INTRACELLULAR BIOCHEMICAL TARGETS OF RUTHENIUM POLYPYRIDYL COMPLEXES IN MULTIPLE CANCER CELL MODELS

By

ADAM S. DAYOUB

Presented to the Faculty of the Graduate School of

The University of Texas at Arlington in Partial Fulfillment

of the Requirements

for the Degree of

DOCTOR OF PHILOSOPHY

THE UNIVERSITY OF TEXAS AT ARLINGTON

Nov 2016

Acknowledgments

I would like to express appreciation for my supervising professor Dr. Frederick M. MacDonnell. His patience and mentoring through these last several years was paramount to my development, not only a graduate student but as a person. I express my gratitude for his patience and skill in my scientific research development. I would not have had this opportunity without his help and confidence in me. He has given me the tools to trust and guide myself in my research endeavors and has shown me that hard work does accomplish many things.

I want to thank my committee members, Dr. Brad Pierce, Dr. Subhrangsu Mandal and Dr. Kayunta Johnson-Winters for their support and the plethora of their ideas and contrasts, which helped the development of this thesis. In particular Dr. Brad Pierce who was kind enough to listen to all my ideas, absurd or no, and guide me with determination and kindness.

I would like to express my deep gratitude for Dr. Malgosia Wilk who has been a guide before my graduate career ever started. The use of her laboratory, she has graciously allowed me to use and perform these experiments in for over 4 years, I will forever be grateful.

Also, an honorable mention to my undergraduate trainee Ali Mohammadi who was paramount to accomplishing this work. Donating his time on weekends and evenings to do work with me and more importantly learn these disciplines in his pre-medical career. I am so proud that this work helped him in acquiring his current position as a medical doctor candidate at UT Southwestern Medical School.

A special thank you to all my current and former lab mates Dr. David Boston, Dr. Nagham Alatrash, Dr. Shreeyukta Singh, Cynthia Griffith, Pooja Ahuja, Eugenia Narh, Chen Yanling, Kai-ling Huang and Matthew West who have supported me personally and professionally. They kept me grounded when I needed to be and have been an amazing ear to speak to in all matters. Their encouragement and support guided and helped me immensely. A special thank you to Cynthia Griffith who introduced me to Dr. MacDonnell and was the catalyst for starting my graduate career.

Thank you to UT Southwestern Hammond Cancer Center and in particular Dr. Rolf A. Brekken and his laboratory, where Chapter 3 and 5 of this thesis were accomplished. The amazing tools and wisdom where such a gift to me in allowing my work to be broadened. My knowledge and skill set was incredibly increased and I have been loving my job every day there. A special thank you in the Brekken lab goes out to Dr. Robin Frink, Jason Toombs, Dr. Dan Ye and Dr. Alan Schroit who are always available to critique and lend ideas for my work development.

I would like to give a special thank you to Dr. Dasgupta and his lab for the use and technical skill with my ICP-MS experiments. From his group, Dr. Charles Phillip Shelor and Brian Stamos, I thank you for your patience and education with these experiments. Also, Dr. Mandal and your group, thank you so much for the use of your lab equipment.

I would like to mention Dr. William Cleaver and Dr. Brian Edwards who have been an ear to my ideas and guides when I had strayed off the course from time to time. To Dr. Heidi Conrad, I am deeply thankful for your hard work with this writing of this thesis. Dr. Peter Kroll, thank you for your support and work with me the past couple of years. You were more understanding than you ever had to be.

Thank you to my graduate school friends Emmanuel Varona, Joya Singh, Shawn Riddlen, John Paul Nimmo , Akop Yapremyan, Diego Lopez and Andy Seal for their friendship and support in so many ways that I can't count on both hands.

Thank you to all the Chemistry and Biochemistry and Biology department staffs for all their hard work and continuous support through my career. They have not only aided me in day to day operations but are also my friends. A special thank you goes to Jill Howard and Linda Taylor for their tirelessly hard work.

I would like to give a deep loving thank you to my family Adib, Helen and Jennifer Dayoub who have been my unwavering support through the dark and hard times and an inspiration through the good. Also, Bryan and Annette Haddad, who spiritually guide me endlessly as well as

my godmother Nawal Dockstader; she was taken from us due to colon cancer and is a driving force for my research. They remind me of where I come from and my mission in life.

I graciously conclude this acknowledgment and thank you to my wife Vilma Veronica Dayoub who for four years has supported me with endless love and understanding. I would not have come so far without her pushing me and knowing what I am capable of accomplishing. I thank her for all the patience, time and love through all this work. She makes me a better person and brings a smile to my face every day. Thank you so much for your love and support. You're my best friend.

November 7, 2016

Abstract

INTRACELLULAR BIOCHEMICAL TARGETS OF RUTHENIUM POLYPYRIDYL COMPLEXES IN MULTIPLE CANCER CELL MODELS

Adam S. Dayoub Ph.D Candidate

The University of Texas at Arlington, 2016

Supervising Professor: Frederick M. MacDonnell

The ruthenium (II) polypyridyl complexes $[(phen)_2Ru(tatpp)Ru(phen)_2]^{4+}$, **RPC4** and $[(phen)_2Ru(tatpp)]^{2+}$, **RPC3** are promising anticancer candidates due to their observed cytotoxic effect against multiple cancer cell lines. These complexes contain a reactive oxygen species (ROS) creating redox-active tetraazatetrapyridopentacene (tatpp) bridge inducing cytotoxic activity against multiple cancer lines and types. Also, they have shown a selectivity towards malignant and normal cell tissue types that are of interest in cellular biological systems and treatment care. They exhibit the ability to regress tumor growth in mouse models, cleave DNA in gel assays and exhibit efficacies in a hypoxic environment similar to that of tumors in vivo.

This thesis is a direct test of the following hypothesis: Ruthenium(II) polypyridyl complexes **RPC3** and **RPC4** both having similar structures and gel based DNA cleaving ability act similarly in cells. The putative targets are the nuclear DNA and/or the mitochondria. Also, we will explore doublets of **RPC3** and **RPC4** with a number of standard care chemo drugs to determine if the RPCs can potentiate a positive response in certain chemo drug resistant cell lines and potentially act in a synergistic fashion.

This thesis develops both hypotheses by an analysis of prior literature research and our biochemical screening approach to test the cytotoxic and intracellular mechanistic ability of these complexes.

In this thesis work, the details of mechanism of action are discussed for complexes **RPC3** and **RPC4** against multiple cancer cell types. Briefly, this examination included methods of cellular entry, RPC cellular compartment localization, their effects on mitochondrial fitness, and the intracellular ROS production levels after inoculation with **RPC3** and **RPC4** and quantification of their DNA cleaving ability in vitro. We first looked at how these complexes differ in their use of active cellular membrane transport and active endocytosis channels. **RPC3** was found to use a great deal of clatherin active transport whereas **RPC4** used a modest amount in comparison. **RPC3** also utilized appreciable lipid raft endocytosis and also gains more entry in ppb into a whole cell vs. **RPC4** which was not found to use any other major transport channel in comparison and passively diffuses through the cell membrane. We also found stark contrasts between intracellular compartmentalization. Our studies elucidate that **RPC4,** is localized heavily in the nucleus of a cell vs. **RPC3,** which was found to be highly localized in the cytoskeleton. This study also exhibits RPCs effects to mitochondrial fitness, ROS production and DNA cleavage ability utilizing confocal fluorescent microscopy of live and fixed cells. We show that **RPC3** and **RPC4** effect mitochondrial membrane potential as well as impair intracellular ATP production against a dosing gradient. We also present evidence of a timed intracellular ROS H_2O_2 production which markedly increases after inoculation with RPCs. Not only was the increase of ROS appreciable but a direct and indirect ROS signal was also found with these RPCs. In the nuclear region of the cells, where **RPC4** is particularly localized, we exhibit an increase of ROS at the 2 h mark vs **RPC3,** highly localized in the cytoskeletal cellular compartment, showing an appreciable ROS increase at 22 h. Last, we demonstrate the DNA cleaving ability using γH2AX to identify double stranded breaks (DSBs) production by **RPC3** and **RPC4.** Very similar to our ROS study, a direct

correlation with **RPC4** showed appreciable DSBs in 2 h vs. **RPC3** exhibiting an indirect yet equal DSB foci formation at 22 h.

We also tested these RPCs in multi-cell tumor spheroids (MCTS) as 3D cell culture more closely resembles in vivo micro-tumor environments. We successfully grew non-small cell lung carcinoma (NSCLC) cells into 3D tumor spheroids and tested **RPC3** and **RPC4** where we identified a shift in inhibitory concentration (IC_{50}) to the right of 2D cell culture inhibition curves. We also noticed in our models these RPCs exhibit differences in morphological effects upon the MCTS. While at IC_{50} doses or above them, **RPC4** did not affect the MCTS spheroid in shape or morphology whereas **RPC3** at small doses was able to disassemble the 3D spheroid.

Lastly, we also examined successful synergy studies with **RPC3** and **RPC4** against a variety of standard care chemotherapy drugs including: cisplatin, etoposide, docetaxel, pemetrexed and gemcitabine. We show in this study that successful doublet combinations with RPCs, cisplatin, etoposide and docetaxel all shifted inhibition curves to the left in a variety of cell lines and types. Not only were they effective but the Loewe synergy index was used to measure these effects as a quantitative synergy proof. We also demonstrate that these RPCs are successful at potentiating cytotoxic efficacies in chemo resistant NSCLC in 2D and 3D cell cultures. Notably, cell lines which were docetaxel resistant, showed a 2-fold or higher synergy when combined with either **RPC3** or **RPC4** and potentiation effects were also found with cisplatin and etoposide resistant cell lines.

In this work we provide evidence that suggests while **RPC3** and **RPC4** are exhibiting similar cytotoxic IC_{50} curves in multiple cell lines and relatively have similar chemical structures, they are behaving in multiple different cellular mechanistic responses in 2D and 3D intracellular environments. We also show that when combined with multiple different standard care chemotherapeutic agents, they are effective as synergistic drug combinations and effective at potentiating responses against chemotherapeutic resistant cancer cell types.

Table of Contents

List of Illustrations

List of Tables

List of Schemes

List of Appendices

Chapter 1

Ruthenium Polypyridyl Complexes and Possible Anti-Cancer Effects

1.1 Modern Ruthenium Drug Cancer Therapy

Rosenberg in the 1960s accidently discovered a metal based antineoplastic agent that is a cornerstone of cancer chemotherapeutics for patients.[1] Shown in Figure 1.1, the compound cis-diamminedichloroplatinum(II), $[PtCL_2(NH_3)_2]$, known as cisplatin commonly, has spawned decades of studies in transition metal chemistry and pharmaceutical research as it pertains to cancer treatment.[1,2] Despite its success in treatment of many cancer varieties, it has been limited due to severe side effects and building drug resistance against many cancer cell types.[2,3] Ruthenium complexes have now been sought after as possible new metal based drugs due to the following: potential for lower cytotoxicity vs their platinum counterparts, [4,5] they have various stable oxidation states and different mechanisms of action [6,7] and ruthenium compound kinetics seem to have several advantages over platinum based drugs.[8] Ruthenium(II) and ruthenium(III) compounds share similar ligand exchange kinetics but are more workable due to their strong influence of coordinated ligands.[9,10] These characteristics make ruthenium complexes useable in biological systems due to their slow ligand exchange rates. [11] These exchange rates play a significant role as ligand exchange is a hallmark determinant of biological activity in platinum complexes. This trait leads many metal based complexes to be substitutionally active at a biological active site or target.[12] Two of the most successful anticancer ruthenium complexes that have emerged from decades of research are NAMI-A and KP1019, shown in Figure 1.1. NAMI-A is believed to interfere with tumor cell interactions in the extra cellular matrix in great extent with actin-dependent cell adhesion and mitosis. [13] This characteristic of NAMI-A is cited as being a reason for its effect on metastases but not established tumor sites.[14] Also KP1019 are proposed to disturb the cellular redox balance of a cancer cell followed by cell cycle arrest in the G2/M phase and mitochondrial apoptotic pathways. [14] New emerging ruthenium complexes with pyridyl- or polypyridyl-based ligands, differ from NAMI-A and KP1019, in that they do not lose ligands and

therefore the entire complex is the biologically active component. They are unique complexes in another right with their photo activating properties.[15] A drawback disadvantage however is many complexes of this variety are cytotoxic against cancer cells once photo-excited, which is problematic in real world standard cancer therapy.[16] Many parts of the human body are not easily accessible for light irradiation and it is not a practical approach, as microscopic tumors and cells would not be easily determined.

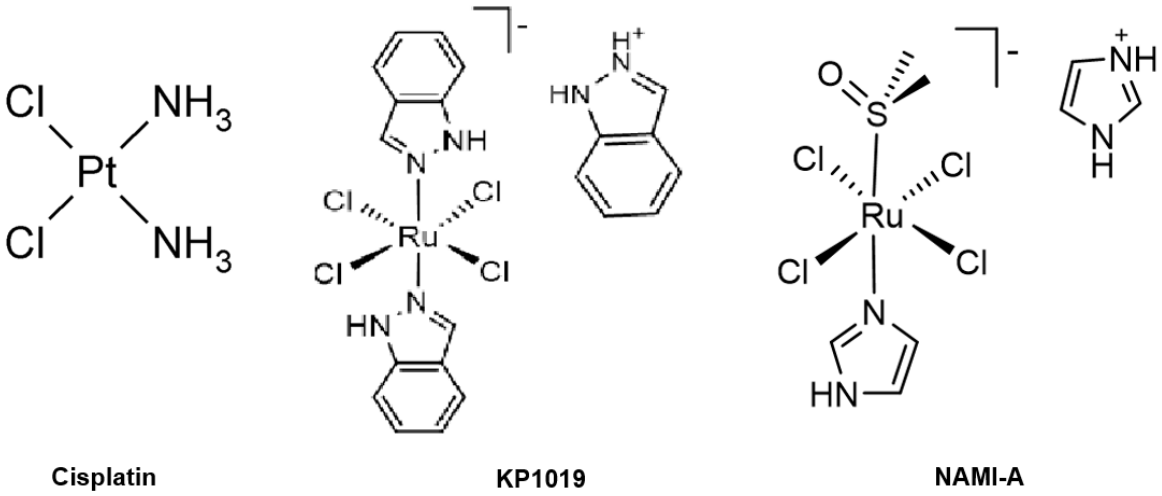

Cisplatin **KP1019** **NAMI-A**

Fig 1.1 Cisplatin and ruthenium anticancer preclinical drugs KP1019 and NAMI-A

1.2 Biological Activity and Description of Ruthenium Polypyridyl Complexes and Current MacDonnell Laboratory Findings

Ruthenium polypyridyl complexes (RPCs) are a family of complexes with extensive studies on $[^{106}Ru(phen)_3]^{2+}$ (RPC1) by Dwyer and Schulman in the 1950 – 1960s.[17] RPC1 differs from the earlier mentioned NAMI-A and KP1019 complexes because it lacks labile ligands and does not form bonds with biological targets.[18] Radiolabeled RPC1 in Dwyer's work demonstrated intact complex cation was the bioactive unit and was not metabolized. [19,20] RPCs have also been

shown to have a high affinity for DNA binding.[107] DNA binding is electrostatic and intercalative with binding constants ranging from $10^1 – 10^7$ M^{-1}.[107 – 100] RPCs have also been shown to inflict

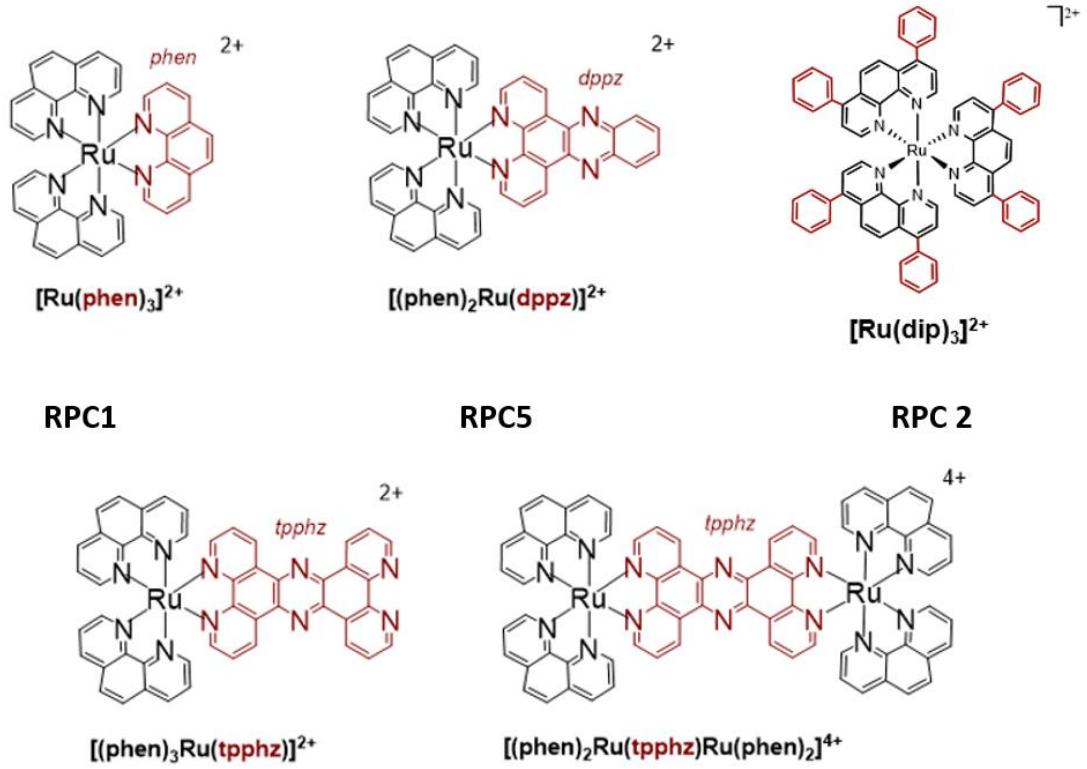

Fig 1.2 Various ruthenium polypyridyl complexes (RPCs) and their different bridging ligands in (red). Also, nomenclature for RPCs 1,2 and 5 are noted.

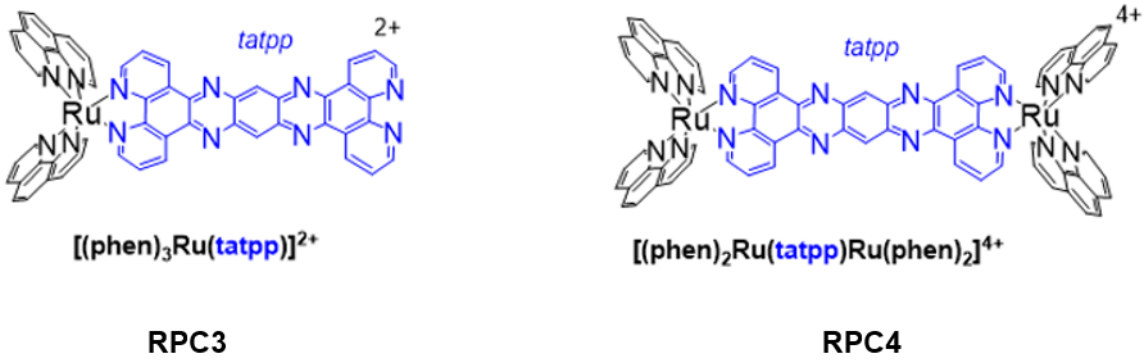

Fig 1.3 RPCs of interest and their nomenclature letters. The (blue) bridge exhibits the novel biological active unit tetraazatetrapyridopentacene (tatpp) ligand.

mitochondrial dysfunction and are thought to be their primary target. [111,112] The ligand varieties that are possible in these coordinative complexes also makes them versatile in their cytotoxicity. Thomas et. al. exhibited that by adding lipophilic ligands the complexes increase their cytotoxicity and also their intracellular primary targets of dysfunction. [11,112] RPCs tend to have reasonable cytotoxicity with the half maximal inhibition concentrations (IC_{50}'s) on the scale of 10^{-4} to 10^{-7} M.[7]. These intracellular targets shown in multiple studies range from lysosomes and peroxisomes to endoplasmic reticulum and mitochondrial dysfunction.[111 - 113] . In this work we focused on similar coordinately saturated and kinetically inert ruthenium(II) complexes containing polypyridyl ligands shown in Figure 1.2

Chemotherapy can be cytotoxic to many healthy cells as well as cancer cells, as such; targeting a complex to cancer cells versus healthy cells would be highly beneficial for cancer treatment. Many RPC's, such as $[Ru(DIP)_3]^{2+}$ (RPC2) (DIP=diphenylphenanthroline), (Figure 1.2) show indiscriminant cell type cytotoxicity with IC_{50}'s around 1-2 μM.[21,22] We initially studied these RPC's and have synthesized planar bridging ligands that could possibly intercalate or target DNA similar to the dppz ligand (dipyridophenazine), $[Ru(phen)_2dppz]^{2+}$ (RPC5) also in Figure 1.2.[22,23] In particular , RPCs containing the tatpp (tatraazatetrapyridopentacene) ligand in dinuclear complex $[(phen)_2Ru(tatpp)Ru(phen)_2]^{4+}$, **RPC4** and mononuclear complex $[(phen)_2Ru(tatpp)]^{2+}$, **RPC3** shown in Figure 1.3 are of interest and the subject of this study as promising anticancer activity complexes. In our previous reported findings, we demonstrated their efficacy with in vitro apoptotic cascades, selectivity between normal and cancer cell types and mouse xenograft tumor models.[24]

Our studies have also demonstrated the DNA cleaving activity of the **RPC3** and **RPC4** tatpp bridge and its ability to cut DNA in gel assays. It is not known however if this was occurring in vitro within the nucleus of a cell.[16,18] In the presence of a mild reducing agent glutathione

(GSH), which is also readily available in most cell types, we believe that the tatpp DNA cleaving ability is due to a redox-cycling mediated by [GSH] and [O2]. [25] We surmise the RPC complexes electrostatically bind to DNA within a cell and the tatpp ligand can exert its redox-active cycling activity and intercalating DNA binding properties. [18,25] [GSH]/[O2] ratio is in a steady state concentration of three redox isomers of **RPC3** and **RPC4** that with low [O_2] and high [GSH] a pathway to ROS production of H_2O_2 is favorable. [25] ROS production of H_2O_2 not only can cleave DNA but the indigenous $Fe^{2+/3+}$ in a cell can also lead to Fenton chemistry producing the damaging $OH^{\cdot -}$ (hydroxyl radical). The scheme of this steady state reaction with **RPC4** is shown in scheme 1.1

We also have examined multiple IC_{50} studies revealing concentrations in the ranges of 8 – 31 μM of both **RPC3** and **RPC4** in multiple cancer lines and types which will be discussed in more detail later. **RPC3** and **RPC4**, after preliminary examination, separate themselves from other antitumor agents by showing selectivity towards carcinoma cells versus normal functioning healthy (non-carcinoma) cells. Normal non-carcinoma cells: HUVEC (Human Umbilical Vein Endothelial Cells), HAVSMC (Human Aorta Vascular Smooth Muscle Cells) and HBE3CKT (Human Bronchial Epithelial Cells) showed a low response to complex treatment, however a high response to complex treatment was observed in carcinoma cells, NSCLC (Non-Small Lung Carcinoma Cells) H358 and H1792 as well as SCLC (Small Cell Lung Cancer) H226 shown in Figure 1.5.[22] We also have also shown their cytotoxic capabilities to be more efficacious in hypoxic environments within certain cancer cell types. [22,24]

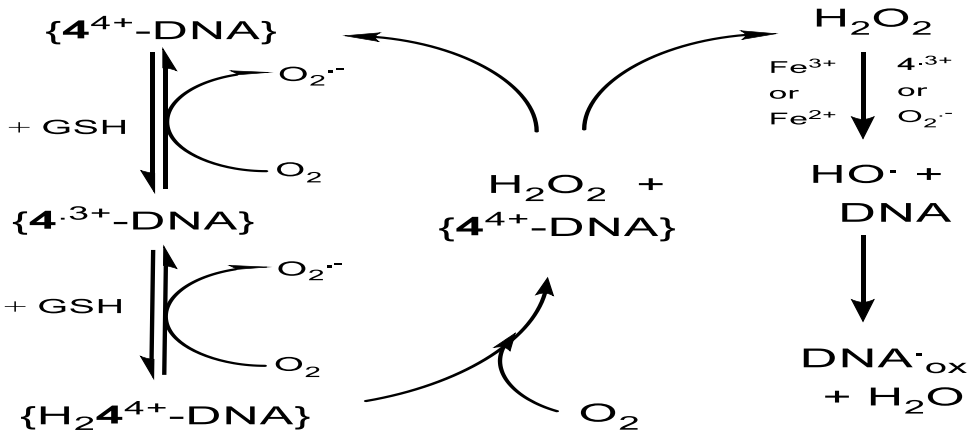

Scheme 1.1 RPCs isoforms created under [GSH] reducing agent and [O_2] in a steady state redox cycle that produces ROS H_2O_2 and hydroxyl radicals responsible for DNA cleavage. The ROS production of H_2O_2 and hydroxyl radicals in the presence of DNA is suspected to cleave DNA in vitro.

This hypoxic environment reveals a possible anti-cancer pathway as most tumors in vivo are hypoxic in nature, due to low vascularization and necrotic cores.[26] Studies conducted under normoxic and hypoxic conditions against NSCLC HOP-62 and Hs-766T (pancreatic tumor), showed an appreciable greater sensitivity with **RPC3** under hypoxic conditions as compared to normoxic conditions. [25,26]

Lastly, we examined a mouse xenograft model with NSCLC H358 against **RPC3** and **RPC 4.** A 60 day study was performed with tumor burden measured as treatment of RPCs and no drug vehicle, phosphate buffered saline (PBS), was administered. In Figure 1.5 we show that with vehicle alone, tumor burden continued increasing while doses of **RPC3** and **RPC 4** significantly regressed tumor growth size. [25]

The ability to cleave DNA, achieve cytotoxicity against different cell types while lowering cytotoxicity against normal cell lines, activity in normoxic and hypoxic environments and regression of tumor burden in mouse models are exciting prospects for a new metal based anticancer drug design.

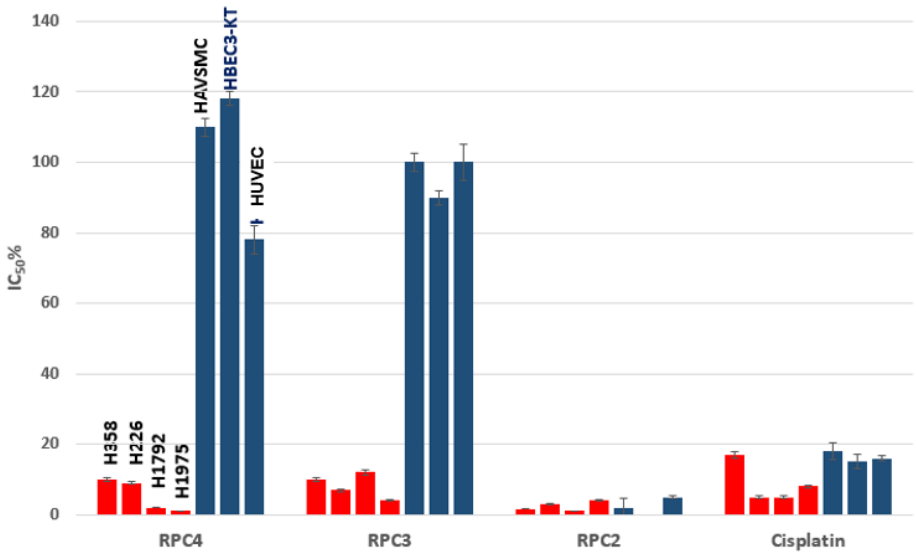

Fig 1.4 Shown are IC_{50}% drug concentrations of RPC2, **3,** and **4** against NSCLC H358, H226 and H1792 as well as SCLC H226 (all in red). Also shown are RPC2, **3,** and **4** against normal non-maligant cells HAVSMC, HBC3-KT and HUVEC (all in blue). In contrast cisplatin was used against all cells as a comparison.

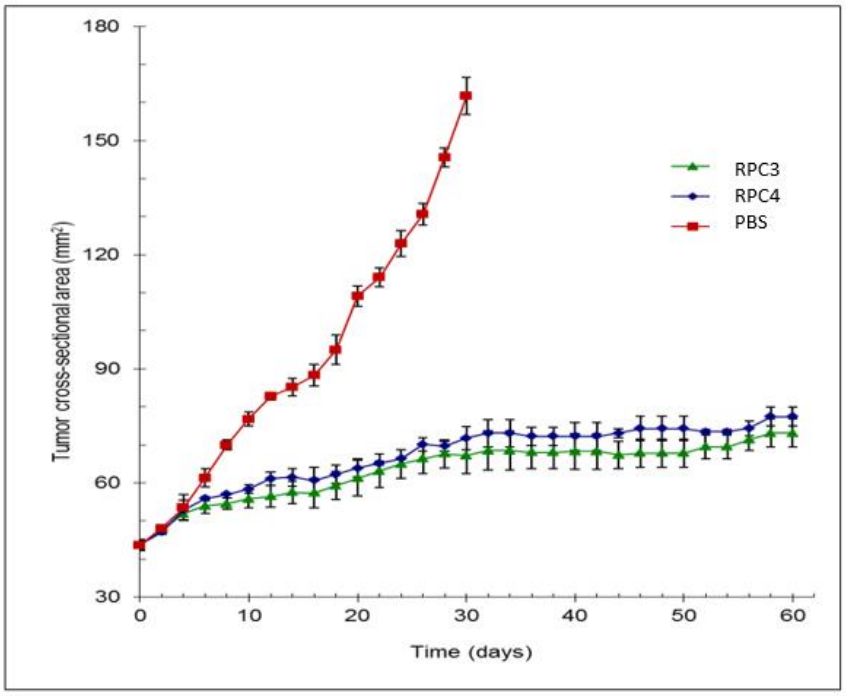

Fig 1.5 Mouse tumor regression model. Phosphate buffer saline (PBS) shows increased tumor growth while **RPC4** and **RPC3** show tumor growth regression over a 60 day period.[18]

1.3 Scope of Thesis

It is postulated that ruthenium polypyridyl complexes (RPC)s $[(phen)_2Ru(tatpp)Ru(phen)_2]^{2+}$, **RPC4** and $[(phen)_2Ru(tatpp)]^{2+}$, **RPC3** will cleave intracellular DNA in vitro within multiple cancer cell types. Studies were also done to examine RPCs against the mitochondria, rather than just examining DNA utilizing different cell models and assays. It is also postulated that combination therapy may be a plausible route of interest for these complexes and a thorough examination will be discussed involving **RPC3** and **RPC4** in multiple cancer cell types and screens.

The first hypothesis of this work states the following: Ruthenium(II) polypyridyl complexes **RPC3** and **RPC4** both having similar structures and gel based DNA cleaving ability, act similarly in cells. The putative targets are the cells nuclear DNA and/or the mitochondria.

The second hypothesis of this works states the following: We will explore doublets of **RPC3** and **RPC4** with a number of standard care chemo drugs to determine if the RPCs can potentiate a positive response in certain chemo drug resistant cell lines and potentially act in a synergistic fashion.

Chapter 2

Examination of RPCs Effects in the Cellular Environments and Organelles in Multiple Cancer Cell Types

2.1 Introduction

While **RPC3** and **RPC4** appear to be promising pre-clinical anti-tumor drugs, little is known about how or even if these complexes enter cells, where they accumulate and what if any cytotoxic efficacies they exert on the cell environment. In this chapter, we examine RPC function in non-small carcinoma lung cells (NSCLC) H358, HOP-62, H1792, H1975, human colon cancer cell HCC-2998 and pancreatic cell Hs766T with detailed studies against several transport channels, accumulation in multiple cell compartments, mitochondrial and nuclear dysfunction as well as intracellular ROS production.

Active transport endocytosis was observed as a function of selective inhibition of specific transport mechanisms. In particular, active transport mechanisms were used by **RPC3** and **RPC4** including: clathrin mediated, lipid raft and GTP couple protein channels as methods of active transport entry through the cell membrane. Once through the cell membrane, cellular location of any drug complex is essential to the preliminary understanding of its function. Inductively coupled plasma-mass spectrometry (ICP-MS) was used to quantify Ru ion content in various cellular compartments to determine localization and mode of active transport across cell membranes of **RPC3** and **RPC4.** Specifically, 4 distinct compartment proteins were analyzed for RPC localization including: cytosol, mitochondria and ER membranes, nuclear and cytoskeleton fractions of various cancer cells.

Mitochondria act as a point of integration for apoptotic signals that are either extrinsic or intrinsic pathways.[27,28] Mitochondrial dysfunction in terms of losing potential, loss of membrane integrity by the release of cytochrome c and ATP inhibition are critical events in triggering various apoptotic pathways.[27-29] Therefore, the status of mitochondria fitness in treated cells was investigated by confocal laser microscopy. We examined mitochondrial potential using the JC-1

aggregate dye as well as a fluorogenic multiplex assay to determine membrane integrity and ATP production in cancer cells.

We also show that DNA is one of the main targets of these RPCs. There has been much attention given to RPC binding with DNA using terms as the “light switch effect“ coined by Barton et. al. but unless activated by light, DNA damage is usually not observed. [29-31] There are many studies that indicate or prove that certain RPCs bind to DNA and it is often assumed that DNA is the biological target.[31,32] Also data and study from several laboratories have indicated that RPCs may target multiple cellular organelles including the mitochondria, [33,34] endoplasmic reticulum,[35] and the extracellular membrane.[36,37]

In this chapter we show that **RPC3** and **RPC4** are effective DNA cleaving agents and initiate double stranded breaks (DSBs) in a variety of cancer cell types. In the previous chapter we introduced that these two complexes catalytically cleave DNA by activation of O_2 through a multi-stage redox-cycling mechanism which generates superoxide and the ROS H_2O_2. We believe that ROS is a major player in the DNA cleavage observed in cancer cells and we will show as well the intracellular ROS production in the cellular environment. It is salient to mention that **RPC3** and **RPC4** cytotoxic action are not due to a light activated process making them an attractive anti-cancer theraputic.

2.2 Experimental

2.2.1 Chemicals

All solvents were reagent and cell culture grade. All reagents and work environments were maintained sterile. **RPCs 1-5**, **ΔΔRPC4** and **ΔRPC3** where provided by the MacDonnell laboratory and were used as received. NSCLC H358, HOP-62 and HCCCL HCC2998 cells were purchased from The National Cancer Institute (NCI) at Frederick Central Repository. Human

lymph node Hs-766T cells and DMEM medium where purchased from American Type Culture Collection (ATCC). H1792 and H1975 were acquired from University of Texas Southwestern (UTSW) Hammond Cancer Center (HCC). RPMI-1640 medium, penicillin/streptomycin, fetal bovine serum (FBS), 100X BME vitamin solution, dimethyl sulfoxide (DMSO), 0.04% trypan blue, bovine serum albumin (BSA), para-formaldehyde (PFA), methanol, nitric acid (HNO_3), sodium azide (NaN_3), 2-deoxy-D-glucose (DOG), sucrose, dynasore hydrate, nystatin, oligomycin, d-(+)-galactose, 4-(2-hydroxyethyl)-1-piperazineethanesulfonic acid (HEPES), digitonin, propidium iodide (PI) and 3-(4,5-dimethylthiazol-2-yl)-2,5-diphenyltetrazolium bromide (MTT), etoposide and cisplatin were purchased from Sigma Aldrich. Phosphate buffered saline 10X was purchase from Biorad. Mitochondrial Tox-Glo Multiplex assay and bis-AAF-R110 substrate were purchased from Promega. JC-1 mitochondrial potential dye was purchased from VWR. The Qproteome Cell Compartment Kit was purchased from QIAGEN. Primary γH2AX monoclonal antibody was purchased from EMD Millipore. Goat anti-mouse IgG (H+L) secondary antibody Alexa Fluor488 and Pro-gold anti-fade mounting agent were purchased from Invitrogen.

2.2.2 Instrumentation

Cell incubation was maintained by a Thermofisher HeriCell CO_2 Incubator. Ruthenium ion concentrations were determined using a Thermofisher-1000 inductive coupled plasma mass spectrometer (ICP-MS). Absorbance data was obtained using a BMG Labtech FLUOstar Omega plate reader. Confocal microscopy was performed using a Zeiss Axio-Plane 540 with mercury lamp and argon laser.

2.2.3 Cell Culture Lines/Maintenance

H358, H1975, H1792, HOP-62 and HCC-2998 cells were grown in RPMI-1640 medium supplemented with 10% FBS, 2 mM L-glutamine, 1 mM sodium pyruvate, 1.1% penicillin/streptomycin and 1X BME vitamin complex solution. Hs766T cells where grown in

DMEM medium supplemented with 10% FBS, 2 mM L-glutamine, 1 mM sodium pyruvate, 1.1% penicillin/streptomycin and 1X BME vitamin complex solution. Cells were grown and passaged in T-25 and T-75 Corning culture flasks at 37^{o}C under 5% CO_2 and humidified atmosphere.

2.2.4 Cytotoxicity and Cell Viability

The cytotoxicity of the RPCs, cisplatin, and VP-16 (Etoposide) were determined by an MTT assay. Cells were seeded into 96-well plates at 1×10^4 cells per well and grown for 24 h at 37 °C in a 5% CO2 incubator; then titrating doses of drug were used ranging from 0.001 - 100 µM. Cells were then incubated with drug for 72 h under the same conditions. The stock MTT dye solution (5 mg/mL) was added to each well for 3.5 h of incubation. The dye was removed and 120 µL of DMSO was added to each well. Plates were read for absorbance at 570 nM using a plate reader. Spheroid cell viability was determined using Promega Cell Titer-Glo for 30 min at rt and read using a luminescent plate reader.

2.2.5 RPC Loci Determination

H358 and HCC-2998 cell lines were seeded, grown and passaged to confluency. Cell lines were then treated with 20 µM concentrations of RPC **1-5** for 12 h. Cell where then removed and washed 3x with ice cold PBS. Each complex/cell treatment pellet was placed into separate 15 ml centrifuge tubes and treated with 4 QIAGEN kit buffers supplemented with 100x protease inhibitor (in sequence per tube) to perform 4 distinct cell compartment isolations. Compartment protein separations (sep1-4) are as follows: sep1-cystoplasmic proteins, sep2-mitochondrial, endoplasmic and lysosomal proteins, sep3-nuclear proteins and sep4-extra cellular matrix proteins. Each cell protein separation was diluted in ddH2O with 1% HNO_3 to remove any cell membrane debris. Each compartment solution was then analyzed for Ru ion concentration using ICP-MS.

2.2.6 Cellular Uptake of RPC complexes

A series of known cell membrane active transport blockers were used to determine entry of RPC **2,3** and **4** in H358 and Hs766T cell lines. H358 and Hs766T cell where seeded, passaged and grown in fresh medium for 24h. Fresh medium was replaced and cells were allowed to acclimate for 6h. Cells were then treated with various active transport endocytosis inhibitors in separated flasks for 1h prior to RPC inoculation as follows: 10 mM Sodium Azide (NaN_3) and 2-deoxy-D-Glucose (DOG), 1 M Sucrose and 300 µM dynasore. In addition 50 µM nystatin was administered for 30 min prior to RPC inoculation. Cells were treated with 40 µM of RPC **2, 3** and **4** for a 6 h period. Each cell protein separation was diluted in ddH2O with 1% HNO_3 to remove any cell membrane debris. Each compartment solution was then analyzed for Ru ion concentration using ICP-MS.

2.2.7 Mitochondrial Potential Determination

H358 cells were seeded on 25x25 mm microscope cover glass slips in BD Falon 60x60 mm tissue culture dishes for 72 h. Cells where then treated with complexes: **RPC3** and 4 at 20 µM for 24 and 48 h. The cover slips was removed and washed 3X in ice-cold phosphate-buffered saline (PBS) to remove residual drug. Cells where blocked with 3% BSA and JC-1 mitochondrial potential dye was adminstered at 1mg/mL in mmH_2O for 10 min and live cell imaging was taken. Confocal microscopy was performed using long pass light filters and a 1.3 airy unit pinhole at 488/529/590 nm. 40x oil immersion objectives were used and digital camera images (DCIM) where captured using ZEN software.

2.2.8 Mitochondrial Membrane Integrity and ATP determination

H358 cells were seeded and passaged in 96 well plates at a cell density of 40,000 cells/mL. At 24 h glucose and L-glutamine containing medium was removed and cells were dosed with DMEM supplemented with 15 mM D-(+)-Galactose and 10 mM HEPES buffer. No bovine serum was added to the medium formulation prior to dosing. Multiplexing assay was carried out by dosing DMEM D-(+)-Galactose supplemented H358 cells with 300 μM stock solutions of **RPC** 1, 2, **3, 4,** 5**,** and Oligomycin as positive control. All stock solutions were prepared in DMEM medium supplemented with D-(+)-Galactose and HEPES buffer previously mentioned with 1% DMSO. Cells were dosed with complexes in a 1:2 dilution series starting at 40 μM. Timings were adhered as described in (Promega G8000, Niles et. al 2007, Marroquin et. al 2007). Eight replicates were kept for untreated ATP chemistry. Digitonin 800 μg/ml was used as a positive membrane integrity toxicity control. A fluorogenic substrate, bis AAF-R110 was used to test membrane integrity based on protease activity measured at 485/525 nm emission with agitation (source). ATP detection was accomplished by scanning for luciferase luminescence using an ATP detection cell titer glow.[38,39]. Fluorescence and luminescence were both measured using a fluorescent/luminescent plate reader.

2.2.9 Measurement of intracellular reactive oxygen species.

The generation of ROS in H358 cells was measured using a ROS sensitive fluorescent probe, 2,7-dichlorodihydrofluorescein diacetate (DCFH-DA). DCFH-DA can be oxidized to 2′ ,7′ -dichlorofluorescein (DCF) by ROS and exhibits green fluorescence intensity. H358 cells were treated with RPC2**, RPC3** and **RPC4** at their respective IC_{50} concentrations for 2, 8 and 22 h. Untreated cells were maintained as the negative control and 10, 20 and 30% H_2O_2 solution in PBS was administered in the cells for 15 minutes as positive control. The cells were passaged and washed 3X in ice cold PBS then suspended in 10 mM DCFH-DA and incubated in the dark for 30 min. The levels of intracellular ROS were examined by confocal microscopy using long

pass light filters and a 1.3 airy unit pinhole at 488/519 nm with a Zeiss axioplane inverted fluorescence microscope.

2.2.10 H2AX Double Stranded Break Assay.

H358, H1792 and H1975 NSCLC cells were seeded on 25x25 mm microscope cover glass slips in BD Falon 60x60 mm tissue culture dishes for 72 h. Cells where then treated with complexes: Etoposide (VP-16), **RPC3** and **RPC4** at their respective IC_{50}'s for 2,8 and 22 h. The cover slips was removed and washed 3X in ice-cold phosphate-buffered saline (PBS) to remove residual drug. Cells where fixed with 4% para-Formaldehyde solution, permeabilized with 0.25% Triton and blocked with 3% BSA. anti-phospho-histone (Ser139) H2AX (1:1000) in 3% BSA/1% sodium azide was administered for 1 h in the dark at room temperature. Cells where then washed 3X in ice-cold PBS and Goat anti-mouse IgG (H+L) secondary antibody Alexa Fluor488 (1:2000) in 3% BSA/1% sodium azide was administered for 2 h in the dark at room temperature. Cells again were washed 3X in ice-cold PBS and then fixed on microscope slide with Pro-Gold antifade reagent. Confocal microscopy was performed using long pass light filters and a 1.3 airy unit pinhole at 488/519 nm. 60x oil immersion objectives were used and digital camera images (DCIM) where captured using ZEN software. Cell sorting and foci count were analyzed with Image J software for an average of 25 cells per image count

2.3 Results and Discussion

2.3.1 Cytotoxicity in 2D Cell Culture.

Cytotoxicity of **RPC2, RPC3, RPC4, ΔRPC3** and **ΔΔRPC4** were evaluated against 7 tumor cell lines. The effect of these complexes were accomplished by looking at their IC_{50} effect of growth on multiple cell lines from multiple tissue types. Lung cancer cell types were represented in 4 NSCLC lines H358, H1975, H1792 and HOP-62 all being adenocarcinoma. Pancreatic lymph node cancer cell line Hs766T as well as one colon adenocarcinoma line HCC-2998 were also used in this screen. As a control, **RPC3** and **RPC4** were tested against normal human cell lines: heart aortic vascular smooth muscle cells (HAVSMC) and human umbilical vascular endothelial cells (HUVEC) to determine any difference in efficacy between cancer and normal cells. Table 1 examines this data and indicates cytotoxic IC_{50} values ranging from 0.1 – 100 μM.

RPCs	H358	HOP-62	H1975	H1792	HCC-2998	Hs766T	HUVEC	HAVSMC
[4]	9.5 ± 5.2	50 ± 4.9	6 ± 3.1	2 ± 5.1	13 ± 5.1	10.0 ± 5.1	119.0 ± 5.0	104.0 ± 4.0
[3]	8.8 ± 5.0	55 ± 4.2	13 ± 4.3	4 ± 4.8	20.0 ± 5.0	31.0 ± 5.9	92.0 ± 5.0	100.0 ± 5.0
[2]	1.7 ± 2.3	6 ± 2.3	3 ± 2.1	1 ± 3.1	1.2 ± 3.2	3 ± 4.3	2.8 ± 5.1	5 ± 4.1
[ΔΔ4]	12 ± 4.2	48 ± 5.6	2 ± 3.9	1.3 ± 4.2	N/A	N/A	N/A	121 ± 5.2
[Δ3]	11 ± 3.8	59 ± 6.1	9 ± 4.1	11 ± 5.1	N/A	N/A	N/A	115 ± 5.1

Table 1.1 shows various IC_{50} values based on concentration of RPC complexes in μM. Carcinoma lines H358, H1975, H1792, HOP-62, Hcc-2998, and Hs766T are compared to normal non-carcinoma lines HUVEC and HAVSMC.

Remarkably, we show that there is a ten-fold difference between HUVEC and HAVSMC and most of the cancer cells with the exception of HOP-62 showing a 2 fold difference. This could put forth a potential targeting scheme toward carcinoma vs healthy tissues. **RPC3** and **RPC4** seem to exert equal cytotoxic behavior among the majority of cells lines with the exception of Hs766T cells where **RPC4** showing a more cytotoxic effect. This data would suggest that both **RPC3** and

RPC4 are behaving with similar mechanisms towards malignant cancer cell types and indicates **RPC3** and **RPC4** are cytotoxic and selective to cell types.

2.3.2 Ruthenium Complex Accumulation in Various Cellular Compartments

Cellular localization and accumulation is a critical first step to understanding the RPCs biological activity. The therapeutic value must exert itself by first reaching its target in the cell and interacting with various cell compartment proteins. Determining whether or not the RPCs are distributing evenly throughout a cell compartment distribution or localized in different concentrations in separate compartments is imperative to understanding their function and various protein interactions. The localization of RPCs **1 – 5** were screened by separating H358 and HCC-2998 cells into multiple compartments after RPC treatment and using ICP-MS measurements to quantify the Ru ion concentration in separate cellular compartments. Please note that RPC 1 was only tested in cell line H358.

Cell compartment proteins were separated into 4 distinct cell compartment types: cytoplasm, cell membranes (mitochondria, golgi and endoplasmic reticulum), nuclear membrane and cytoskeleton. After treating cell lines H358 and HCC-2998 with RPC complexes, cell compartments were separated and analyzed. Results for compartment loci can be seen in Figure A/B 2.1 where (A) is H358 and (B) is HCC-2998. Ru ion content, was measured in ppb and then later translated to a percentage based on the total amount of Ru ion in the whole cell. The top left corner of each plot is a ppb representation of total Ru ion entry per complex in (non-fractionated) whole cells. **RPC4** was normalized for 1 ruthenium per other RPCs so as to reflect whole complex localization per cell compartment.

RPC complexes 1,2 and 5 were also examined as a controls representing a closely-related but non-redox active cationic ruthenium polypyridyl complex. As seen in Figure A/B 2.1, **RPC4** showed an increase in nuclear compartment localization up to 38% in H358 and 30% in HCC-2998 showing a significant difference from RPC 5. Barton et. al. demonstrated that RPC 5 intercalates but does not cleave DNA in the nucleus and the nuclear center of the cell is the target

due to its hydrophobicity.[40] Overall **RPC4** shows a greater presence in the nucleus as compared to all other RPCs tested. Also RPC 1 was localized the least in the nuclear region of H358 as it localized the other compartments more equally. **RPC4** and 5 also showed appreciable mitochondrial localization where cytotoxic ability might occur. A 30% localization of RPC 5 and a 25% localization of **RPC4** in the mitochondrial regions of H358 and 19% equally of RPC 5 and **RPC4** in the mitochondrial regions of HCC-2998 were observed. Markedly, a stark contrast was found with complexes RPC2 and **RPC3** highly localized in the cytoskeleton of both cells H358 and HCC-2998. RPC 2 shows an almost 90% location within the cytoskeleton region of H358 and HCC-2998. **RPC3** was also pronounced in the cytoskeleton at approximately 75% in H358 and 90% in HCC-2998. At first, this seemed unusual that RPC 2 was so localized in the cytoskeleton but multiple studies do state its effects are exerted on the mitochondria.[41,42] Also, **RPC3** being so heavily localized in cytoskeleton proteins of both cell lines was a surprising contrast from its counterpart **RPC4**.

We can assume that **RPC3** and **RPC4** localization indicate possible bioactive action sites based on their cell compartment loci but the surprising discovery was the deviation and difference between the RPCs loci from one another in cells. Their IC_{50}s would suggest that they behave very similar to each other but based on this data they may be mechanistically acting differently.

2.3.3 Ruthenium Complex Cellular Membrane Transport

The localization of **RPC3** and **RPC4** in the cell lines H358 and HCC-2998 was examined in the previous section; now the route of cellular entry will be elucidated. Endocytosis active transport through the cellular membrane is energy dependent, whereas passive diffusion is not.[40] Endocytosis, being an energy dependent pathway, is susceptible to modulation were passive diffusion is an energy independent pathway less prone to its effects.[43] This is a crucial step in identifying the RPC complexes different attributes, if any, by their method of entry into a cell membrane. The mechanism of cellular entry was examined as a function of active transport

channels. Cell lines H358 and Hs-766T were inoculated with various RPCs and certain cell membrane channels where inhibited. ICP-MS was used to detect Ru ion content that had passed through the membranes into cells.

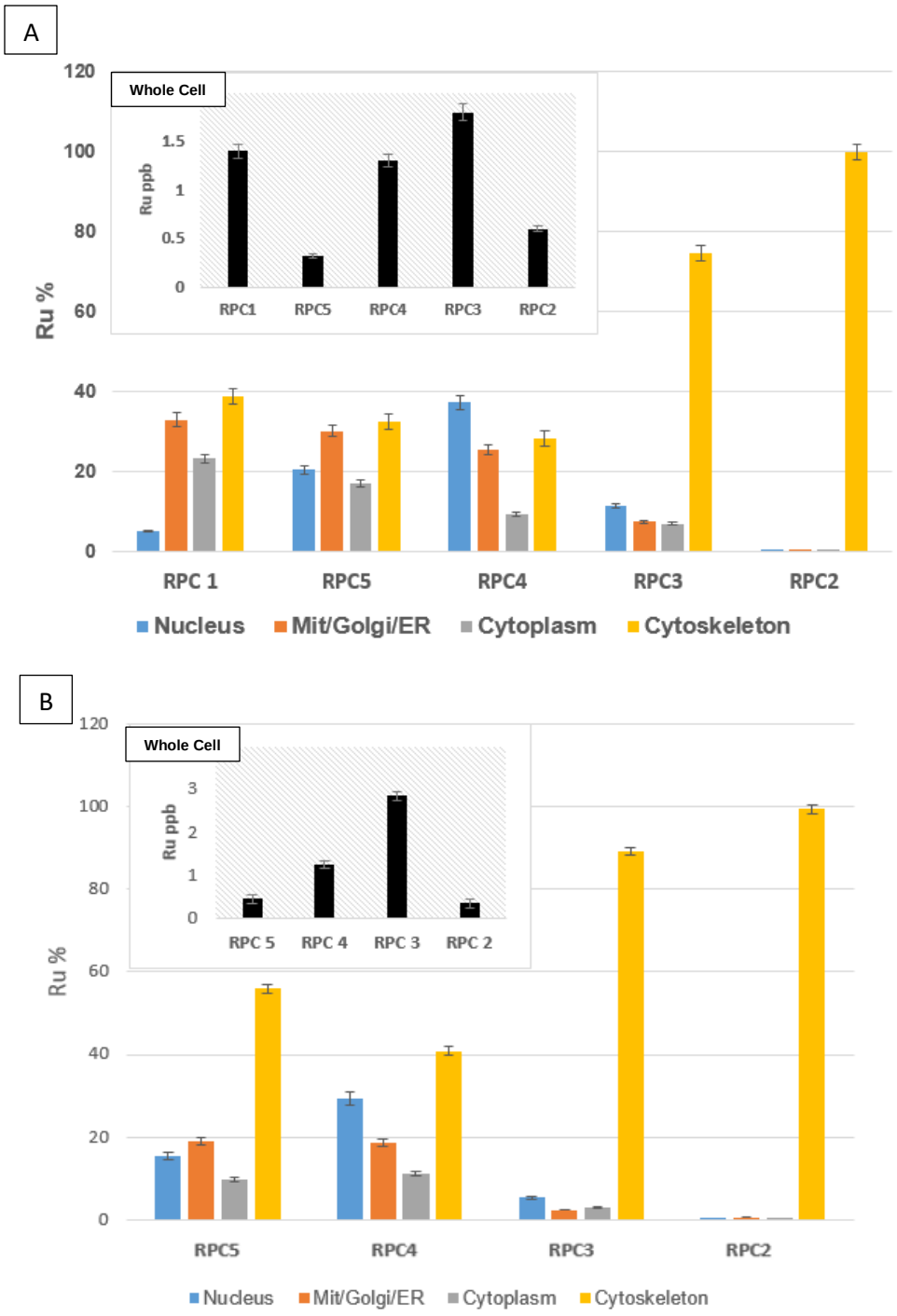

Fig 2.1 A/B Cell lines H358 (A) and HCC-2998 (B) were inoculated with 20 µM of RPC 1 - 5 for 12 h. Cells were then compartmentalized into for separate compartments: nucleus, cell organelles, cytoplasm and cytoskeleton and Ru ion was analyzed using ICP-MS. Top left bar graph shows Ru amount inside unfractionated (whole) cells. **RPC4** was /2 as to be compared to all other mononuclear RPC complexes.

Active mediated endocytosis inhibitors were used to examine cell membrane transport receptors used by **RPC3** and **RPC4**. RPC2 was used a positive control as it is cytotoxic to all cell lines tested indiscriminately. Various active transport inhibitors were employed to study relative complex concentrations penetrating the cell membranes as they gain entrance which was plotted in Figure A/B 2.2. Treatments of sodium azide (NaN_3) and 2-deoxy-D-glucose (DOG) were administered due to their known active transport energy inhibition actions.[40] A 23% inhibition of **RPC4** was observed as compared to internalization of the control and an appreciable 65% inhibition of **RPC3** was found compared to the control as well. This finding was remarkable as again **RPC3** and **RPC4** are showing a difference in their respective actions. Due to this discovery a further test was examined to look at specific active endocytosis transport channels. The study of these transport channels were examined by inhibition of lipid raft, clatherin and GTP-protein active receptor mediated endocytosis as the three main routes of cell entry.[44] Phagocytosis inhibition was not studied since H358 and Hs766T cell lines as well as most cancer cell lines do not exhibit this function.[29,40] First we employed sucrose, a clathrin mediated endocytosis inhibitor, exhibiting a cell entry inhibition of 50% for **RPC4** and 81% inhibition of **RPC3** entry as compared to the control. RPC 2 showed a 30% inhibition as well. This suggests the clathrin transport mechanism is the main action of entry for these RPCs. In addition, nystatin, a lipid raft mediated endocytosis inhibitor, showed a 32% inhibition entry for **RPC3** in Hs766T and an 80% inhibition in H358 whereas no appreciable difference in entry was inhibited **RPC4**. RPC2 showed a modest inhibition with lipid raft at 20%.

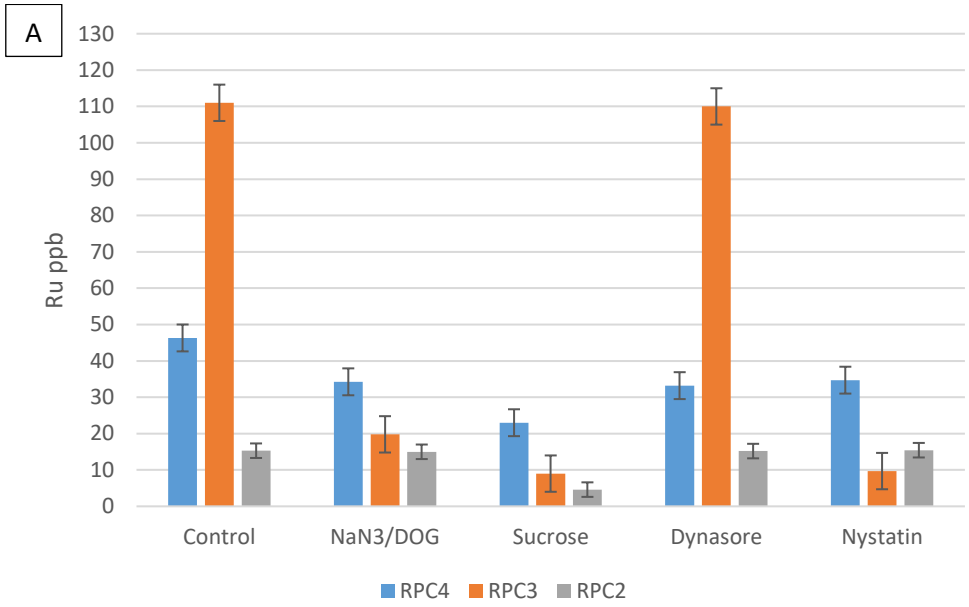

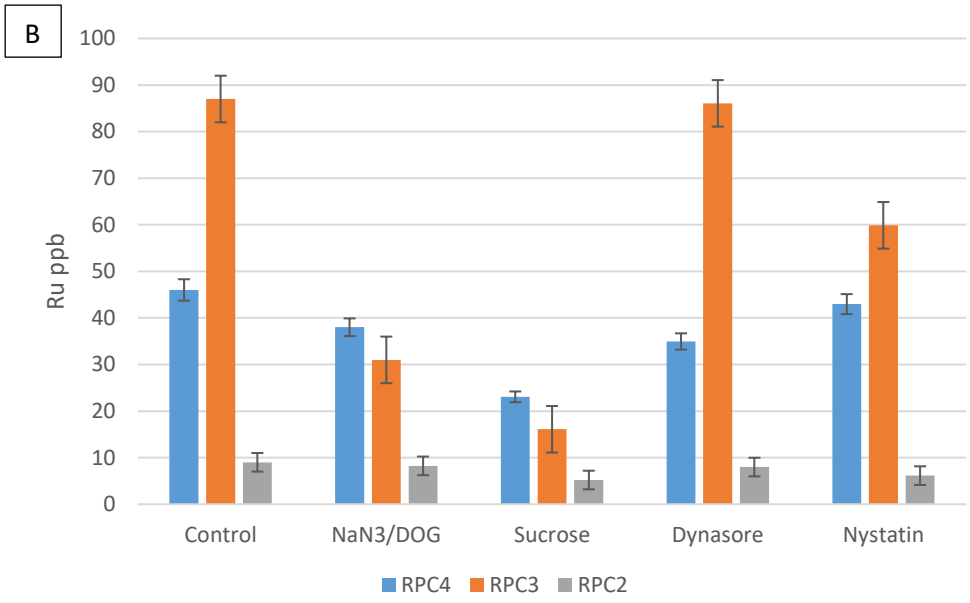

Fig 2.2 (A/B) Separate active mediated endocytosis inhibitors were inoculated to H358 (A) and Hs766T (B) cells separately and were inoculated with 40 μM of various complexes. Detection of Ru ion content was performed with ICP-MS. The control is 40 μM of various complexes without any inhibitor. **RPC4** was nominalized as to be compared to mononuclear complex **RPC3** and 2.

This data suggested that a moderate form of lipid raft mediated endocytosis is being utilized by **RPC3**. Lastly dynasore, a GTP-binding protein inhibitor, which is a main component of receptor mediated endocytosis, also showed a 33% inhibition of **RPC4** entry into the cell membrane as compared to the control. No appreciable change can be seen with **RPC3** and RPC 2. Studies by Guo W. et. al. showed that RPCs can bind to extracellular serum proteins which can promote cellular uptake.[43] For this reason fetal bovine serum (FBS) was not removed from the media as in human blood a similar plasma is present.

From this study we conclude that **RPC3** and **RPC4** are exhibiting active mediated endocytosis into the outer cell membrane and using different mediated cell membrane receptors to accomplish their entry albeit **RPC3** is highly using more. While **RPC3** and **RPC4** are both using clathrin mediated endocytosis they exhibit differences in other forms of cell membrane mediated receptor entry. In addition to the clathrin mediated channel**, RPC4** utilized a modest amount of GTP protein binding endocytosis whereas **RPC3** used an appreciable amount of lipid raft dependent endocytosis. It should also be noted that appreciably more **RPC3,** in ppb, is able to enter the cell as compared to **RPC4** as this could be the case of more active transport being used. This further demonstrates significant differences in the abilities of **RPC3** and **RPC4** in cells.

2.3.4 Mitochondrial Potential Determination

Since the discovery of $[(bpy)_2Ru(dppz)]^{2+}$ and RPC5 and their ability to fluoresce, there has been an interest in using their fluorescent properties to observe RPC complexes in live cells.[45,46] Barton and co-workers showed the dppz ligand bound DNA, by upon reversible binding of dsDNA, the luminescence appears quenched in aqueous media but in the excited state fluoresces when intercalated with dsDNA.[46] Thomas et. al. did similar studies involving the $[(phen)_2Ru(tpphz)]^{2+}$ family of complexes using live imaging to determine mitochondrial dysfuntion within MCF-7 cancer cells.[46] Another advantage is the ability of some RPCs to illuminate when intercalated with dsDNA, making them usable visible targets inside of cancer cells.[45,46,47]

Unfortunately, **RPC3** and **RPC4** do not show significant fluorescence even when intercalated with DNA. The same concept however can be applied from a “reverse engineering” standpoint. To study the action of **RPC3** and **RPC4,** various fluorescent cellular probes were employed to see where and what possible damage actions these complexes were exerting inside of a cell.

The actions of **RPC3** and **RPC4** on the mitochondrial membrane potential within H358 cancer cells were examined. JC-1 is a mitochondria specific dye which is widely used in apoptotic studies to monitor mitochondrial health. The dye exhibits a fluorescent emission shift from green red (~590 nm) to green (~529 nm) as the mitochondrial potential fails. Green JC-1 aggregates are formed when mitochondrial potential has failed whereas red JC-1 aggregates are formed in the presence of functioning mitochondrial proton motive force.[40] H358 cells were inoculated with **RPC3** and **RPC4** for a period of 24 and 48 h. A collection of these images in real time is presented in Figure 2.4 and 2.5.

Image tracks in Figure 2.4 and 2.5 show **RPC3** and **RPC4** and their effects on mitochondrial potential. As can be seen in both image tracks (top row left to right) the first 24 h there is roughly a 50% reduction in mitochondrial potential as both functioning and nonfunctioning signals can be seen somewhat equally. At 48 h in both image tracks (bottom row left to right) all potential has failed in both studies. This is to be expected being the dosing for both these experiments are well over the IC_{50} for the H358 cell line and at 48 h the cells are more than likely entering the final stages of apoptosis. These results could correlate with multiple studies that many RPCs are mitochondrial targeting toxins in cancer cells. [47]

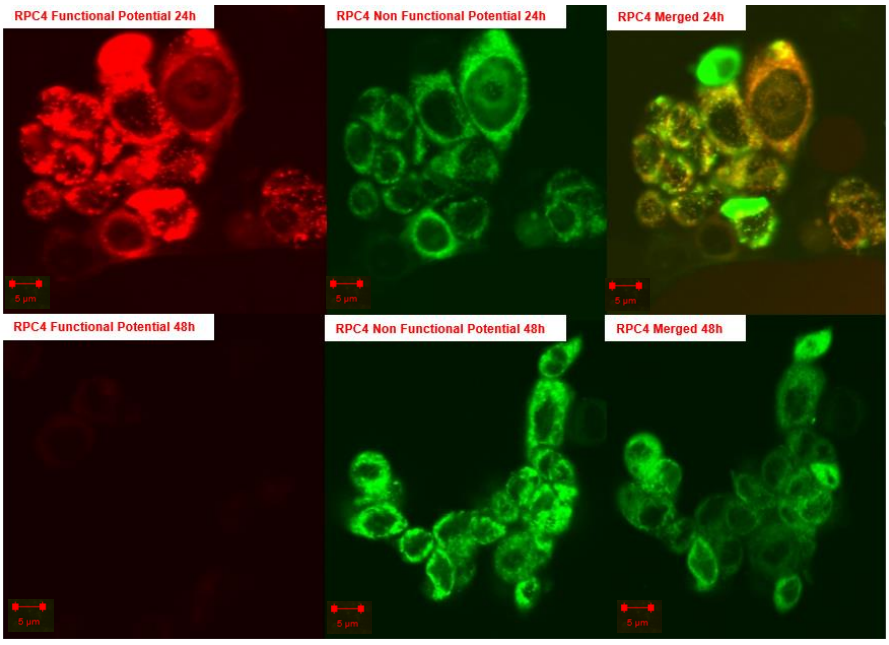

Fig 2.4 Real time JC-1 live imaging stain with **RPC4** indicating functional mitochondrial potential (red), failed mitochondrial potential (green), and the last column merges the two channels (red/green) for 24 and 48 h inoculation.

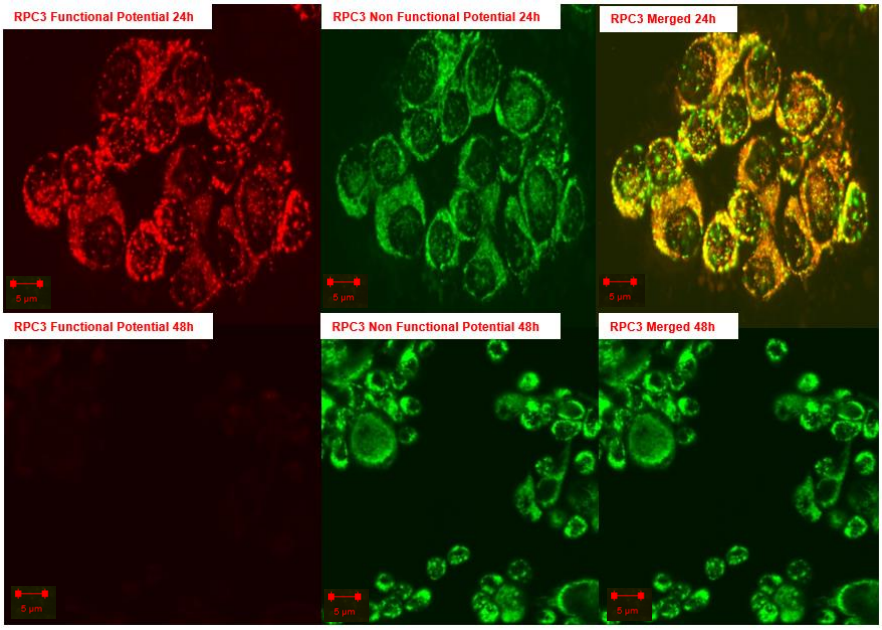

Fig 2.5 Real time JC-1 live imaging stain with **RPC3** indicating functional mitochondrial potential (red), failed mitochondrial potential (green), and the last column merges the two channels (red/green) for 24 and 48 h inoculation.

2.3.5 Mitochondrial Membrane Integrity and ATP determination

Multiple studies involving RPCs show the depolariation activity of these complexes. However, these studies do not reveal how the potential failed which could be due to reasons involving membrane perfusion, mitochondrial complex electron short circuiting or ATP synthase dysfunction. Multiple complex toxins and inhibitors exist as it pertains to mitochondrial dysfunction: Rotenone and Capsaicin in Complex I, Antimycin A and Stigamatelin in Complex III, Cephaloridine in Complex IV and NSAIDS and Oligomycin in Complex V.[48] Many of these mentioned toxins can effect mitochondrial potential dysfunction in one way or another. To better understand what **RPC3** and **RPC4** are doing to the mitochondria the following study was performed to determine hall mark signs of mitochondrial membrane integrity as well as ATP production dificiencies**.**

To elucidate whether or not RPCs are indeed disrupting mitochondrial membrane integrity, H358 cells were dosed with RPCs 1 -5 and a Promega fluorogenic substrate, bis AAF-R110. [38,39] The mechanism of the substrate upon entrance into a broken mitochondrial membrane will fluoresce brightly whereas intact membrane will prevent this effect.

Another way in which mitochondrial potential on the membrane can be disrupted is via the ATP synthase channel or complex V. So while we were determining membrane integrity dysfunction ATP production was also studied by using a cell Titer-Glo luciferase assay. Glucose free media was administered to ensure no route to ATP production through glycolysis was observed. Together these two studies are a multiplex assay and can be seen in Figure 2.6 and 2.7.

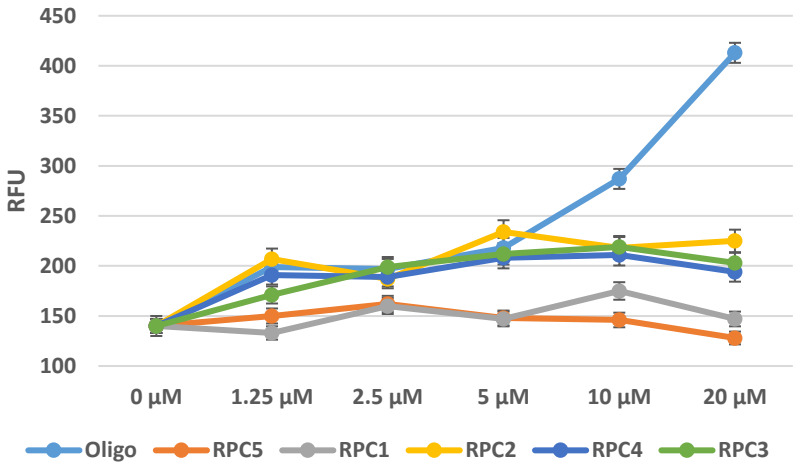

Fig 2.6 Multiplex assay using bis AAF-R110 showing mitochondrial membrane integrity after titrating doses (µM) of RPCs 1-5 for 12 h. Oligomycein was a positive control as a known mitochondrial toxin. Upon mitochondrial membrane loss of integrity the substrate fluoresces and the x-axis indicates fluorescent relative units.

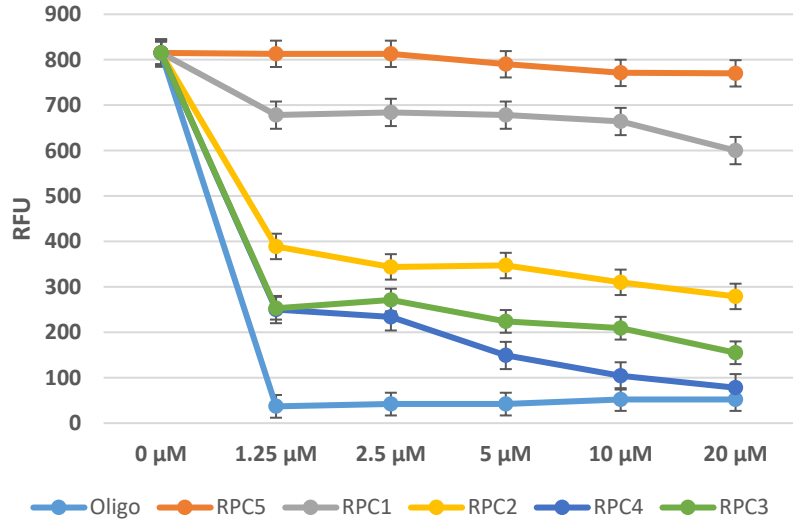

Fig 2.7 Multiplex assay showing] ATP production using luciferase Tox-Glo after titrating doses (µM) of RPCs 1-5 for 12 h. Oligomycein was a positive control as a known mitochondrial toxin. Glucose free media was used for the ATP study.

As seen in Figure 2.6 there was minimal membrane integrity loss upon RPC inoculation with any of the complexes. This suggests mitochondrial membrane potential dysfunction observed by using JC-1 dye. The change and differentiation between the RPC complexes presents itself in Figure 2.7 were ATP production was either being progressed or halted depending on the RPC being inoculated. RPC 1 and 5 did not appreciably hinder ATP production as these two RPCs are not very cytotoxic in cells. The cytotoxic RPCs 2-4 showed a significant decrease in ATP production as compared to the control Oligomycein which is a known inhibitor of ATP synthase Complex V in the mitochondria.[48] Jenkins et. al. also reports, in his Pfizer pharmaceutical work, that cationic metal complexes are almost always Complex V ATP synthase inhibitors by an uncoupling mechanism.[48] RPC 2 which is primarily found in the cytoskeleton and a presumed mitochondrial toxin agent, showed less ATP inhibition as did **RPC3** and **RPC4.** This finding could indicated that **RPC3** and **RPC4** are uniquely different from other RPCs and that an uncoupling mechanism of ATP synthase complex V is occurring. As **RPC3** and Oligomycein levels of ATP inhibition are almost reached equally as the titrating dose increases, **RPC4** does eventually reach the level of Oligomycein also. Important as well, **RPC3** and **RPC4** levels that reduce ATP at Oligomycein levels, are relatively near the IC_{50} values of H358 cells. To our knowledge no ruthenium complex or RPC is reported to perform this ATP activity inhibition.

2.3.6 Measurement of intracellular reactive oxygen species

As discussed in chapter 1 of this work, **RPC3** and **RPC4** are proposed to exert their cytotoxic effect through production of ROS. Cellular oxidative stress is known to trigger apoptotic signaling, cell death and are commonly used signal cascades within a cell.[49,50] However, the addition of ROS production by **RPC3** and **RPC4** could initiate apoptosis and DNA damage. DNA damage will be studied in the next section as in this section we will be examining intracellular ROS in H358 cells. To assess the capacity of **RPC3** and **RPC4** to generate intracellular ROS, H358 cells were inoculated with the relative IC_{50} of **ΔΔRPC4**, **ΔRPC3** and RPC2 shown in Table

1.1. Inoculation was carried out for 2, 8 and 22 h and cells where then stained with 2',7'-dichlorofluorecein diacetate (DCFH-DA).[51] DCFH-DA is an oxidation sensitive dye that fluoresces brightly and is measured in the green when intracellular ROS is generating in a cell. DCFH-DA was commonly and inaccurately thought to be a H_2O_2 marker but has seen been shown to be a reliable ROS detection dye in general.[52] As can be seen in Figure 2.8, image tracks exhibit ROS production within the H358 cells environments with RPCs 2-4. For positive control (second column going down in sequence) 10%, 20% and 30% H_2O_2 solution was given to non-RPC treated cells for 15 min. as a positive marker.

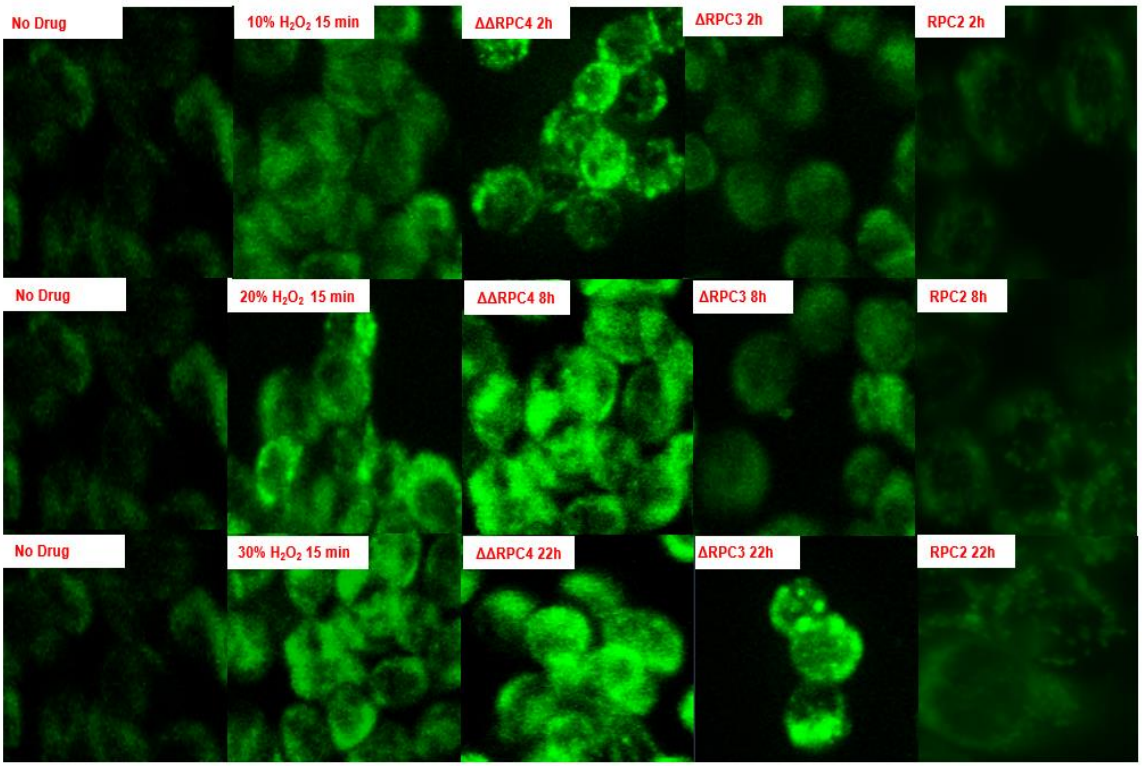

Fig 2.8 Real time DCFH-DA stain with RPC **ΔΔRPC4, ΔRPC3**and 2 in H358 cells. Intracellular ROS increase with RPC **ΔΔRPC4** and **ΔRPC3** are clearly shown with time points (top to bottom per column) of inoculation at 2, 8 and 22 h. No drug image tracks show natural ROS production in living cells.

As can be seen in Figure 2.8 there is a markedly increased production of intracellular ROS inside H358 cells with RPCs. The no drug image (left column) shows normal ROS production signaling within all mammalian cells.[53] It should be noted that the signal is strongly coming from the outer layers of the nucleus of the cell as ROS production signaling is a cytosol dependent process in general.[53] The ability of **ΔΔRPC4** and **ΔRPC3** to increase ROS production is strongly present inside the H358 cell line. **ΔΔRPC4** (middle image track column going down with time) shows strong ROS production throughout the entire cell including the nucleus. This correlates strongly with compartmentalization experiments showing its loci within the nucleus of the same cell line. Interestingly enough **ΔRPC3** (fourth column to the right, top to bottom) shows a delayed response to the increase in ROS activity and is clearly localizing on the periphery of the nuclear compartment. This would be in tandem with the complex loci highly in the cytoskeleton of the cell line as in the previously mentioned section. RPC2 (furthest to the right column top to bottom) shows very small increase in ROS production which was an odd finding as many studies presume RPC2's main influence is mitochondrial damage and the release of damage proteins (BCL-2 and cytochrome c) would increase intracellular ROS. [53] Many studies show ROS increase production with ruthenium complexes as interacting with cascade signals or damaging organelle compartments.[54,55] For example, 2-Phenylimidazo[4,5-f][1,10] phenanthroline derivatives and different rates of intracellular ROS were concluded to present themselves due to upregulation of TrxR.[56] This study with **ΔΔRPC4** and **ΔRPC3** in terms of ROS production, are believed to exist in the nucleus of the cell with electrostatic binding to DNA but this hallmarks the vast traits of RPCs in general. [26] We show evidence that suggests **ΔΔRPC4** produces vast amounts of ROS, by fluorescent signal whereas **ΔRPC3** creates low intracellular production in the nucleus of the cell until the 22 h time point. However, there still is ROS production in the cellular nucleus in minute amounts as compared to RPC 2 which shows minimal ROS production in the cytosol. Every examination of **RPC3, RPC4, ΔΔRPC4** and **ΔRPC3** has yielded contrasting intracellular effects other than their inhibition cell growth properties.

2.3.7 Measurement γH2AX in Double Stranded DNA Break Sites

The DNA cleavage observed in our prevously published work can also be observed in cultured human NSCLC H358, H1792 and H1975 cells. In this case, we used the γH2AX assay to look for DNA double stranded breaks (DSBs) in the nucli of treated cells. When DSB occur, damaged histone H2AX sites at the ser-139 residues in mammalian cells are phosphorylated at these DSB recruitment sites.[57,58] When these discrete nuclear foci formations are formed, as a result of H2AX phosphorylation, they are a sensitive method of DSB detection, with each DSB corresponding to one foci formation which can be seen in the nuceus of cells. [59] Nuclear DSBs present themselves as yellow-green foci upon fixing and staining cells with a monoclonal γH2AX primary antibody as seen in Figure 2.9. For a classic positive control, H358 cells were irradiated (IR) with 1.8 Gy and show numerous DSB foci within 30 minutes [60,61] and is compared to the negative control of untreated H358 cells, which shows no signal. Etoposide was also used as a positive control, as it is known to stabilize transient covalent complexes between topo 2 and DNA, converting them to DSBs.[62,63] As seen in Figure 2.9, cells treated with the IC_{50} of etoposide at 1.0 μM show numerous DSBs at 2 h which progress numerously at longer time periods, 8 and 22 h, respectively.[62,63]

The next two columns in Figure 2.9 show the nuclear effects upon treating H358 cells with **RPC4** (10 μM) and **RPC3** (12 μM) at their IC_{50} dose. As well as H1975 and H1792 cells in Figure 2.10 with **ΔΔRPC4** (2 μM) and (1 μM) and **ΔRPC3** (9 μM) and (11 μM) respectively. Cells treated with **RPC4** and **ΔΔRPC4** are quite similar to etopside, with numerous DSBs evident after the 2 h time period and large increases seen in the foci count with 8 and 22 h time point. **RPC3** and **ΔRPC3** exhibits a lack of DSB events at the 2 and 8 h time points, suggesting that the ability of **RPC3** and **ΔRPC3** to directly induce DSBs is an indirect method as compared to **RPC4 and ΔΔRPC4.**

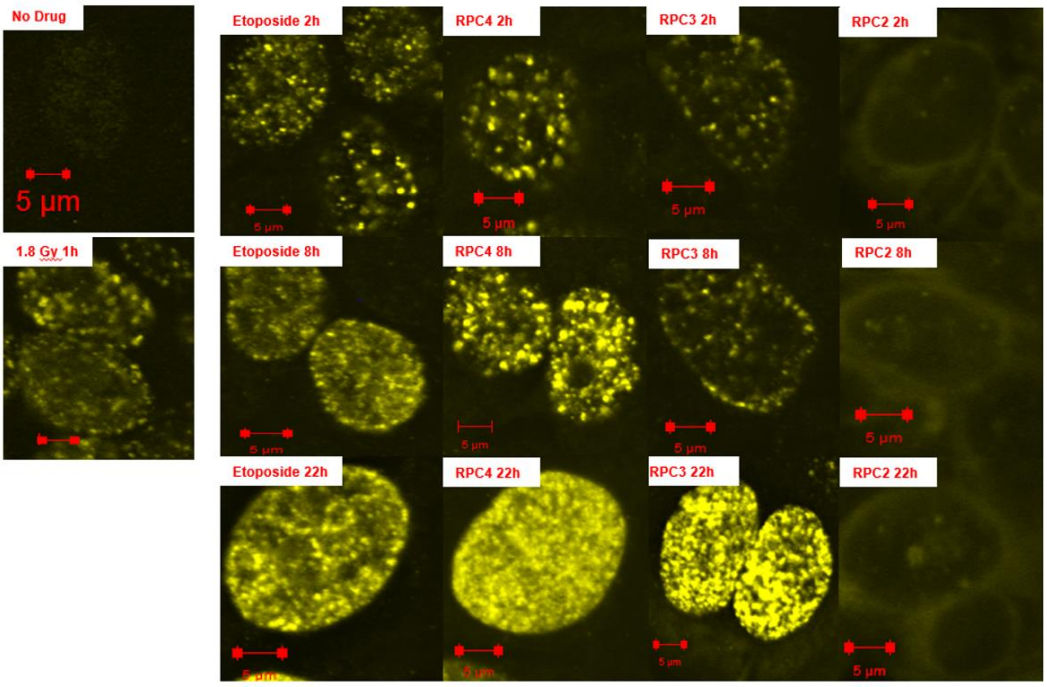

Fig 2.9 γH2AX phosphorylated foci sites in H358 cells dosed with 1.0 µM Etoposide, 10 µM RPC **4**, 12 µM **RPC3** and 1 µM RPC 2 at 2, 8 and 22 h.

The appearance of numerous DSBs after 22 h as in Figures 2.9 and 2.10 are considered indirect repsonses whereas strong DSB responses in the first 2 h of treatment can be considered the direct method of apoptosis.[64]

To quantify the foci count, Image J software package was used which gives a count of the foci per 25 cells.[65] As shown in Figure 2.11 with H358 cells, the results seen in Figures 2.9 and 2.10 are supported by the quantitation with foci formations. Etoposide and **RPC4** show a similar response after 2 h, whereas **RPC3** is only slightly above the negative control. At the 8 h time point, **RPC4** has now exceeded etoposide in foci formation and an almost 5 fold more foci count than cells treated with **RPC3**. Only after 22 h, do the foci count become near equal and the extensive number of foci (over 250 each) which is indicative of an apoptotic event. **RPC4** and

ΔΔRPC4 clearly shows mechanistic similarities to clinically used chemotherapy DNA cleavage agent etoposide and can be argued as competative as well, measured by this assay.

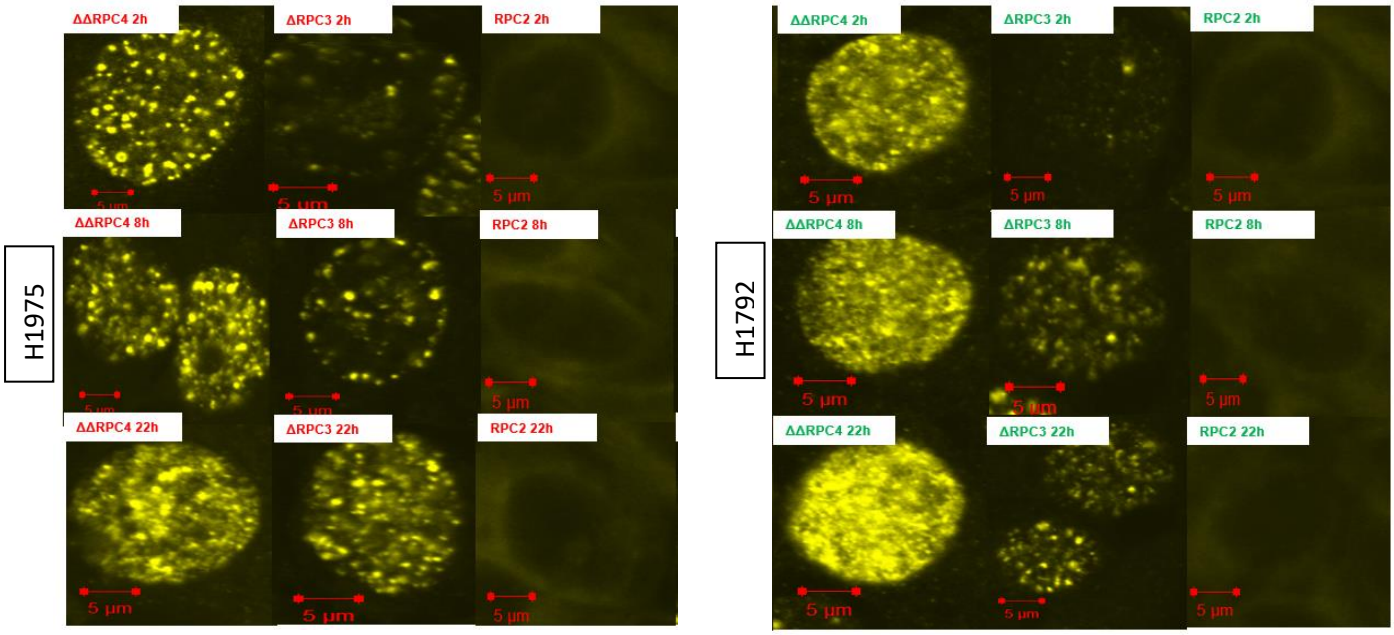

Fig 2.10 γH2AX phosphorylated foci sites in H1975 and H1792 cells dosed with **ΔΔRPC4** 2 µM and 1 µM and **ΔRPC3** 9 µM and 11 µM respectively at 2, 8 and 22 h.

The DSB data for **RPC3** and **ΔRPC3** indicates a different and indirect pathway, despite near identical behavior as previously mentioned in chapter 1. This result is particularly intriguing as both **RPC3, ΔRPC3, RPC4** and **ΔΔRPC4** are essentially equitoxic as measured by IC_{50} values to H358 cells, and show similar tumor gowth inhibition in mouse tumor models.[25]

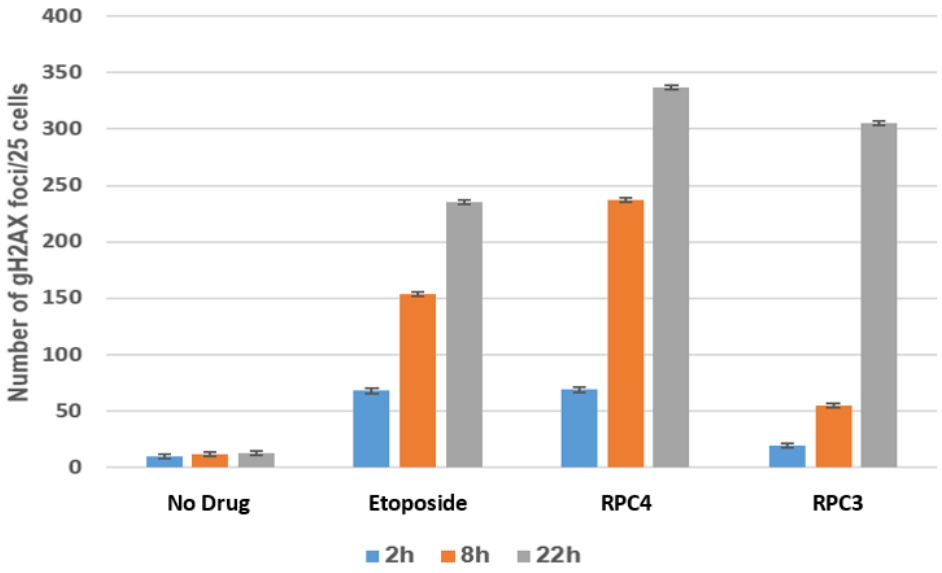

Fig 2.11 Quantitative analysis of γ-H2AX foci in H358 cell line for Etoposide, **RPC4** and **3** using image J software. An average of 25 cells per count were used in tandem with double phase light contrast particle count.

2.4 Conclusions

In summary, this study has shown that **RPC3** or **ΔRPC3** and **RPC4** or **ΔΔRPC4** are two separate and unique cancer anti-proliferating agents against several cancer lines and types studied. A contrast in cellular localization in NSCLC H358 and HCC-2998 was observed showing **RPC4** localizing in a significant amounts in the nucleus of cells were **RPC3** was highly localized in the cytoskeleton. In this study we also show evidence that suggests variant forms of active endocytosis transport channels are in play. Entrance into H358 and pancreatic cancer cells Hs766T are shown to be kinetically driven where **RPC4** seems to using modest amounts of clatherin and G protein coupled transport as **RPC3** using appreciable clatherin, lipid raft transport and overall more appreciable active transport. Mitochondrial potential dysfunction was shown

that with complexes **RPC3** and **RPC4** potential across the membrane was disrupted. Also, H358 cell membrane integrity was shown not to be a factor in dysfunction with these RPCs instead the evidence suggests that the ATP synthase complex V channel was targeted and uncoupled. **RPC3** and **RPC4** in multiple gel assay show ROS production that cleaves plasmid DNA and where in this chapter we show that intracellular ROS was created in the cellular environment. **RPC3** produced intracellular ROS at a slower rate than **RPC4** which showed ROS production as short as 2 h. This data also matched in tandem with the DSB data that was observed with **RPC4** indicating DNA DSB damage in the short 2 h time mark. Also, **RPC3** showed the same indirect production of DNA DSBs at the similar rate as ROS production. The same response was also seen with the enantiopure samples of the RPCs as well. This would suggest that the ROS production is indeed a major player in the DSB activity that is shown in H358, H1792 and H1975 cell lines. Furthermore it can be concluded that though **RPC3** and **RPC4** act similar in most respects with in vitro gel assays once inside the cell environment are very different and unique complexes.

Chapter 3

Examination of **ΔRPC3** and **ΔΔRPC4** in 3D Multiple Cell Tumor Spheroids

3.1 Introduction

The current mode of research on the efficacy of cancer drugs are performed with 2D cell culture models. 2D cell cultures studies are beginning to be questioned as a true indicator of in vivo effectiveness of cancer treatment developments.[66] Most studies that have promising chemotherapeutic drug designs in 2D have a paltry performance when moved in vivo to roughly an 8% success rate.[67] Attributing factors include absence of cell-cell or cell-extracellular matrix interactions in 2D cell models, gap junctions interference or lack thereof, protein shape disfigurement as the connections the cell makes to polystyrene plates are not natural and the basal/apical polarity of the cell in 2D where nothing lays on top of the cells.[68] Therefore, the development of cell culture models that can elucidate a more accurate representation of drug interaction and effect in a cell vs the 2D cell experiments is critical to our understanding of future in vivo studies. Also, the financial cost of in vivo experiments can be costly as many drug discovery designs from 2D to in vivo studies do not correlate with one another.[69,70] Multicellular tumor spheroids (MCTSs) are heterogeneous cellular aggregates that have many of the properties of solid tumors including nutrient, O_2 and CO_2 gradients, hypoxic/necrotic cores, cell-cell matrix signaling, and proper gene expression. [71] Therefore, we produced MCTs of varying NSCLC lines to detect the formation potentials of these lines and if they respond the same or at all to drug stimulus as their 2D counterparts.

3.2 Experimental

3.2.1 Chemicals

All solvents were reagent and cell culture grade. All reagents and work environments were maintained sterile. RPCs **ΔΔRPC4** and **ΔRPC3** where provided by the MacDonnell laboratory and were used as received. NSCLC H358, H1792, H1975, H2073, H2126, H322, H1993, H460, HCC1792 and HCC4017 were acquired from University of Texas Southwestern (UTSW) Hammond Cancer Center (HCC). RPMI-1640 medium, penicillin/streptomycin, fetal bovine serum (FBS), etoposide, cisplatin and docetaxel were purchased from Sigma Aldrich. Phosphate buffered saline 10X was purchase from Biorad. Cell Titer-Glo was purchased from Promega. Nuncone low adherent 96 well titer plated were purchased from Thermofisher.

3.2.2 Instrumentation

Cell incubation was maintained by a Nuair CO_2 Incubator. Luminescence data was obtained using a BMG Labtech FLUOstar Omega plate reader. Phase contrast microscopy was performed using a Zeiss inverted microscope.

3.2.3 Cell Culture Lines/Maintenance

H358, H1792, H1975, H2073, H2126, H322, H1993, H460, HCC1792 and HCC4017 cells were grown in RPMI-1640 medium supplemented with 10% FBS, 2 mM L-glutamine and 1 mM sodium pyruvate. Cells were grown and passaged in T-25 and T-75 Corning culture flasks at 37^{o}C under 5% CO_2 and humidified atmosphere.

3.2.4 Formation and Analysis of Multi Cell Tumor Spheroids (MCTs)

MCTs were cultured using a low adherent hemisphere plate well method. H358, H1792, H1975, H2073, H2126, H322, H1993, H460, HCC1792 and HCC4017 cells were passaged once confluent and approximately 1500 cells/mL suspension was transfered to low adherent plates containing complete RPMI-1640 medium. The single cells formed MCTs aggregates within 24 h and noticable 100 - 200 μM spheroids in 48 h in 37°C under 5% CO_2 and humidified atmosphere. Formations were imaged using a Zeiss Axio phase contrast microscope using 10X and 20X objectives to monitor color of tumor and drug, size, morphology and diameter.

3.2.5 Cytotoxicity and Cell Viability

The cytotoxicity of RPCs, etoposide, cisplatin and docetaxel were determined by a Promega Cell Titer-Glo ATP detection reagent. Cells were dosed with various drug for 96 h and afterwards plates are removed from incubator and allowed to come to rt for 30 min. Cell Titer-Glo is then administered in equal amounts to media per well for 45 min. at rt. Plates are read for luminescence using a BMG Labtech FLUOstar Omega plate reader and ATP values were monitored in terms of cell viability.

3.3 Results and Discussion

3.3.1 MCTS Formation

In an effort to first produce MCTS we cultured a variety of NSCLC cells to view their formation potentials into spheroids. As seen in Figure 3.1 a variety of cell lines were cultured and MCTS where attempted. Cell lines HCC1172 and HCC4017 formed aggregate sphere morphologies and was not considered a MCTS. Cell lines H322, H358, H460, H1993, H2126, H1792, H1975 and H2073 all formed successful MCTS as shown in Figure 3.1. The successful formation of MCTS allowed us now to study inhibition effects of multiple chemotherapeutic drugs against a 3D model vs only a 2D cell model.

3.3.2 MCTS Viability against RPCs

Due to the MCTS difference in nutrient gradients, O_2 concentrations, hypoxic centers and cell adhesion differences it is prudent to examine cell viability with RPCs **ΔΔRPC4** and **ΔRPC3** and look for shift changes in IC_{50} curves. Many 3D cell dosing examinations show differences from 2D to 3D; either 2D matching with 3D, as with cisplatin and H4006 [72] or shifting far to the right, as with cisplatin and A549 serving as two examples.[73] We examined MCTS H358, H1792 and H1975 for IC_{50} curves with **ΔΔRPC4** and **ΔRPC3** and contrasted them with their 2D counterparts.

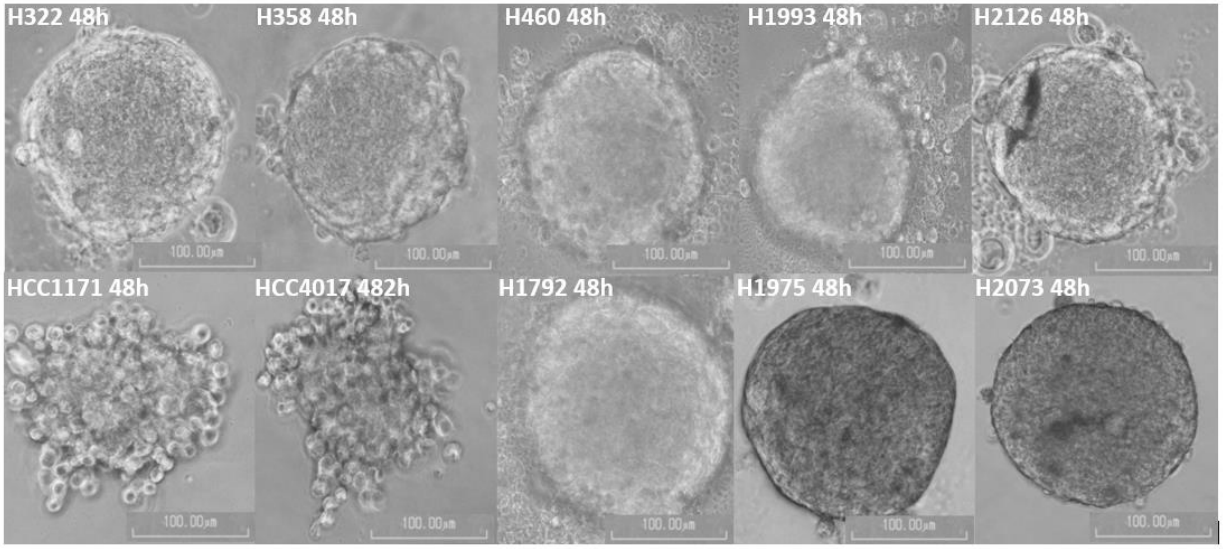

Fig 3.1 Multiple NSCLC formed into MCTS and imaged after 48 h incubation. H322, H358, H460, H1993, H2126, H1792, H1975 and H2073 formed tumor sphere morphologies. HCC1171 and HCC4017 formed aggregate sphere morphologies. Scale bar is at 100 µM.

Drugs	H358	H1792	H1975
ΔΔRPC4 (3D)	22 ± 5.2	20 ± 4.7	28 ± 4.8
ΔRPC3 (3D)	27± 4.9	29 ± 5.1	21 ± 5.1
ΔΔRPC4 (2D)	12 ± 4.2	7.0 ± 3.9	1.7 ± 4.2
ΔRPC3 (2D)	11 ± 3.8	9.0 ± 4.1	3.0 ± 5.1

Table 1.2 exhibits IC_{50} values for **ΔΔRPC4** and **ΔRPC3** in 3D and 3D cell cultures. These values are in µM.

In Figure (A/B/C) 3.2, we plot cell lines H358, H1792 and H1975 IC_{50} curves and observe them shifted to the right. These values can also be seen in Table 1.2. In Figure (A) 3.2 we show 2D H358 cells IC_{50} of **ΔΔRPC4** (12 µM) and **ΔRPC3** (11 µM) shift to the right in MCTS exhibiting **ΔΔRPC4** (22µM) and **ΔRPC3** (27 µM) respectively. Similar results were found for H1792 in Figure (B) 3.2 showing **ΔΔRPC4** (20 µM) and **ΔRPC3** (29 µM) and H1975 Figure (C) 3.2 **ΔΔRPC4** (28 µM) and **ΔRPC3** (21 µM). The exhibited 3D MCTS drug inhibition curves to the right could signify properly functioning signaling between cells that are

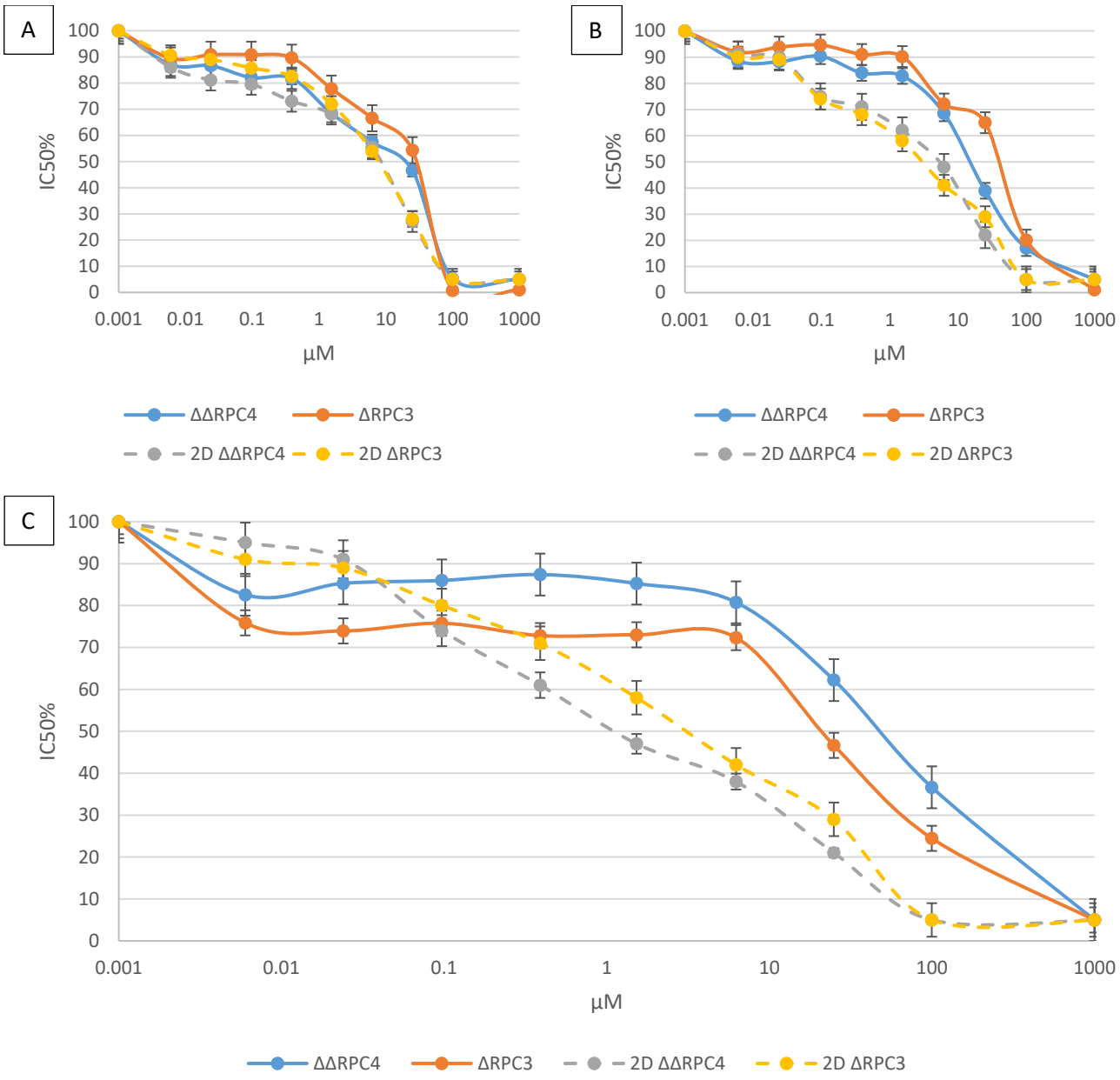

Fig 3.2 MCTS **ΔΔRPC4** and **ΔRPC3** dosing in 2D (dotted curves) and 3D (solid curves) for (A) H358 MCTS, (B) H1792 MCTS and (C) H1975 MCTS.

not present in the 2D ridged cell shape form or a complex penetration issue through the tumor walls. However, **ΔΔRPC4** and **ΔRPC3** are reaching inhibitory cytotoxic levels still making them

attractive for possible therapy routes. Future studies will be performed to elucidate the mechanism of action occurring in MCTS tumor formations and **ΔΔRPC4** and **ΔRPC3.**

3.3.3 MCTS Morphology with RPCs and Chemotherapy Drugs

In an effort to examine dosing effects in MCTS we imaged all spheroids during dosing regimens to examine if any morphological change events are occurring to the MCTS. This approach provides us with a view of effect as to drug influence on morphology that is very limited in 2D cell culture formations. In Figure 3.3 we show a 4-fold titrating dosing scheme on MCTS H358 with RPCs **ΔΔRPC4** and **ΔRPC3** for the first 48 h of dosing regimen.

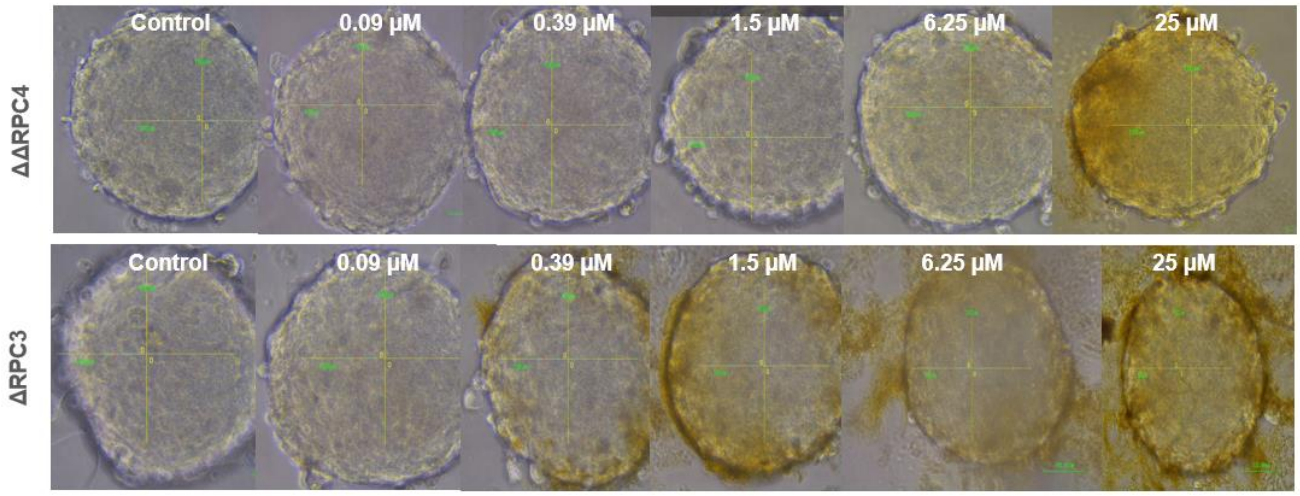

Fig 3.3 MCTS H358 was dosed with **ΔΔRPC4** and **ΔRPC3** with a 4-fold titrating dosing scheme for 48 h. **ΔΔRPC4** (top image track) treated MCTS keep their spheroid formation whereas **ΔRPC3** (bottom image track) at lower doses is causing significant morphological changes. Drug color indicates **ΔRPC3** is kinetically entering the spheroid at a higher rate than **ΔΔRPC4**. Scale cross hair bar is at 100 μM^2.

The MCTS exhibit two distinct differences after being dosed with **ΔΔRPC4** and **ΔRPC3;** the amount of drug entering the spheroids and morphology of the tumorsphere. In Figure. 3.3 (bottom image track) 0.39 μM of **ΔRPC3** enters the periphery of the MTCS membranes at a faster kinetic rate than **ΔΔRPC4** (top image track). In Chapter 2 we discussed **ΔRPC3** enters the cell at 132 ppb vs **ΔΔRPC4** at 85 ppb in 2D cell assays. This contrast in permiability through the cell membrane and high use of active transport for **ΔRPC3** would seem to carry over into 3D MCTS. Also, Figure 3.3 indicates **ΔRPC3** fully occupies the MCTS at 6.25 μM where as **ΔΔRPC4** exhibits a much lighter color throughtout the sphere at the same concentration. Morphological changes are also noticed as well involving cell disembly as a MCTS. **ΔΔRPC4** dosed MCTS Figure 3.3 (top image track) shows the sphere containing its spheroid shape through the top dose of 25 μM whereas **ΔRPC3** dosed MCTS (bottom image track) starts disembling at the 6.25 μM dose and the effect gets stronger at 25 μM. We also tested two additional MCTS that exhibit strong IC_{50} effects in 2D with **ΔΔRPC4** and **ΔRPC3**; H1792 (**ΔΔRPC4** (7.0 μM) and **ΔRPC3** (9.0 μM)) and H1975 (**ΔΔRPC4** (1.7 μM) and **ΔRPC3** (3.0 μM)) which at these doses exhibited the same morphicological phenomena shown in Figure 3.3 after 48 h. **ΔΔRPC4** dosed in H1792 and H1975, Figure 3.4 (top image track), exhibites similar effects with H358 MCTS in Figure 3.3 in terms of drug color throughout the spheroid and cell adhesion is remaining in spherical shape. **ΔRPC3** dosed in both cell lines as well in Figure 3.3 (bottom image track) however, exhibits the same cell disembly as H358 in Figure 3.3 MCTS. A stark contrast between **ΔΔRPC4** and **ΔRPC3** is revealed in 3 separate MCTS to behaving different from one another not only in 3D cell assays but 2D cell cultures as well. Possible reasons for the cell disembly effect seen with **ΔRPC3** could range from possible mitotic catastrophy [74], VEGF and EGFR inhibition [75,76], and gap junction disposition.[77,78] Future studies will be conducted to determin the mechanism of effect shown in this study.

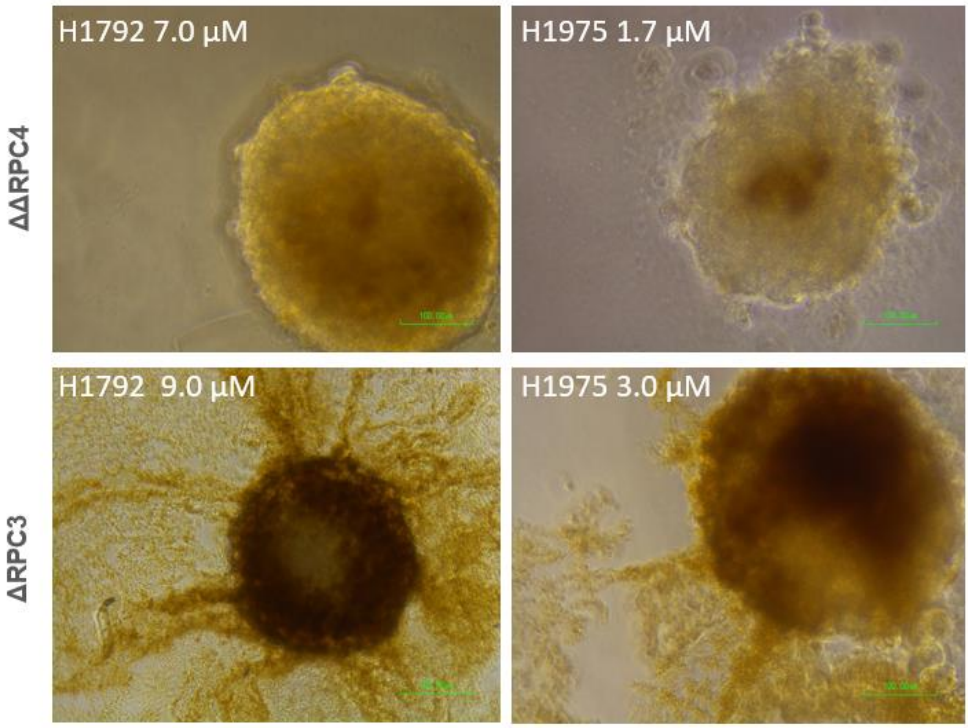

Fig 3.4 MCTS H1792 and H1975 are dosed with **ΔΔRPC4** (top image track) and **ΔRPC3** (bottom image track) at their IC_{50} concentrations for 48 h. Scale bar is 100 µM.

3.4 Conclusions

In summary we have exhibited that 2D and 3D cell culture differed from one another in terms of **RPC3** and **RPC4's** effect on them. The evidence suggests that an MCTS is vastly different in its ability to resist drug effect that is apparent in the 2D models. Also, the stark contrast of **ΔΔRPC4** and **ΔRPC3** in there imposed morphology on MCTS was remarkable. We exhibited that **ΔΔRPC4** colored the spheroids at higher concentrations indicating a a slower kinetic diffusion constant than **ΔRPC3** which could be visibly seen at lower concentrations. This is in agreement with the 2D model cell compartmentalization and active trasnport studies in chpater 2 that show faster kinetic and concentration uptake of **ΔRPC3.** The contrast of MCTS morphology

was also striking in the loss of cell cohesion with **ΔRPC3 vs. ΔΔRPC4** leaving the MCTS in a tumor shape and model. Lastly, we show that IC_{50} curves shifted to the right indiciating the psuedo-in vivo environment that the 3D MCTS are immitating in terms of more functional cell activity for repair and survival mechanisms than in 2D models, however the IC_{50} with each MCTS adn **ΔΔRPC4** and **ΔRPC3** was accomplished making these still attractive drug studies.

Chapter 4

Examination of RPC Doublet Drug Combination Efficacy with Standard Care Chemotherapy

4.1 Introduction

Drug combination studies and the aim of obtaining a more robust effect against a certain disease, is a well established approach.[79] We have seen this approach used in doublet antibiotic regimens for complex infections and anti-retroviral agents.[80] Oncology research has studied drug combination trials for hematologic malignancies and solid tumors for decades.[81,82] In the clinic, the priniciple benefit is higher antitumoral effect while reducing patient side effect.[83] The concept of synergy is a quagmire and contentous debate among many disciplins and in biochemistry and cell biology R&D. Synergy, additivity and antagonism are used carelessly by many examiners to explain a simple effect increase which is additive in nature but is claimed to be synergistic.[84,85] In practical terms, when two drugs are combined and the activity from that result is similar to the cumulitive action of each individual drug, the combination is considered additive.[86] Synergy occurs when the action of a drug combination is greater than the sum of the activity of each individual agent when mono-dosed.[87] There are may algorithems and mathmatical fields to calculate synergy that extend back to the 1970s.[88,89] Methods that are effect base driven compared to individual effects of drugs are: the combination threshold, highest single agent (HSA), Chou Talay method, Loewe response additivity and Bliss independent model.[90-92] As the purpose of this chapter is not to discuss synergy methods but possible drug doublet studies, the algorithm for determining synergy for **RPC3** and **4** will be the Loewe additivity. We chose the Loewe additivity method because it is an industry standard for determining synergist combinations.[93] Loewe additivity incorporates the dose equivalence priniciple and the sham combination principle. Briefly, the dose equivialnce principle states that for a given effect, dose of drug A is equivalent to dose b_a of drug B and the recipricol of both where as the sham

combination principle states that b_a can be added to any other dose b of drug B to make an additive drug combination.[93,94]

In this chapter we examine standard care chemotherapy and doublet dosing with **RPC4** and **RPC3.** We will show that certain combinations are indeed synergistic, additive and antagonistic with respect to the type of drug and cell type studied. Three cell lines were screened against multipe standard care chemotherapies and **RPC4** and **RPC3** including: cisplatin (nuclear DNA adduct forming cytotoxin)[103], etoposide (topoisomerase II inhibitor)[104], docetaxel (taxen tubuline stabilizer)[105] and gemcitabine (anti-metabolite DNA damage agent)[106] shown in Figure 4.1. We examined those screens for IC_{50} growth curves and put them through the Loewe additivity algorithm to identify synergistic hits and combinations.

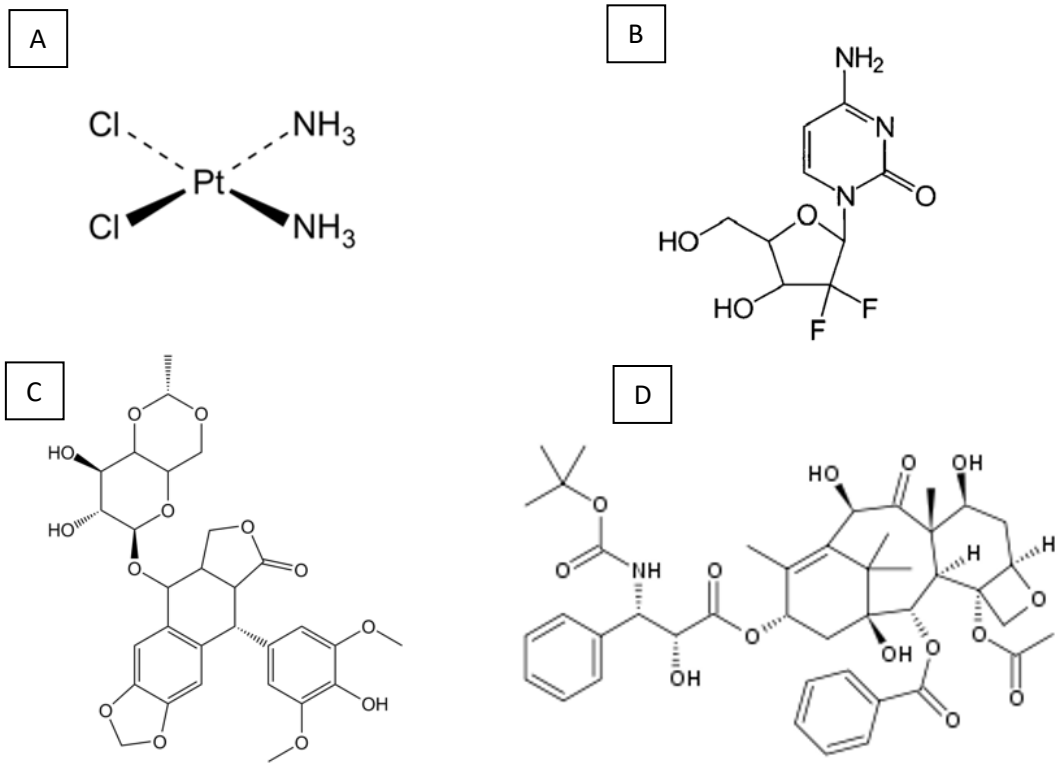

Fig 4.1 Standard care chemotheraputic drugs: (A) cisplatin, (B) gemcitabine, (C) etoposide and (D) docetaxel.

4.2 Experimental

4.2.1 Chemicals

All solvents were reagent and cell culture grade. All reagents and work environments were maintained sterile. **RPC3** and **RPC4** where provided by the MacDonnell laboratory and were used as received. NSCLC H358, HOP-62 and HCCCL HCC2998 cells were purchased from The National Cancer Institute (NCI) at Frederick Central Repository. RPMI-1640 medium, penicillin/streptomycin, fetal bovine serum (FBS), 100X BME vitamin solution, dimethyl sulfoxide (DMSO), 0.04% trypan blue, bovine serum albumin (BSA), para-formaldehyde (PFA), methanol, sodium azide (NaN_3), propidium iodide (PI), crystal violet, ethanol, 3-(4,5-dimethylthiazol-2-yl)-2,5-diphenyltetrazolium bromide (MTT), gemcitabine, docetaxel, cisplatin and etoposide were purchased from Sigma Aldrich. Phosphate buffered saline 10X was purchase from Biorad.

4.2.2 Instrumentation

Cell incubation was maintained by a Thermofisher HeriCell CO_2 Incubator. Absorbance data was obtained using a BMG Labtech FLUOstar Omega plate reader. Liquid colony assay count was performed using a Zeiss Axio-Plane 540 inverted light microscope.

4.2.3 Cell Culture Lines/Maintenance

H358, HOP-62 and HCC-2998 cells were grown in RPMI-1640 medium supplemented with 10% FBS, 2 mM L-glutamine, 1 mM sodium pyruvate, 1.1% penicillin/streptomycin and 1X BME vitamin complex solution. Cells were grown and passaged in T-25 and T-75 Corning culture flasks at 37^oC under 5% CO_2 and humidified atmosphere.

4.2.4 Single Dose Cell Viability Assay

The cytotoxicity of the RPCs, cisplatin, etoposide, docetaxel and gemcitabine and all their corresponding drug doublets were determined by an MTT assay. Cells were seeded into 96-well

plates at 1 × 10^4 cells per well and grown for 24 h at 37 °C in a 5% CO2 incubator; then titrating doses of drug were used ranging from 0.001 - 100 µM. Cells were then incubated with drug for 72 h under the same conditions. The stock MTT dye solution (5 mg/mL) was added to each well for 3.5 h of incubation. The dye was removed and 120 µL of DMSO was added to each well. Plates were read for absorbance at 570 nM using a plate reader.

4.2.5 Doublet Dose Cell Viability Assay

Drug combinations were designed with Drug A in all dosing regimens to be the titrating drug dose whereas drug B was always at a steady concentration at the IC_{10} of each cell line respectively being tested. Titrating doses of drug A were used ranging from 0.001 - 100 µM. Cells were then incubated with drug for 72 h under the same conditions. The stock MTT dye solution (5 mg/mL) was added to each well for 3.5 h of incubation. The dye was removed and 120 µL of DMSO was added to each well. Plates were read for absorbance at 570 nM using a plate reader.

4.2.6 Data Analysis

We assumed that exponential growth therefor the number of cells at any given time *t* and 0 were defined by the expression N(*t*)=N(*t*=0 h) * (mu*t), where mu is the growth constant that depends on each individual cell line respectively. Drug effect was measured by MTT assay and Drug A and B doublet IC_{50} was compared to growth curves of IC_{50} for drug A alone and drug B alone at its IC_{10} as a steady constant throughout each drug screen study. We employed two synergy models the Loewe Additivity Test and the Bliss Model. The Loewe model, which is an industry standard, predicts that the additive effects of drugs A and B depend on the individual does effect curves and are to be expressed as Effect → $(E)(a+b) = E_a(a + b_b) = E_B(b_a + b) = E_{AB}$ where E_A is measured as a drug effect curve of drug A, $(a+a_b)$ giving the overall effect E_{AB} and the reciprocal for drug B. The Loewe method makes the assumption drugs have a constant

potency ratio between themselves.[94,95] An isobologram that has a drug combination curve which falls below 1 is consider additive - synergistic with far below 1 accepted as synergy. Above 1 is considered to be antagonistic. All combination data is shown in the form of combination index in bar graph form.

4.3 Results and Discussion

4.3.1 Single Dose Treatment Screen

IC_{50} Values for drugs **RPC3, RPC4,** cisplatin, etoposide and gemcitabine alone were determined using cells lines H358, HOP-62 and HCC-2998. These values can be seen in table 1.3 and are expressed in μM.

Drugs	H358	HOP-62	HCC-2998
RPC4	9.5 ± 5.2	50.0 ± 4.9	13.0 ± 5.1
RPC3	8.8 ± 5.0	55.0 ± 4.2	20.0 ± 5.0
Cisplatin	17.0 ± 4.9	3.5 ± 3.4	16.0 ± 3.6
Etoposide	1.0 ± 2.1	5.0 ± 4.3	0.10 ± 4.2
Gemcitabine	0.1 ± 1.4	0.001 ± 1.3	0.10 ± 1.1
Docetaxel	0.003 ± 1.2	0.003 ± 1.1	0.006 ± 1.3

Table 1.3 IC_{50} values of cell lines H358, HOP-62 and HCC-2998 with **RPC3, 4,** cisplatin, etoposide, gemcitabine and docetaxel using MTT assay for 96 h. These values are in μM.

When examining these complexes IC_{50} growth curves, all drug studies shown in table 1.2 fully reached cell death at high drug concentrations. Because there were full growth and death curve slopes there was no need for an effective dose (ED_{50}) or adjusted IC_{50}. As such we are able to perform the Loewe method, discussed in the following section, as all the data will fit into the same

IC_{50} curve category. A sample growth curve of all complexes can be seen in Figure 4.2 for cell line H358 to elucidate this point. Our values for H358 cell line against chemo drugs shown in the plot agree with current literature.[101]

4.3.2 The Doublet Combo Drug Screen

Our effort to identify combinations for IC_{50}s of cancer cells H358, HOP-62 and HCC-2998 was performed in an unbiased manner were we screened drug doublets with a 2-fold dilution factor of drug A. Drug A in all cases was the titrating drug whereas drug B is always the steady concentration of drug at the IC_{10} of cell lines tested. Drug B was chosen to be IC_{10} as the B drug could not be at a concentration where enough was present to achieve cytotoxicity in great amounts on its own.

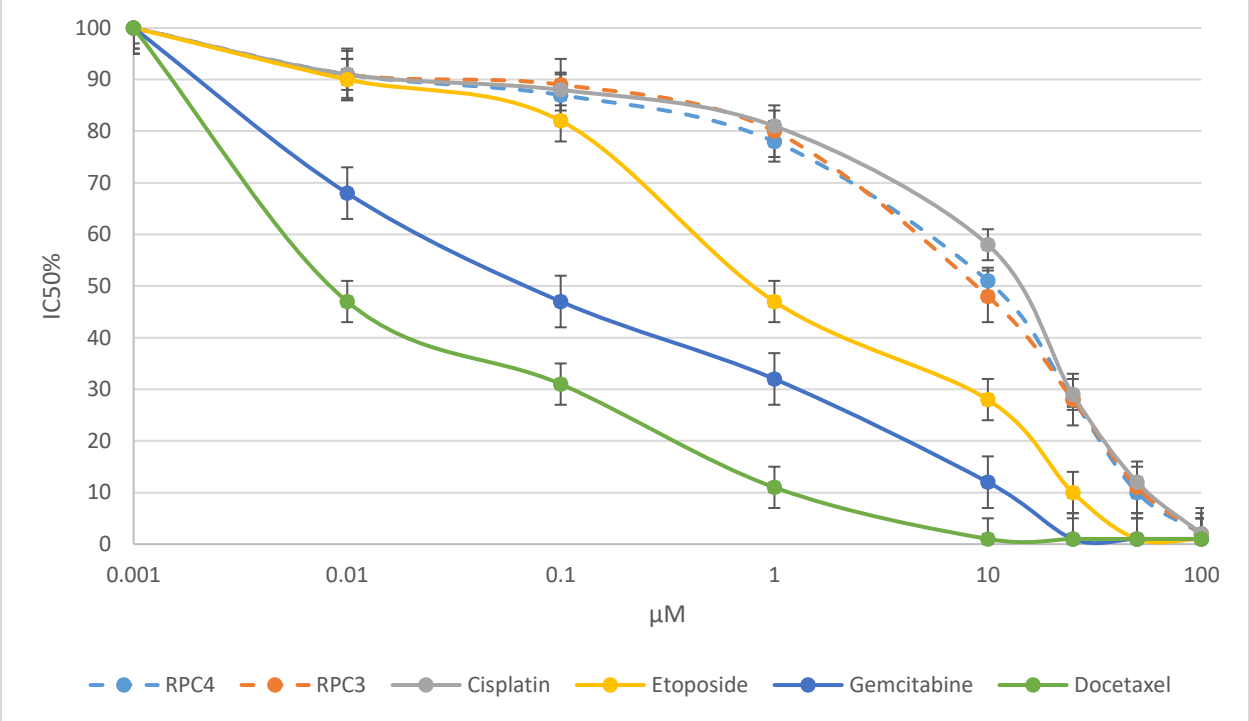

Fig 4.2 IC_{50} drug curves for cell line H358 with **RPC3** and **RPC4 (**dotted line)**,** cisplatin, etoposide, gemcitabine and docetaxel using MTT assay for 96 h.

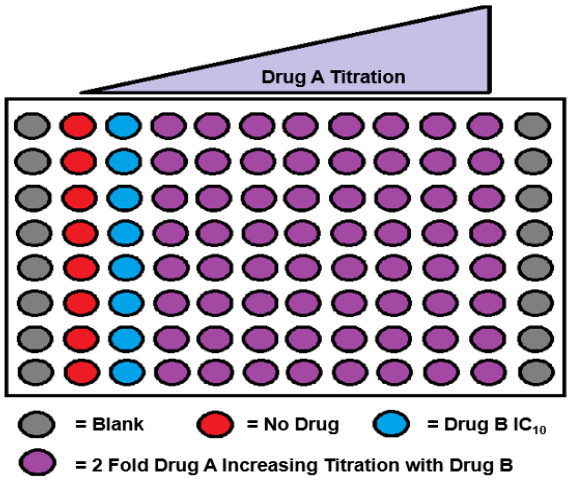

Fig 4.3 Drug doublet experimental setup indicating: grey = no cells and drug, red = cell and no drug, blue cell and drug B at IC_{10} concentration and purple = increasing 2 fold drug A concentrations.

The data analysis using the sham method can correct for any drug amount in theory but for practical reasons it is usually a consitutent to leave drug B at a single dose and reletively below theraputic values.[96] In Figure 4.3 we show a representation of doublet assay setup in terms of dosing gradient in 96 well titer plates.

After running a full panel of doublet runs with each drug combination and multiple cell lines we identified IC_{50} values that were below and above the single dose response curves. For ease of comparison the drug combinations have been separated by drug A independently per graph with drug B and cell lines along the x-axis in each case.

We first examine **RPC3** and **RPC4** as shown in Figure (A/B) 4.4 in bar graph format. An anecdotel summation of the data can suggest which combination of RPC and standard care drug seem to be synergistic or at a minimum additive. Approximately 50% of **RPC4** doublet treatments showed markedly lower responses in terms of IC_{50}s as with **RPC3**, as many as 70% of doublets responded in a more efficacious inhibition cell growth response. The combination of **RPC4** and **RPC3** with cisplatin seemed to be a cytotoxic drug combo across all 3 cell lines with H358 and

HCC-2998 indicating a broad spectrum drug combination. Due to the DNA base (especially guanine) adduct forming capability of cisplatin, it is resonable to suggest that under DNA repair duress in the presence of cisplatin, production of ROS by **RPC3** and **4** could in effect exert more DNA damage. As cisplatin damage is taking effect, heterochromatin would be unwinding making DNA more exposed to ROS damage.[101,103] We show **RPC4** against all 3 cell lines has IC_{50}s greater than 10 μM but when combined with cisplaltin H358 and HCC-2998 are below 1 μM and also astonishingly HOP-62 which alone with **RPC4** inhibites cell growth at 50 μM is reduced to a remarkable 3 μM. Also, **RPC3** against all three cell lines in combination with cisplatin is lowered to <1 μM as well. This in itself is an exciting prospect as many cisplatin resistent cancer emerge in the clinic at an alarming rate.[96] The potential for combination therapy with cisplatin leads to a plausible theraputic window. As with another nuclear cytotoxic agent etoposide, 2 lines responded with **RPC4** and etoposide albeit for HCC-2998 however, **RPC3** was a broad spectrum succcess with etoposide against all lines. Etoposide, being a topoisomerase II inhibitor, yielding a mechanism to to prevent successful re-winding of the DNA helix and again would leave access to ROS damage in the nucleus of cells.[104] We now have evidence that shows in a preliminary screen, two very successful, in clinic nuclear target anti-cancer agents combined with RPCs, are showing an appreciable effect.

When we look at an extracellular matrix toxin in terms of tubulin destabilization, the drug docetaxel was also combined with RPCs **3** and **4.** Interstingly enough there was a split in effect with both RPCs.

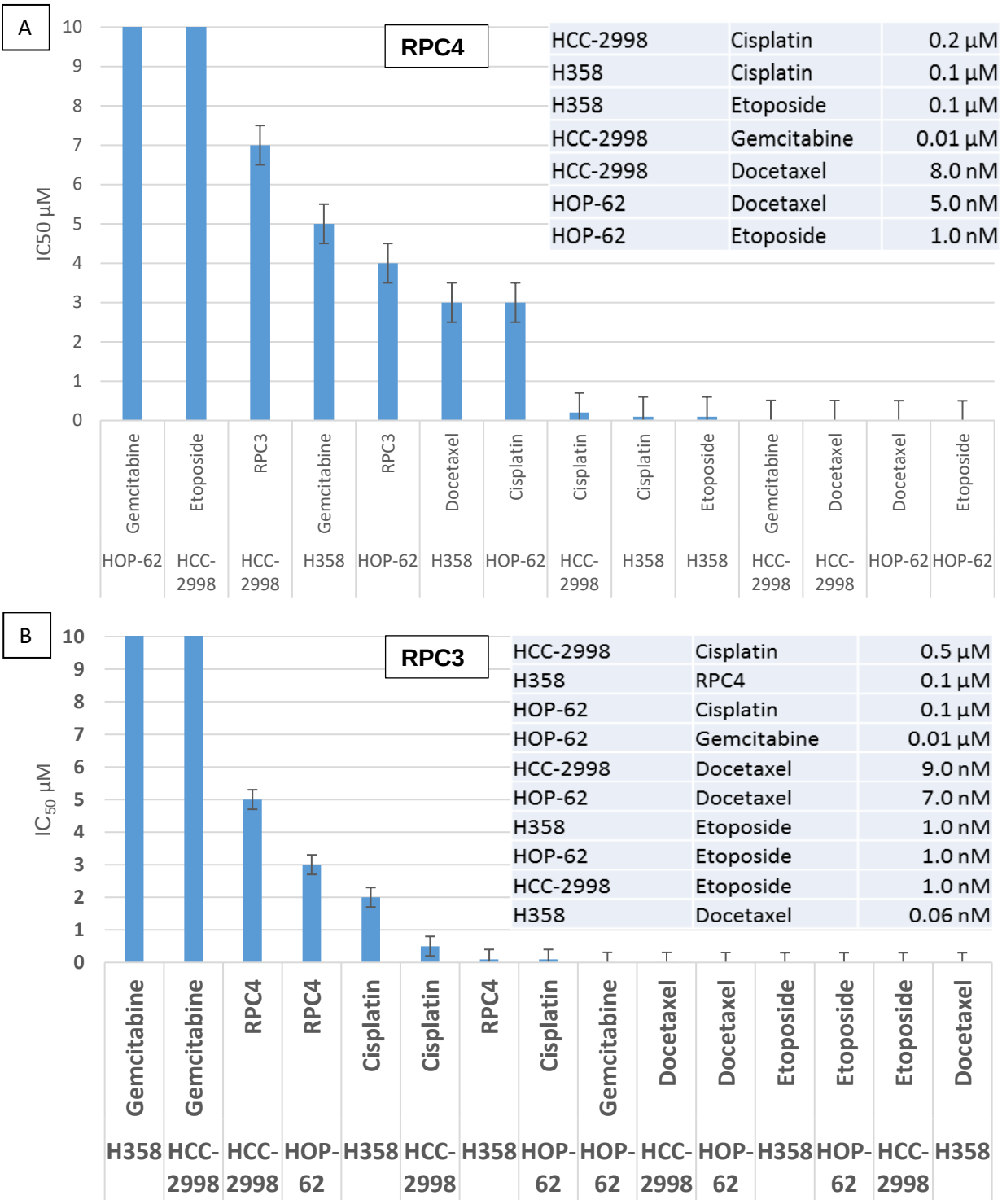

Fig 4.4 A/B Graph (A) = titrating dose of **RPC4** against constant drug B (IC_{10}) dosing and cell lines along x-axis. Graph (B) = titrating dose of **RPC3** against constant drug B (IC_{10}) dosing and cell lines along x-axis. All IC_{50} values that are visually below 0.5 µM are listed in the upper right hand box of each figure respectively.

RPC4 only showed an appreciable effect in HOP-62 in terms of increased efficacy whereas **RPC3** performed well in H358. On a graph scale the results look promising but when the inhibition effect for docetaxel for most of these cell lines in roughly 3 nM, there was no response that truly came below that threshold. This could be a result of docetaxel hindering cell division and stalling a cascade response when **RPC3** and **RPC4** are in the DNA environment not allowing full apoptosis.[105] Last, gemcitabine was the worst performer of this study group. Gemcitabine performed somewhat the same as docetaxel in terms of mono-dosing inhibition with these cell lines which **RPC3** and **RPC4** were not able to overcome. It can be argued for instance that with cell line HOP-62, the IC_{50} with **RPC4** and gemcitabine was 0.01 µM but with gemcitabine alone the efficacy against this cell line is 3 nM action. This effect showed great antagonism as competitive effects may be occurring with antimetabolite drug combinations. Lastly, we also did drug combination with **RPC3** and **RPC4** as both drug A and B with each other. Interestingly, we did not get near the same response as we saw with cisplatin and etoposide but there were some shifts in there combination cytotoxicity in the cell types. Most notably H358 showed the greatest effect with the **RPC3** and **RPC4** combo at 1 µM. Although the RPC combinations with themselves was not an effective combination as their combinations with cisplatin or etoposide were. This is important as a more likely drug pairing in real world therapy is more sought after with a known agent and a new upcoming drug.[80] These findings will be discussed in terms of true synergistic effects in the next section.

The next part of this study we examine standard drugs and use them as the drug A model that was just examined with **RPC3** and **RPC4.** In Figure (A/B/C) 4.5 we illustrate the same experimental study explored with these drugs now being titrated. It is reasonable to assume that the same effect would be shown when the inhibition curves would equal each other. If drug A is (X) µM with drug B constantly dosed at (Y) µM achieved an IC_{50} (Z), the same should be achieved when their reciprocals are dosed in the same manner. This may not always be the case however if drug A becoming B is held steady well below (X) µM never allowing the synergy effect to take

place at all. With that argument standing, reversing the study to demonstrated drug A as the standard care drugs with the RPCs being drug B is salient to a full study.

When **RPC4** and **RPC3** are used in combination with cisplatin and etoposide, we see evidence of inhibition growth of cells when the RPCs are held constant at a value well below their respective IC_{50}s, in this case is <10 µM for all cells tested. RPC concentration was held at 2 µM for each doublet examination and we still achieve significant response with cisplatin and etoposide indicating a

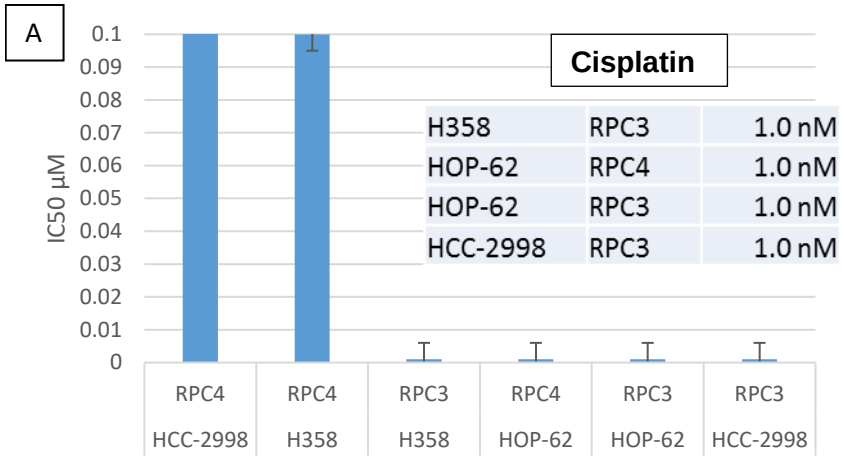

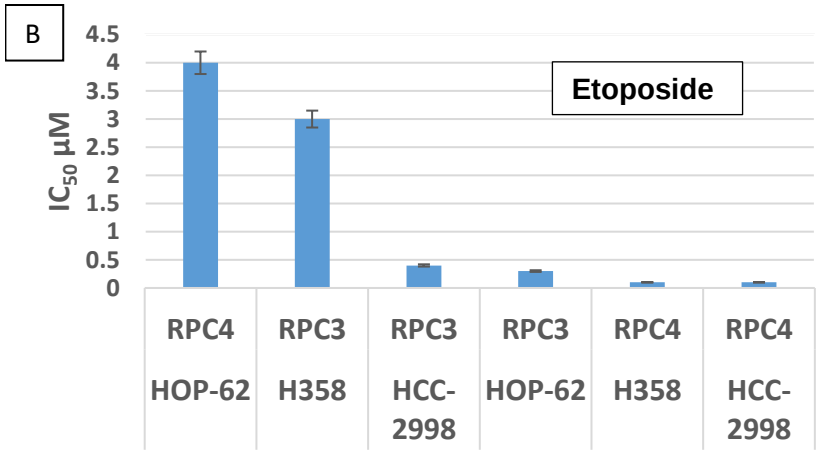

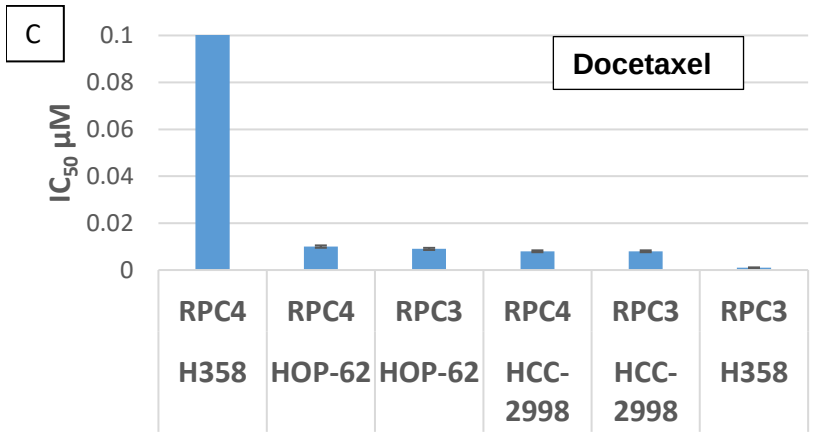

Fig A/B/C 4.5 Graph (A) = titrating dose of cisplatin against constant drug B (IC_{10}) dosing and cell lines along x-axis. Graph (B) = titrating dose of etoposide against constant drug B (IC_{10}) dosing and cell lines along x-axis. Graph (C) = titrating dose of docetaxel against constant drug B (IC_{10}) dosing and cell lines along x-axis. All IC_{50} values that are visually below 0.5 µM are listed in the upper right hand box of each figure respectively.

synergistic effect is taking place. Cisplatin as the titrant drug and 2 µM of **RPC4** shows an appreciable effect in H358 and HCC-2998 with an inhibition of 0.1 µM considering the IC_{50}s for cisplatin with these cell types is 8 µM and 16 µM respectively. Also, etoposide showed great efficacy against all 3 cell types with **RPC3** exhibiting inhibition in the 1 nM range. It should be mentioned that **RPC4** as drug B with cisplatin and etoposide did not show synergy with all cell lines. Lines such as HOP-62 with cisplatin and HCC-2998 with etoposide still were additive at best making RPCs an attractive doublet cocktail for possible therapeutic regimens.

4.3.3 Synergy Combination Index Analysis

As mentioned in the previous section the drugs of choice for this screen were chosen due to their full cytotoxic inhibition curves allowing for true IC_{50}s as opposed to EC_{50}s or ED_{50}s. There are many opponents to the effect based approached as the argument is always based on ways to

determine what curve for each individual drug produces the same quantitative effect as a doublet.[96] The additive effect of a combination is fully dependent on the individual dose and its effect which lends to words like synergy, additivism and antagonism. One must determine what study to pursue for the data that is being presented and achieved. To answer this question we used a dose approach method which relies on the dose effect approach known as the Loewe method.[97] A brief description of this method is warranted to understand the data that will be presented in this study.

The Loewe method utilizes the dose equivalence principle that states: for a given effect, doses of drug A are equivalent to dose b_a of drug B and the reciprocal of both.[98] This concludes that the effects of drugs A and B depend on the individual dose curves which were elucidated in the previous section as single drugs and as doublets. This expression can be shown by the work of Tallarida et. al. as the following:[98]

$$\text{Effect } (a+b) = E_a(a+a_b) = E_B(b_a + b) = E_{AB} \qquad 1.$$

E_A is measured on the dose effect curve of drug A, where $(a + a_b)$ corresponds to A dose leading to the overall effect of E_{AB} and also for drug B. This however assumes that drugs have a constant potency ration effect when in real world settings dose effect curves have varying constant ratios of doses at all levels of effect and have individual maximum drug effects as well.[98] This leads to a relation between all pairs of doses (a and b) producing the combo effect E_{AB} and the single doses to carry out said effect which leads to the math relation that is the Loewe additivity or synergy index:

$$(2): V_{Loewe} = (E)(a+b) = E_a(a + b_b) = E_B(b_a + b) = E_{AB} \qquad 2.$$

$$(3): V_{Loewe} = (a/A)+(b/B) = 1 \qquad 3.$$

Hence the synergy index in related on the 0 -1 scale with any curve under 1 being considered synergistic.

This model allows us to deduce the combination data and indicate which drugs are synergistic combinations together for possible therapeutic windows. It is important to stress that in the introduction we state multiple forms of synergy algorithms and all have their strong points as well as weaknesses.[84-91] The Loewe method was preferred for this study as it is an industry standard for determining therapy windows.[94-96]

4.3.4 Synergy Index

Previously we indicated that several of the drug combinations tested appeared to be synergistic towards the 3 cell types tested. In Figure (A/B) 4.6 the combination index for **RPC3** and **RPC4** as drug A show their combinations based on V_{Loewe} and drug combinations below 1 are only shown. This allows us to discuss the synergistic drug combos of the data set from the previous section.

When these drug combination IC_{50} values are applied in Loewe fields, indications that many of these drug combinations were synergistic towards the cell types tested. Cisplatin across the study with **RPC3** and **RPC4** showed a pronounced synergy with V_{Loewe} values ranging from 0.7 - 0.3. Also, etoposide showed efficacy as a drug combination with RPCs exhibiting index values ranging from 0.3 – 0.05. Not shown in Figure (A/B) 4.5 is HOP-62 which has an index value of 1.01 making it additive but still a successful drug combination avoiding antagonism. For a table of all V_{Loewe} index values please see [appendix 1.1] This data matches what was seen in the IC_{50} inhibition study in terms of each IC_{50} in combination drug was lower or competitive with each dose of drug A and B individually.

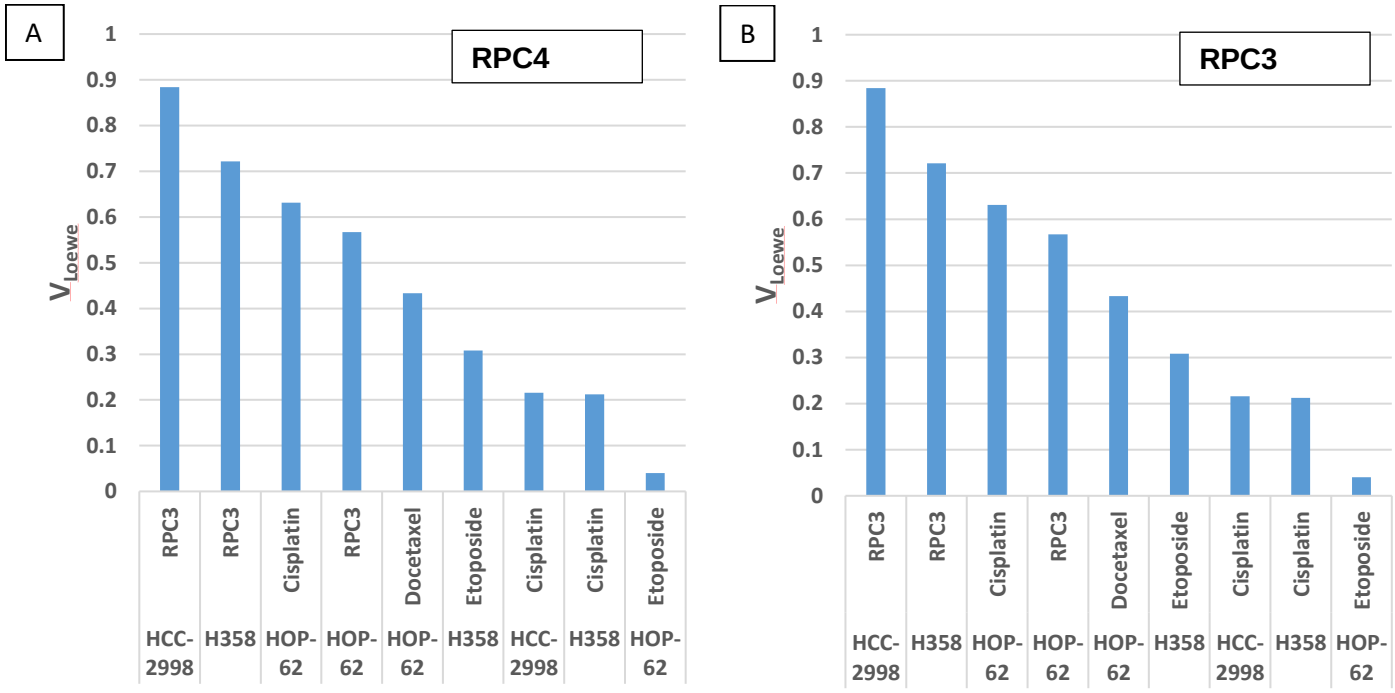

Fig A/B 4.6 Graph (A) = titrating dose of **RPC4** and its V_{Loewe} index against constant drug B (IC_{10}) dosing and cell lines along x-axis. Graph (B) = titrating dose of **RPC3** and its V_{Loewe} index against constant drug B (IC_{10}) dosing and cell lines along x-axis.

The appreciable amount of synergy shown with standard care chemo drugs cisplatin and etoposide are very attractive for future studies with a broader range of cell types.

Docetaxel and gemcitabine were not as broad spectrum synergistic combos as cisplatin and etoposide. **RPC3** only showed a true synergistic effect with H358 and docetaxel with an index value of 0.2 where **RPC4** was synergistic with HOP-62 and docetaxel at an index value of 0.44 . The other docetaxel combinations with RPCs where additive at best and not under 1 on the V_{Loewe}. Gemcitabine as well did not break the synergy threshold whatsoever suggesting that an antimetabolite like gemcitabine may not be the best choice in combination with **RPC3** and **RPC4.**

Again when cisplatin, etoposide and docetaxel where combination dosed as drug A we also analyzed their combination index based on V_{Loewe}. In Figure (A/B/C) 4.7 shown are the combination indices for these 3 drugs with drug B combinations.

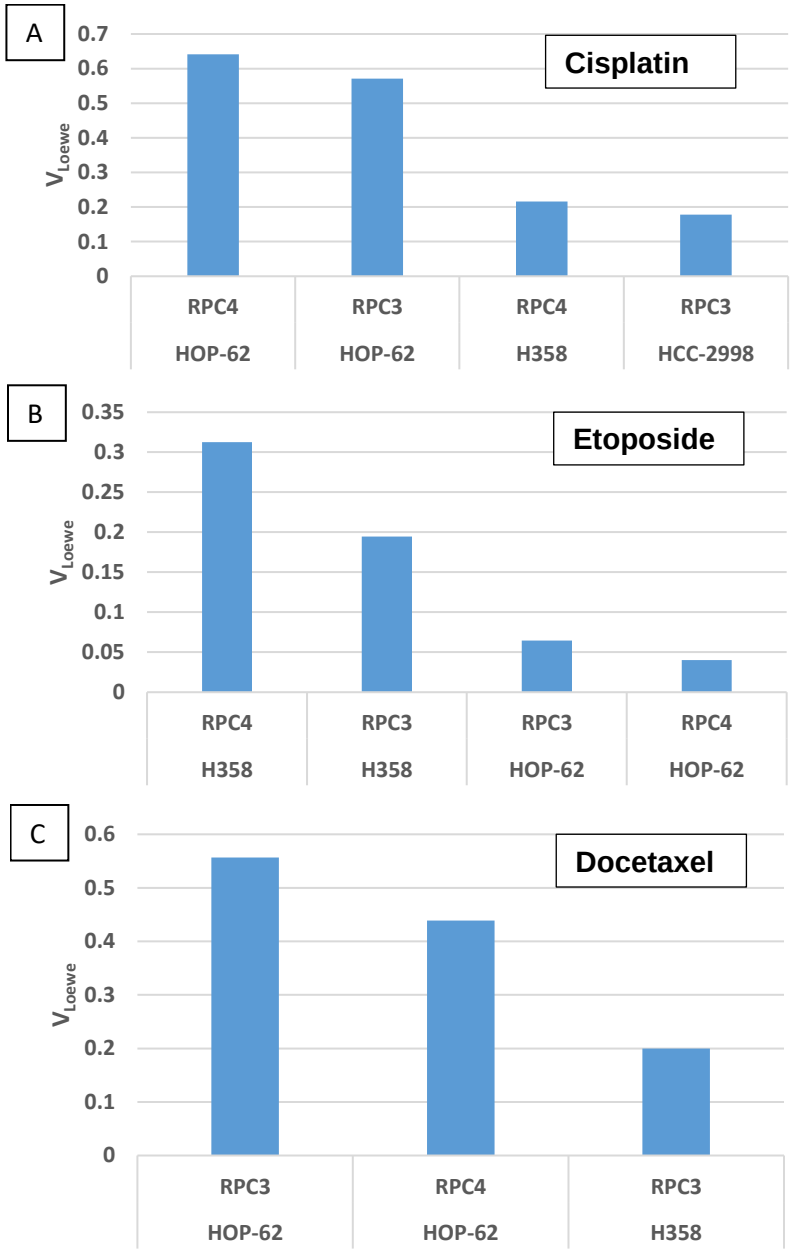

Fig. A/B/C 4.7 Graph (A) = titrating dose of cisplatin and its V_{Loewe} index against constant drug B (IC_{10}) and cell lines along x-axis. Graph (B) = titrating dose of etoposide and graph (C) = titrating dose of docetaxel and their V_{Loewe} index against constant drug B (IC_{10}) and cell lines along x-axis.

.

Figure (A/B/C) 4.7 confirms that cisplatin in combination with **RPC3** and **RPC4** in most cell types tested are indeed synergistic. HOP-62 showed synergy with both RPCs **3** and **4** with index values approximately at 0.6 as well as H358 with **RPC4** and HCC-2998 with **RPC3** approximately at index values of 0.2 for both. Also, etoposide again is confirmed to be synergistic with both RPCs in cell lines H358 and HOP-62. In [appendix 1.1] the full list of additive and antagonistic drug combination hits can be observed. Lastly Figure (A/B/C) 4.7 indicates that **RPC3** and **RPC4** were only synergistic in HOP-62 with index values approximately 0.55 and 0.44 respectively with **RPC3** only being synergistic in H358 with docetaxel. Gemcitabine again is not discussed as it was extremely antagonistic and its values can be seen in [appendix 1.1].

4.4 Conclusions

We have shown data that suggests that **RPC3** and **RPC4** can have potential of being used in combination therapy with certain anti-cancer chemotherapeutics that are currently in the clinic. We demonstrated that **RPC3** and **RPC4** in combination with nuclear anti-cancer chemotherapeutics cisplatin and etoposide were in almost all cases synergistic drug combinations. There combination indices were well below $V_{Loewe} < 0.6$ indicating synergy but also matching in IC_{50} values that agree with the data. Docetaxel is seen to be synergistic with RPCs in HOP-62 and **RPC3** alone in H358 but overall additive would describe RPCs and docetaxel at best in this study. Gemcitabine as mentioned before was antagonistic and future studies with antimetabolite drugs should be considered to verify this find. We intend to broaden this study to a greater size of cell line types to examine the efficacy of cisplatin and etoposide combinations with RPCs **3** and **4.** To our knowledge there is no known ruthenium complex anti-cancer drug that has yet to show these synergistic effects in vitro and with standard care drugs that significantly inhibit cancer cell growth as a combination then with each drug by itself respectively.

Chapter 5

Potentiation Study with **ΔΔRPC4** and **ΔRPC3** on Resistant Non-Small Lung Carcinoma Lines and Standard Care Chemotherapy

5.1 Introduction

Anticancer monotherapies, whether they are cytotoxic agents or specific site targeting molecules, are limited in their ability to have a durable clinical response.[99] In the recent decade this is most likely due to factors including multiple dependency during tumorigenesis and cellular resistant mechanisms.[100] Combination therapy has been in the clinic for over 50 years and what separates certain doublet studies from one another is the overall synergistic effect question. Potentiation and synergy are synonymous terms with numerous studies exhibiting large drug screens and combining any two drugs to acquire a response.[102] Potentiation of a drug response is different from synergy in a subtle but important way: synergy is the effect of two drugs efficacy greater than the sum of each individual drug whereas potentiation is using drug B to elicit an effect in drug A without drug B itself having noticeable effect.[103] We have studied a panel screen of multiple NSCLC and their effects with multiple drug combinations and **ΔΔRPC4** and **ΔRPC3.** The goal was to look at **ΔΔRPC4** and **ΔRPC3** resistant cells and elicit a higher cytotoxic effect by potentiating them with multiple other standard care chemotherapeutics. Also, we reversed the study by using **ΔΔRPC4** and **ΔRPC3** as potentiation complexes to elicit a response in chemotherapeutic resistant cells. We show an effect with potentiation in cells with resistant to drugs: cisplatin, etoposide, docetaxel and pemetrexed (an antimetabolite). We also studied potentiation in terms of synergy by comparing them to the Loewe additivity index to determine if they were synergistic together as well. We present in this chapter a full panel screen on 2D and 3D NSCLC potentiation screens with these novel anticancer complexes **ΔΔRPC4** and **ΔRPC3.**

5.2 Experimental

5.2.1 Chemicals

All solvents were reagent and cell culture grade. All reagents and work environments were maintained sterile. RPCs **ΔΔRPC4** and **ΔRPC3** where provided by the MacDonnell laboratory and were used as received. NSCLC H2073, H460, HCC515, HCC1359, H2126, H1975, H1648, H647, H1792, H322, HCC1171, H1993, H1819, H596, HCC15 and HCC4017 were acquired from University of Texas Southwestern (UTSW) Hammond Cancer Center (HCC). RPMI-1640 medium, fetal bovine serum (FBS), etoposide, cisplatin and docetaxel were purchased from Sigma Aldrich. Phosphate buffered saline 10X was purchase from Biorad. Cell Titer-Glo was purchased from Promega. Nuncone low adherent 96 well titer plated were purchased from Thermofisher.

5.2.2 Instrumentation

Cell incubation was maintained by a Thermofisher HeriCell CO_2 Incubator. Luminescence data was obtained using a BMG Labtech FLUOstar Omega plate reader. Liquid colony assay count was performed using a Zeiss 500 light microscope. MCTS visulization was performed using a Zeiss Axio-Plane 540 inverted light microscope.

5.2.3 Cell Culture Lines/Maintenance

NSCLC H2073, H460, HCC515, HCC1359, H2126, H1975, H1648, H647, H1792, H322, HCC1171, H1993, H1819, H596, HCC15 and HCC4017 cells were grown in RPMI-1640 medium supplemented with 10% FBS, 2 mM L-glutamine, 1 mM sodium pyruvate and 1X BME vitamin complex solution. Cells were grown and passaged in T-25 and T-75 Corning culture flasks at 37^{o}C under 5% CO_2 and humidified atmosphere.

5.2.4 Single Dose Cell Viability Assay

Cytotoxicity drug effects with NSCLC lines and RPCs, cisplatin, etoposide, docetaxel and pemetrexed and were determined by an (2-Aminoethyl MethaneThioSulfonate Hydrobromide) MTS assay. Cells were seeded into 96-well plates at 1×10^4 cells per well and grown for 24 h at 37 °C in a 5% CO2 incubator; then 4-fold titrating doses of drug were used ranging from 0.00001 - 100 µM. Cells were then incubated with drug for 96 h under the same conditions. The stock MTS dye solution (5 mg/mL) plus 1 mL PMS/20 mL MTS was added to each well for 1-2 h of incubation. Plates were read for absorbance at 570 nM using a plate reader.

5.2.5 Doublet Dose Cell Viability Assay

Cytotoxicity drug combination effects with NSCLC lines and RPCs, cisplatin, etoposide, docetaxel and pemetrexed were designed with Drug A in all dosing regimens to be the 4-fold titrating drug dose whereas drug B was always at a steady concentration at the ~IC_{10} of each cell line respectively being tested. Titrating doses of drug A were used ranging from 0.00001 - 100 µM. Cells were then incubated with drug for 96 h under the same conditions. The stock MTS dye solution (5 mg/mL) plus 1 mL PMS/20 mL MTS was added to each well for 1-2 h of incubation. Plates were read for absorbance at 570 nM using a plate reader.

5.2.6 Doublet Dose Cell Liquid Colony Assay

Liquid colony assay formation on NSCLC and RPCs, cisplatin, etoposide, docetaxel were carried out in 6-well plates with roughly 100 – 200 cells/mL suspension seeded in random areas in each plate well. Dosing for drug A in all dosing regimens was the 4-fold titrating drug dose whereas drug B was always at a steady concentration at the ~IC_{10} of each cell line respectively being tested. The top dose for drug A was the IC_{50} for each doublet line respectively based on MTS assay due to the stringency of this assay. Colonies were allowed to form for 15 – 21 days (undisturbed) depending on cell line viability and growth rates. When approximately 50 cells per

colony were noticed each cell colony formation well was fixed and stained with 30% ethanol/5 mg crystal violet solution for 1 h. Cells were then gently washed under DI water, as not to disturb colonies, 3X until stained colonies were clearly visible and supernatant solution as completely removed. Cell colonies were then counted under light microscopy.

5.2.7 Formation and Analysis of Multi Cell Tumor Spheroids (MCTS)

MCTs were cultured using a low adherent hemisphere plate well method. H358, H2126 cells were passaged once confluent and approximately 1500 cells/mL suspension was transfered to low adherent plates containing complete RPMI-1640 medium. The single cells formed MCTs aggregates within 24 h and noticable 100 - 200 μM spheroids in 48 h in 37^{o}C under 5% CO_2 and humidified atmosphere. Formations were imaged using a Zeiss Axio phase contrast microscope using 10X and 20X objectives to monitor color of tumor and drug, size, morphology and diameter.

5.2.8 Doublet Dose MCTS Cell Viability Assay

Cytotoxicity drug combination effect of RPCs and docetaxel with NSCLC line H460 were designed with Drug A in all dosing regimens to be the 4-fold titrating drug dose whereas drug B was always at a steady concentration at the ~IC_{10} of H460. Cells were dosed with various drug for 96 h and afterwards plates are removed from incubator and allowed to come to rt for 30 min. Cell Titer-Glo was then administered in equal amounts to media per well for 45 min. at rt. Plates are read for luminescence using a BMG Labtech FLUOstar Omega plate reader and ATP values were monitored in terms of cell viability.

5.2.9 Data Analysis

We assumed cell exponential growth and therefor the number of cells at any given time *t* and 0 were defined by the expression N(*t*)=N(*t*=0 h) * (mu*t), where mu is the growth constant that depends on each individual cell line respectively. Drug effect was measured by MTS or cell Titer-Glo assay and Drug A and B doublet IC_{50} was compared to growth curves of IC_{50} for Drug A alone and IC_{10} of Drug B alone. Drug B concentration was constant throughout each drug screen study. We employed the Loewe Additivity Model to detect synergy. The Loewe model, which is an industry standard, predicts that the additive effects of drugs A and B depend on the individual does effect curves and are to be expressed as Effect → $(E)(a+b) = E_a(a + b_b) = E_B(b_a + b) = E_{AB}$ where E_A is measured as a drug effect curve of drug A, $(a+a_b)$ giving the overall effect E_{AB} and the reciprocal for drug B.[94-96] The Loewe method makes the assumption drugs have a constant potency ratio between themselves.[94] Any isobolagram that has a drug combination curve that falls below 1 is consider additive to synergistic with far below 1 accepted as synergy. Above 1 is considered to be antagonistic. All combination data is shown in the form of combination index in bar graph form.

5.3 Results and Discussion

5.3.1 Single Dose Treatment Study

IC_{50} Values for drugs **ΔΔRPC4**, **ΔRPC3,** cisplatin, etoposide, docetaxel and pemetrexed alone were determined using NSCLC H358, H2073, H460, HCC515, HCC1359, H2126, H1975, H1648, H647, H1792, H322, HCC1171, H1993, H1819, H596, HCC15 and HCC4017. All of these NSCLC cell lines except, (H358, H1792 and H1975), are resistant to **ΔΔRPC4** and **ΔRPC3.** RPCs **ΔΔRPC4** and **ΔRPC3** that had IC_{50}s above 25 µM were considered poor responders and were capped at this concentration to preserve drug. For this reason all cells, except (H358, H1792 and H1975) are considered to have an IC_{50} of 25 µM against all cell lines in this study. Poor cell lines responders to standard chemotherapy drugs cisplatin, etoposide, docetaxel and pemetrexed were used to determine what RPC, if any, could potentiate a more successful

inhibition curve response in these drug resistant cells. The same approach was used for RPC resistant cells with standard chemotherapy drugs as well. These resistant NSCLC were chosen from a database of over 150,000 cell lines from the DIVSA program at UT Southwestern Hammond Cancer Center. Cell that are resistant vs. sensitive were based on median IC_{50} values in association with current chemotherapy dosing across all cell lines used in clinic. These poor cell and drug responders can be seen in Table 1.4 (cisplatin, etoposide and pemetrexed) and are expressed in µM. Cells dosed with docetaxel are presented in nM.

Docetaxel		**Pemetrexed**		**Cispltain**		**Etoposide**	
H2073	580 ± 2	H1975	1000 ± 3	H322	18.5 ± 4	H1648	31 ± 2
H460	62 ± 3	H1648	1000 ± 4	HCC1171	8.65 ± 3	H1819	20 ± 4
HCC515	1000 ± 2	H2126	1000 ± 2	H1993	9.8 ± 3	H322	47 ± 3
HCC1359	78 ± 4	H647	1000 ± 3	HCC4017	8.15 ± 2	H647	11 ± 3
H2126	11.5 ± 2	H1792	1000 ± 3	H1648	4.9 ± 3	H596	10 ± 4

Table 1.4 Various drugs that are resistant to NSCLC are listed above. Cisplatin, etoposide and pemetrexed and are expressed in µM. Cells dosed with docetaxel are presented in nM. Resistant vs. sensitive cell lines were chosen over a median of 150,000 cells in DIVSA software program at UT Southwestern Hammond Cancer Center.

5.3.2 Potentiation Drug Study

The potentiation of these various NSCLC were done in an unbiased manner and were screened as a doublet drug screen much like the previous chapter. However, differences include a 4-fold titrated dilution factor of drug A, each cell line is resistant to drug A in terms of efficacy,

and 2-aminoethyl methane thiosulfonate hydrobromide (MTS) assay were employed. Drug A, in all cases was the titrating drug whereas drug B is always the steady concentration of drug at the IC_{10} of cell lines tested. Drug B was chosen to be IC_{10}, to ensure it alone could not be responsible for appreciable cell death. In Figure 4.2, from the previous chapter, shows a representation of the doublet drug assay.

After running a full battery of MTS assays with each potentiation drug combination, we achieved IC_{50} data points for each cell line. This study can be seen in Figure A/B 5.1. For ease of comparison, the drug combinations in each graph have been separated by drug A (top of each plot) with drug B and cell line results on the x-axis in each case.

We first examine **ΔRPC3** and **ΔΔRPC4** reistant NSCLC as shown in Figure A/B 5.1. Due to the 25 μM dosing cap, all cell lines that are at 25 μM can be consider over that IC_{50} value. Inhibition curve values for all doublets can be found in Appendix Table 1.2.

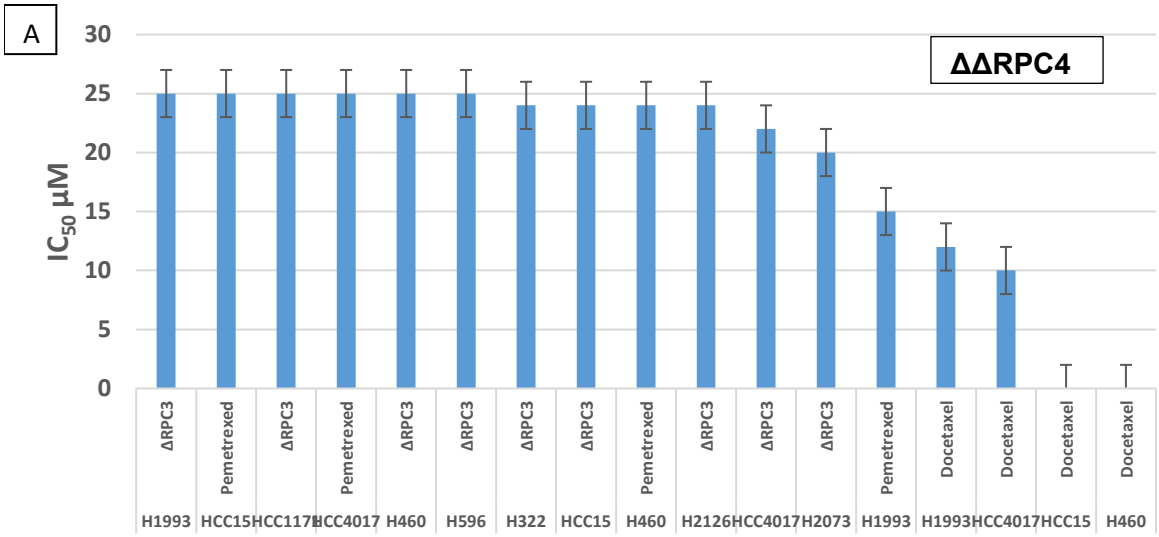

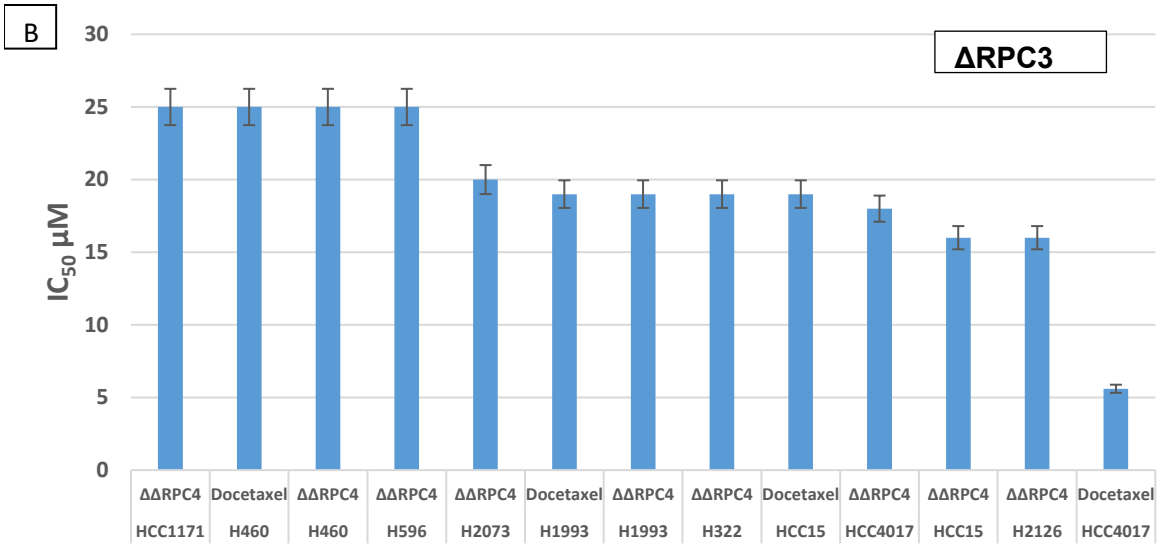

Fig A/B 5.1 Potentiation study with Drug A (titrating dose) either being **ΔΔRPC4** (graph A) and **ΔRPC3** (graph B) with drug B and cell lines (x-axis) show IC_{50} of each combination in µM from MTS assay. All IC_{50} in each NSCLC with **ΔRPC3** and **ΔΔRPC4** alone exceeded 25 µM. Any IC_{50} of doublets below 25 µM can be considered at a minimum, an additive potentiation. All data was assayed with MTS.

When comparing **ΔRPC3** and **ΔΔRPC4,** docetaxel was the only drug to potentiated any significant response in terms of IC_{50} values. HCC15 and H460 lowered from 25 uM (**ΔΔRPC4**) to ~1 nM with docetaxel. HCC4017 and H1993 showed a similar 2-fold docetaxel potentiated response lowering 25 µM (**ΔRPC3** and **ΔΔRPC4)** to a 8 – 12 µM range. Also, any potentiation with **ΔRPC3** and **ΔΔRPC4** with each other did not yield appreciable results other than additive 5-10 µM flucuations for several of the cell lines in Figure (A/B) 5.1.

In Figure (A-D) 5.2 we examined resistant NSCLC to standard chemotherapy care drugs cisplatin (A), etoposide (B), docetaxel (C) and pemetrexed (D).

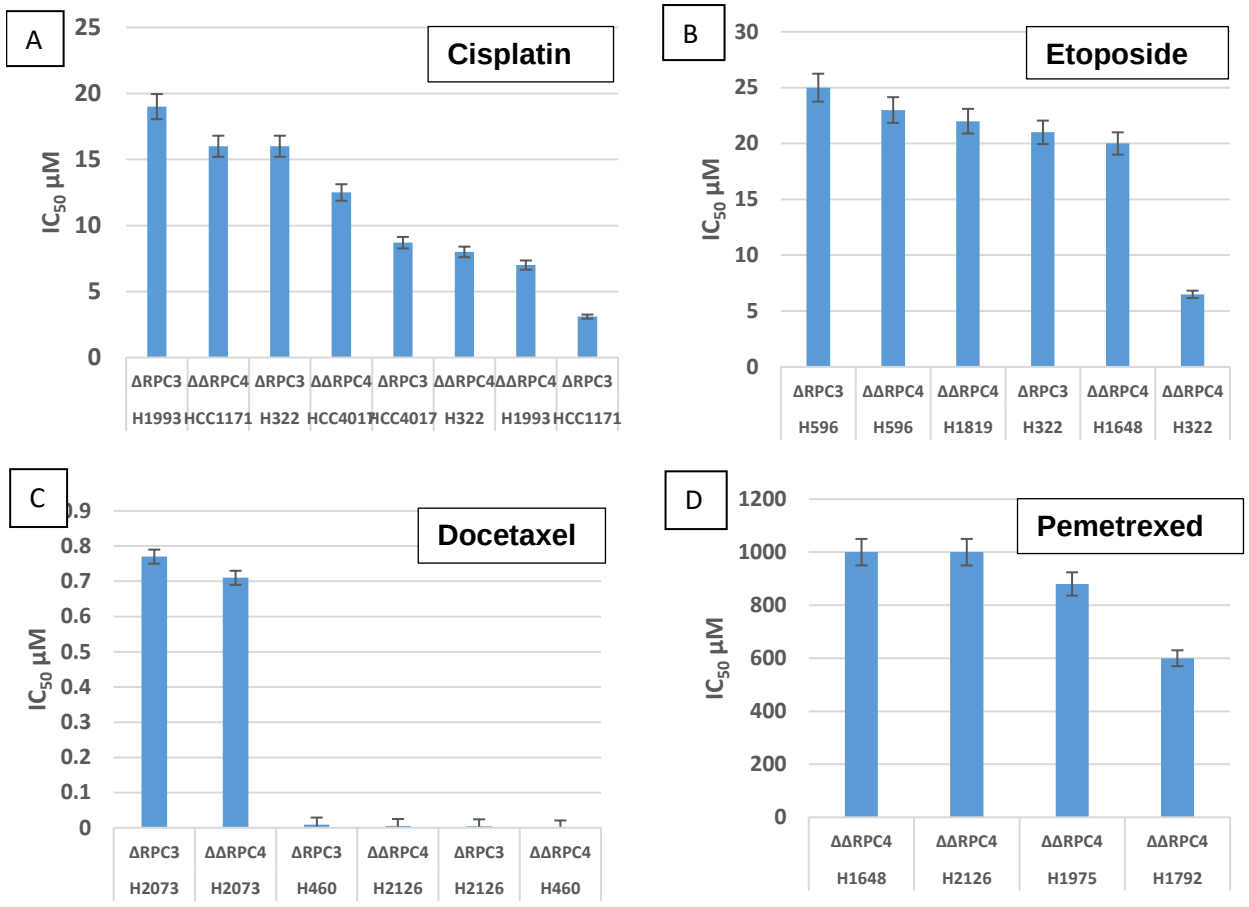

Fig (A/B/C/D) 5.2 Examines potentiation study with Drug A (titrating dose) resistant against NSCLC with: (graph A) cisplatin, (graph B) etoposide, (graph C) docetaxel and (graph D) pemetrexed. Drug B (constant IC_{10} dose) and cell lines are on the x-axis. IC_{50} of each combination is in µM from MTS assay.

In Figure 5.2 (A) we attempted potentiation response of cisplatin resistent NSCLC lines with **ΔRPC3** and **ΔΔRPC4. ΔΔRPC4** was able to potentiate some modest responses with H1993 from 9.8 µM (cisplatin) to 3.6 µM with **ΔΔRPC4** as well with H322 from 18.5 µM to 8 µM respectively. **ΔRPC3** exhibited a modest effect with HCC1171 potentiating a response from 8.5 µM (cisplatin) to 3 µM. All other combinations were antagonistic, were the IC_{50} curves raised well above the

cisplatin only curves appreciably. With another nuclear chemotheraputic agent, etoposide, lines resistent to it were also examined for potentiation in Figure 5.2 (B) with **ΔRPC3** and **ΔΔRPC4.** H1648 shows a potentiated response from 31 μM (etoposide) to 20 μM with **ΔΔRPC4.** A more significant potentiation was in H322 where an appreciable drop in resistance from 47 μM (etoposide) to 7 μM with **ΔΔRPC4** and even more so with **ΔRPC3** further potentiating a response to 3 μM. With both nuclear acting standard chemotherapy agents, cisplatina and etoposide, H322 showed appreciable potentiated responses with both **ΔRPC3** and **ΔΔRPC4.** HCC1171 had a modest effect with **ΔRPC3** wereas **ΔΔRPC4** showed modest effects as well with H1648 and H1993. Figure 5.2 (C) examined possible potentiation with anti-metabolite chemotherpay drug pemetrexed with **ΔRPC3** and **ΔΔRPC4.** NSCLC H1792 reveals a modest response when potentiated with **ΔΔRPC4.** RPC **ΔΔRPC4** lowered the IC_{50} curve from 1000 μM (pemetrexed) to 600 μM. All other combination were not effective and **ΔRPC3** was not shown in Figure 5.2 (C) as no movement in the curve was noticed. This cooresponds to our previous doublet study with gemcitabine and its failed attempt at producing synergistic results. These findings would suggest that antimetabolite chemotheraputics and RPCs do not have an efficacious effect together. The largest potentiation response came from **ΔRPC3** and **ΔΔRPC4** potentiating docetaxel resistant lines in Figure 5.2 (D). H460 exhibits a potentiation from 6.5 nM (doccetaxel) to 1 pM with **ΔΔRPC4** and 6 pM with **ΔRPC3.** Also, NSCLC H2126 showed an appreciable response from 11 nM (docetaxel) to 1 nM with **ΔΔRPC4** and 0.5 nM with **ΔRPC3.** Other than H2073 showing an antogonistic response from 580 nM (docetaxel) to ~700 nM with **ΔRPC3** and **ΔΔRPC4** these potentiation findings with docetaxel resistent lines **ΔRPC3** and **ΔΔRPC4** are remarkably exciting prospects. Cisplatin and etoposide resistant lines also showing some NSCLC that exhibited potentiation potentials but not at the same fold difference as docetaxel.

5.3.3 Liquid Colony Verification of Potentiation Data

Due to the remarkable potentiation study with certain cell lines, the results with docetaxel had to be validated as the potentiation was so efficacious with **ΔRPC3** and **ΔΔRPC4** as well as with cisplatin and etoposide. We utilized the liquid colon assay to verify our findings and 11 potentation effects were selected to represent each group of drug respectively. Pemetrexed was not chosen for this study as no potentiation effect of appreciable value was observed with NSCLC.

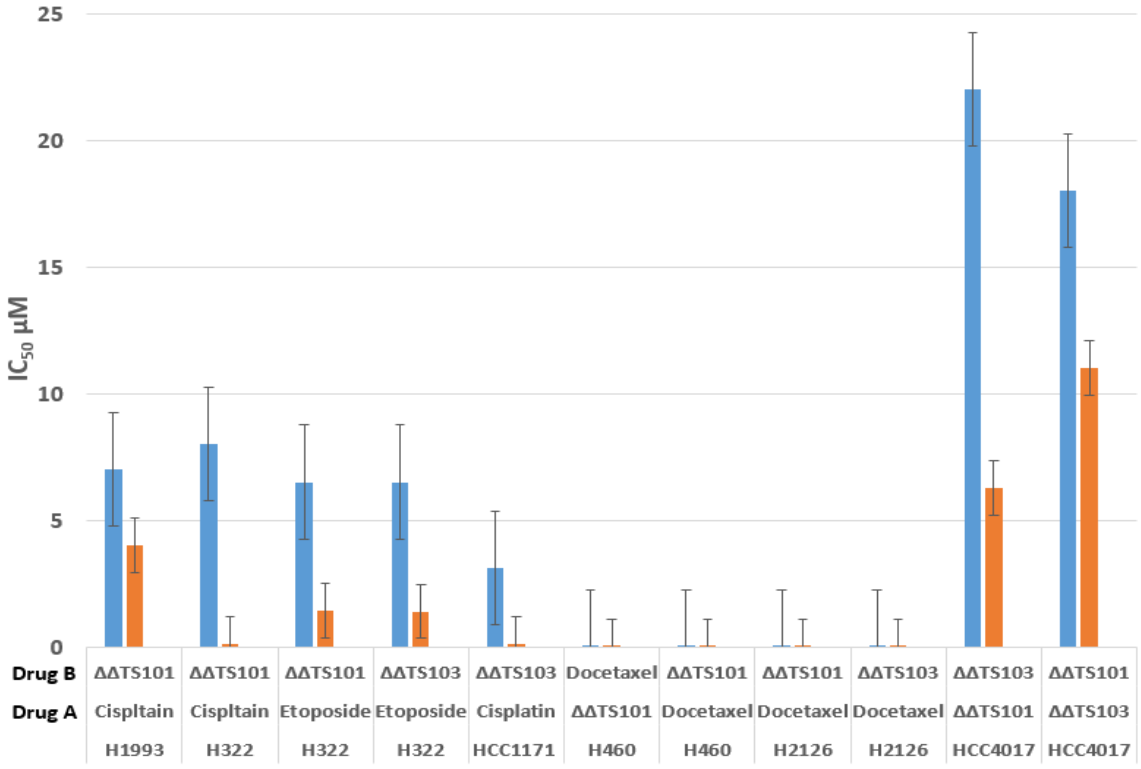

Fig 5.3 Liquid colony assay formation with 11 potentiation drug combination hits. Blue bar graphs represent inhibition concentration by MTS assay and orange bar graphs represent inhibition concentration from liquid colony assay. Drug a (titrating dose) with drug B (constant IC_{10} dose) and NSCLC are on x-axis. Drug concentrations are represented in µM.

We plot this data in bar graph form in Figure 5.3 as well as in Table 1.4 as a function of IC_{50} values in μM. Cisplatin drug combo represented their effecacy in liquid colony showing **ΔΔRPC4** potentiating an appreciable response in NSCLC H1993 (4 μM) and H322 (0.12 μM).

NSCLC	Drug A	Drug B	MTS	Liquid Colony
H1993	Cisplatin	ΔΔRPC4	7.0 μM	4.0 μM
H322	Cisplatin	ΔΔRPC4	8.0 μM	0.12 μM
H322	Etoposide	ΔΔRPC4	6.5 μM	1.4 μM
H322	Etoposide	ΔRPC3	6.5 μM	1.4 μM
HCC1171	Cisplatin	ΔRPC3	3.1 μM	0.12 μM
H460	ΔΔRPC4	Docetaxel	0.1 nM	0.06 nM
H460	Docetaxel	ΔΔRPC4	0.8 nM	0.03 nM
H2126	Docetaxel	ΔΔRPC4	5.0 nM	1.0 nM
H2126	Docetaxel	ΔRPC3	4.0 nM	2.0 nM
HCC4017	ΔΔRPC4	ΔRPC3	22 μM	6.2 μM
HCC4017	ΔRPC3	ΔΔRPC4	18 μM	11 μM

Table 1.5 Liquid colony assay inhibition concentrations with doublet drugs A and B. Each value is shown as either MTS or liquid colony assay drug inhibition studies.

Also, cisplatin was also potentiated in HCC1171 with **ΔRPC3** (0.12 μM). As with cisplatin, etoposide showed similar results with H322 after being potentiated with both **ΔRPC3** and **ΔΔRPC4** (1.4 μM) respectively. The remarkable docetaxel potentiations also exhibited positive responses in liquid colony with H460 potentiated with **ΔΔRPC4** (0.03 nM) as well as H2126 being potentiated by both **ΔΔRPC4** (1.0 nM) and **ΔRPC3** (2.0 nM). Lastly, we studied one of the additive **ΔΔRPC4** and **ΔRPC3** potentiations with each other in HCC4017. The data does hold up

to scrutiny in the liquid colony assay as each was able to potentiate a response from one another at **ΔΔRPC4** (11 μM) and **ΔRPC3** (6.2 μM). The stringency of the liquid colony assay validates these doublet combination responses. All 11 doublet potentiations were upheld to be a true effect in both MTS and liquid colony assay formats.

5.3.4 Synergy Index

Now that we validated the potentiation effects seen in the 11 NSCLC hits we used the Loewe additive method and combination index for **ΔRPC3** and **ΔΔRPC4** as V_{Loewe} as discussed in the previous chapter. Drug combinations below 1 are only shown for brevity.

When the 11 potentiation hits were put into the Loewe method formulations 9 out of 11 were successful in being synergistic. HCC4017, with **ΔRPC3** and **ΔΔRPC4** doublets potentiating each other, were not considered synergy by this model and therefore excluded. All V_{Loewe} indices can be viewed in [appendix 1.2]. In Figure 5.4 the combination index for the 9 potentiation drug hits in ascending order from most synergistic 0.1 to borderline additive 0.8 is presented.

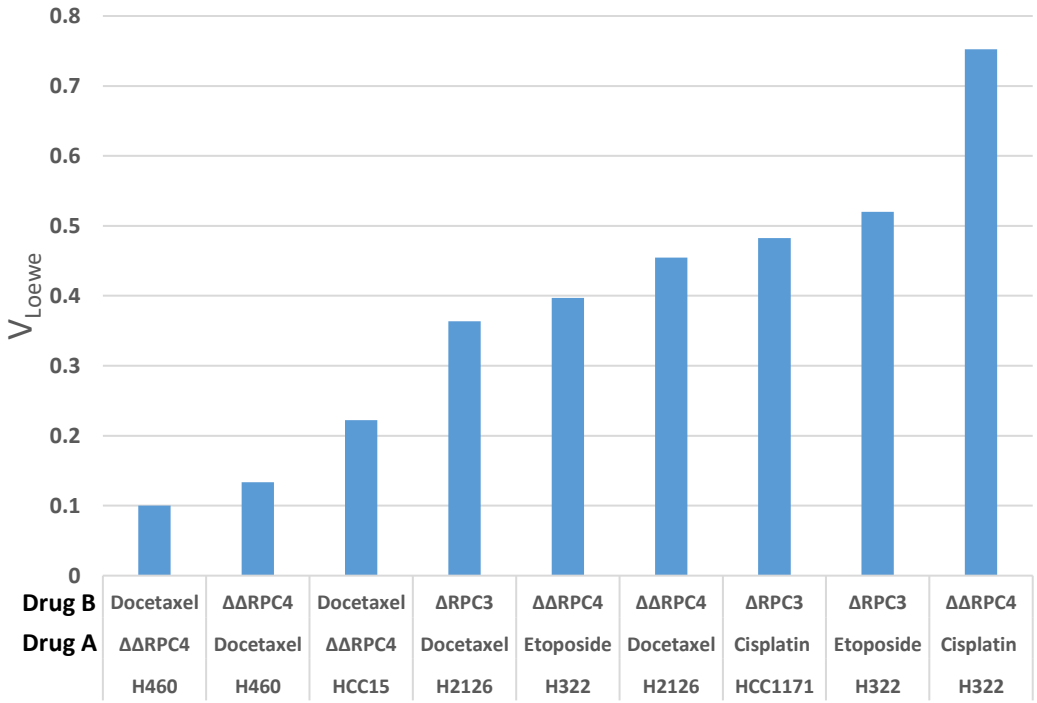

Fig 5.4 Loewe combination index of successful potentiation drug combinations with drug A (titrating dose) and B (constant IC_{10} dose) reflected in the x-axis with NSCLC used.

Cell nuclear cytotoxic compounds cisplatin exhibits synergy with **ΔΔRPC4** in H322 at V_{loewe} 0.75 were **ΔRPC3** was synergistic with cisplatin in HCC1171 at V_{Loewe} 0.47. As well with etoposide **ΔRPC3** and **ΔΔRPC4** both were synergistic in H322 with V_{Loewe} values **ΔRPC3** (0.51) and **ΔΔRPC4** (0.4).

The very synergistic potentiation however came from docetaxel doublets with **ΔRPC3** and **ΔΔRPC4.** H2126, 460 and HCC15 all exhibited **ΔRPC3** and **ΔΔRPC4** potentiating docetaxel resistent cell lines. HCC15 and H2126 **ΔΔRPC4** potentiated responses with V_{Loewe} index values of 0.22 and 0.45 respectively. Also, H460 and **ΔΔRPC4** show synergy V_{Loewe} values at 0.1. With the combination of the doublet inhibition concentrations, liquid colony and Loewe combination index these potentiated effects are exciting for possible theraputic windows. Resistent drug cell

types could possibly gain these potentiation benefits from new drug types that all but foregin to them.

5.3.5 Potentiation Effects in MCTS

We have discussed the possibility of theraputic windows with the drug potentiations and in this section we examine the doublet dosing in 3D cell culture MCTS. As stated in the previous chapters MCTS mimic tumors in vivo vs. their 2D counterparts. Due to the overwhelming success in the potentiation study with docetaxel it was a logical drug combination to test in 3D. We examined doublet docetaxel with **ΔΔRPC4** in H2126 and H420 as well **ΔRPC3** and docetaxel in H2126.

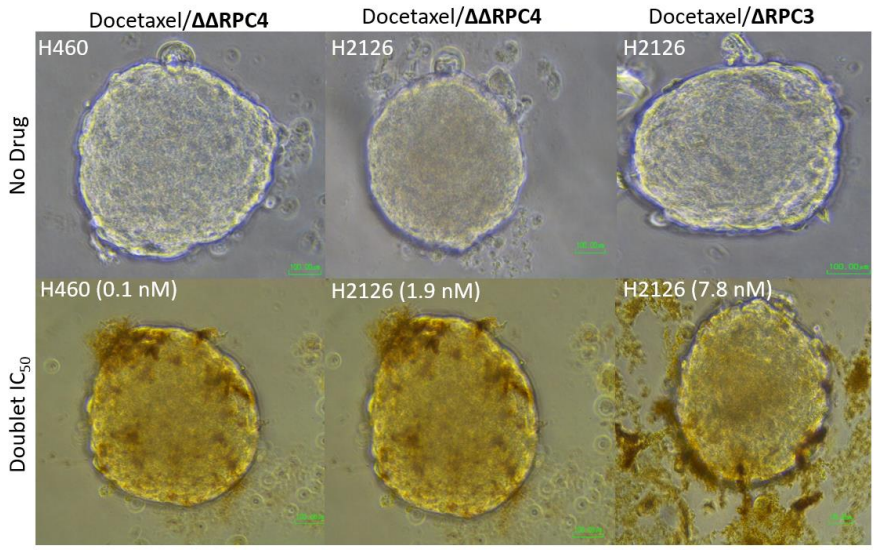

Fig 5.5 Docetaxel potentiated by **ΔΔRPC4** in H2126 and H420 MCTS as well as docetaxel and **ΔRPC3** in H2126 MCTS. Tumors were imaged at IC_{50} dose achieved by MCTS cell viability cell Titer-Glo. Images were taken by a Zeiss 500 light phase contrast microscope at 10X objective. Scale bar is 100 µM.

In Figure 5.5 we first examine the morphological changes occurring in the MCTS at the IC_{50} dosing concentration of each doublet found in Table 1.4. As in the MCTS chapter previously

discussed, we noticed the same morphological changes in H2126 and H460 dosed with docetaxel and **ΔΔRPC4**. The cell adhesion of the tumor, in the 3D shape, remain cohesive and 4 μM of **ΔΔRPC4,** as constant concentration drug B, is still able to greatly color the tumor (bottom image track). H2126 with docetaxel and **ΔRPC3** show the same cell disassembly as noticed in all other MCTS we imaged with **ΔRPC3** (bottom image track)**.**

In Figure (A/B) 5.6 we also demonstrate the MCTS IC_{50} in cells H2126 and H460 with these synergy doublets. We demonstrate docetaxel is potentiated with **ΔRPC3** and **ΔΔRPC4** in MCTS H2126 as a noticeable shift to the left (**ΔRPC3** 7.8 nM and **ΔΔRPC4** 1.9 nM) in the IC_{50} curve is attained (graph A solid function lines) vs. the docetaxel solo (125 nm) dosing curve (graph A dotted function line). Also, docetaxel potentiated by **ΔΔRPC4** in MCTS H460 we noticed the same effect (**ΔΔRPC4** 0.1 nM) where there is a shift to the left (graph B solid function line) vs. the docetaxel solo (0.4 nM) dosing curve (graph B dotted function line).

We show that 3D evidence suggests the potentiation effect may not be strictly limited to in vitro assays but a similar effect in vivo may prove true in future studies.

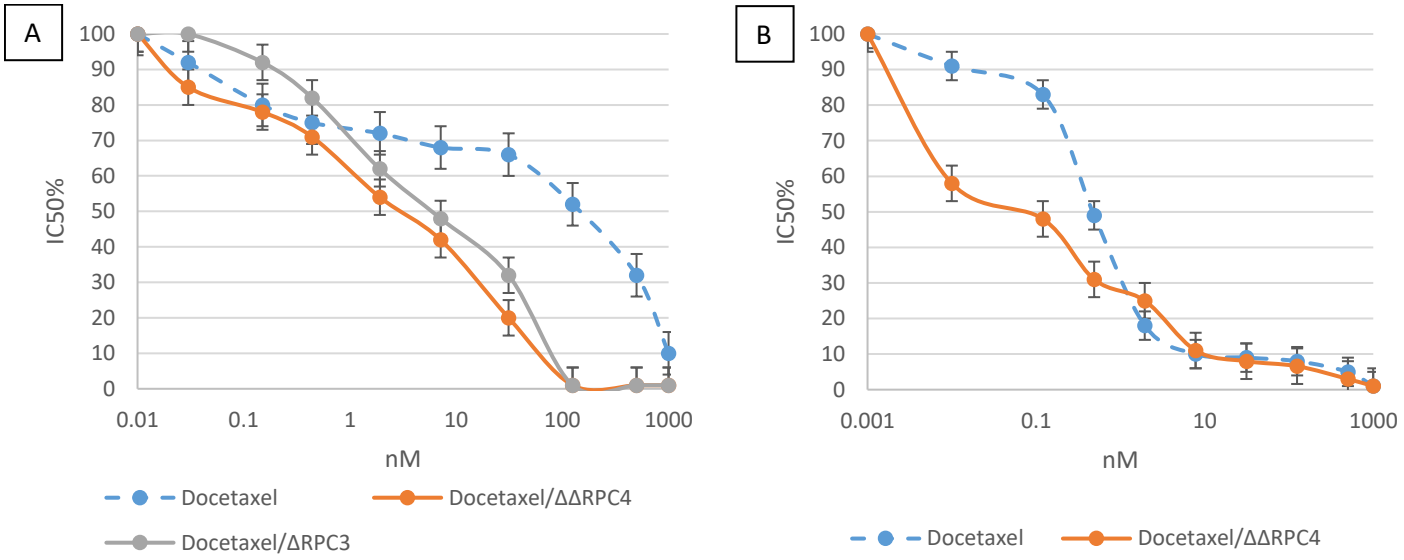

Fig A/B 5.6 Docetaxel potentiated with **ΔRPC3** and **ΔΔRPC4** in MCTS H2126 (A) and docetaxel potentiated with **ΔΔRPC4** in MCTS H460 (B) were the dotted function represents docetaxel as a solo drug in each MCTS respectively. MCTS viability was determined by cell Titer-Glo assay.

5.4 Conclusions

Potentiation is a common and more used technique emerging every decade with anticancer therapy. We have demonstrated in a thorough NSCLC study with **ΔΔRPC4** and **ΔRPC3** and with various chemotherapeutic agents that we were able to elicit responses with certain combinations. We show that **ΔΔRPC4** and **ΔRPC3** are indeed able to elicit potentiated responses in resistant NSCLC with cisplatin and etoposide. We also showed an even greater effect with the ability of **ΔΔRPC4** and **ΔRPC3** to potentiate response in docetaxel resistant cell lines. Most notably we examined two docetaxel resistant lines, H2126 and H460 in a 3D MCTS environment to mimic in vivo response types and great efficacy with **ΔΔRPC4** and **ΔRPC3** was determined. This opens many routes to possible drug combination discovery

that can be beneficial to future cell studies and quite possibly going beyond the dish to patient trials. There are a plethora of drug combinations used in the clinic and the ever growing fear of drug resistance warrants studies like this in finding new potentiate drugs combinations. Not only synergistic drug combinations but also drug combinations well tolerated in patients. In our previous work, we demonstrated the preliminary targeting capability of **ΔΔRPC4** and **ΔRPC3** in normal cell tissue types vs cancer types was evident and when that is taken into consideration, several synergistic combinations could be useful in possible future clinic studies.

Granted, we are not at the clinic door but the road is open to studies that we will push forward in the near future to exploit the effects of **ΔΔRPC4** and **ΔRPC3** to their full potential. Possible expansion of potentiation data studies as well can look for more drug combination hits that can prove to be beneficial in cancer therapy.

Chapter 6

Hypothesis Summation

6.1 Hypothesis Discussion

Chapter 1.3 recap (Hypothesis 1) -- *The first hypothesis of this work states the following: Ruthenium(II) polypyridyl complexes **RPC3** and **RPC4** both having similar structures and gel based DNA cleaving ability act similarly in cells. The putative targets are the nuclear DNA and/or the mitochondria.*

As we have shown in this examination of both **RPC3** and **4** with their enantiomer variants, the first hypothesis is hereby disproven. Both RPCs did exhibit similar traits in their ability to induce cancer cell death and mouse tumor burden but it is clear from the evidence we have shown that they are indeed two uniquely different complexes. The stark differences they exhibit from **RPC4** highly localized in the intracellular nucleus whereas **RPC3,** in almost all its intracellular amounts, is localized in the cytoskeleton. Also in contrast is **RPC3**'s use of different active transport channels in comparison to **RPC4**. Their clear ability to cleave dsDNA and increase ROS intracellular production in a direct fashion with **RPC4** in as little as 2 h whereas **RPC3** takes a very indirect route taking as long as 22 h to accomplish the same effect. We also show that in MCTS formations the effect of **RPC3** to dissemble a tumor sphere is in contrast to **RPC4** leaving the same sphere and cell type intact. They showed similarity in their ability to disrupt the mitochondria of the cell, in particular the ATP synthase channel. The truly amazing aspect of these complexes is their kinetic ability to be cytotoxic at almost the same values of growth inhibition but are completely different in every way we studied them thus far.

Chapter 1.3 recap (Hypothesis 2)--*The second hypothesis of this works states the following: We will explore doublets of **RPC3** and **RPC4** with a number of standard care chemo drugs to determine if the RPCs can potentiate a positive response in certain chemo drug resistant cell lines and potentially act in a synergistic fashion.*

.

The second hypothesis through synergy and doublet examination appears to hold true. Combination of variant drugs that are effective in different cell compartments and **RPC3** and **RPC4** do show synergy against certain cell types and lines. We show that with a topoisomerase II inhibitor, etoposide, with **RPC4** and **RPC3** potentiated an effect against H322. The nuclear toxin cisplatin was potentiated with these RPCs in H1993 and H322 as well. Docetaxel, a tubulin stabilizer and cytoskeletal toxin, was most effective in being potentiated with these RPCs in multiple cell lines H322, H460 and H2126. Many more cell lines were also shown to be effected by doublets with **RPC3** and **RPC4** in an additive fashion but successful still. We also examined doublet studies H358, HOP-62 and HCC-2998 which were not resistant to etoposide, cisplatin or docetaxel and still yielded incredible synergistic effects based on the Loewe combination indices. Lastly, we show that with MCTS H460 and H2126, docetaxel resistant lines, shifted to left when potentiated with **RPC3** and **RPC4** in 3D cell culture.

These RPC complexes are novel in their ability to kill cancer cells in two distinct fashions, show selectivity between normal and cancer cells, cleave DNA with DSBs in competition with a current chemotherapeutic agent in the clinic, potentiate effects with standard care chemotherapeutic resistant cell types and their ability to have a redox-active bridging ligand that is functional with the intracellular reducing agents present in almost every mammalian cell.

The vast majority of this work needs to be continued to further elucidate these complexes. They offer the potential to help people someday against the ever growing concern of cancer treatment.

Appendix 1.1

H358	V_{Loewe}	HOP-62	V_{Loewe}	HCC-2998	V_{Loewe}
RPC3/Etoposide	0.1921	RPC4/Etoposide	0.04002	RPC3/Cisplatin	0.1326
Etoposide/RPC3	0.1944	Etoposide/RPC4	0.04022	Cisplatin/RPC3	0.1778
RPC3/Docetaxel	0.1999	RPC3/Etoposide	0.0642	RPC4/Cisplatin	0.2158
Docetaxel/RPC3	0.2001	Etoposide/RPC3	0.0647	Cisplatin/RPC4	0.2064
RPC4/Cisplatin	0.2123	RPC3/RPC4	0.0887	RPC3/RPC4	0.5962
Cisplatin/RPC4	0.2164	RPC4/Docetaxel	0.4333	RPC4/RPC3	0.8842
RPC3/RPC4	0.2254	Docetaxel/RPC4	0.4388	RPC4/Docetaxel	0.9965
Cisplatin/RPC3	0.3085	Docetaxel/RPC3	0.5564	Docetaxel/RPC4	0.9998
RPC3/Cisplatin	0.3047	RPC3/Docetaxel	0.5642	Docetaxel/RPC3	1.0212
RPC4/Etoposide	0.3084	RPC4/RPC3	0.5668	RPC3/Docetaxel	1.0132
Etoposide/RPC4	0.3124	Cisplatin/RPC3	0.5710	Etoposide/RPC3	14.000
RPC4/RPC3	0.2214	RPC3/Cisplatin	0.5721	RPC3/Etoposide	15.000
RPC4/Docetaxel	0.9652	RPC4/Cisplatin	0.6312	RPC4/Gemcitabine	19.000
Docetaxel/RPC4	0.9662	Cisplatin/RPC4	0.6412	Gemcitabine/RPC4	20.000
RPC4/Gemcitabine	20.000	RPC3/Gemcitabine	10.000	RPC4/Etoposide	21.602
Gemcitabine/RPC4	21.000	Gemcitabine/RPC3	11.000	Etoposide/RPC4	22.000
RPC3/Gemcitabine	1000.0	RPC4/Gemcitabine	2000.0	Gemcitabine/RPC4	28.000
Gemcitabine/RPC3	1000.0	Gemcitabine/RPC4	2000.0	RPC4/Gemcitabine	28.000

Appendix 1.1 Combination Index V_{Loewe} for H358, HOP-62 and HCC-2998 cell lines. Drug A (titrating dose) with drug B (constant IC_{10} dose)

Appendix 1.2

Cell Line	Drug A	Drug B	V_{Loewe}
H1993	ΔΔRPC4	Docetaxel	1200
H1993	ΔΔRPC4	Pemetrexed	750.6
H1993	Cispltain	ΔΔRPC4	0.992
H1993	ΔRPC3	Docetaxel	1900
H1993	Cispltain	ΔRPC3	2.698
H1993	ΔΔRPC4	ΔRPC3	2.000
H1993	ΔRPC3	ΔΔRPC4	0.760
H322	Etoposide	ΔΔRPC4	0.396
H322	Cispltain	ΔΔRPC4	0.752
H322	Etoposide	ΔRPC3	1.282
H322	Cispltain	ΔRPC3	1.504
H322	ΔΔRPC4	ΔRPC3	1.920
H322	ΔRPC3	ΔΔRPC4	1.520
HCC15	ΔΔRPC4	Docetaxel	0.223
HCC15	ΔΔRPC4	Pemetrexed	167.6
HCC15	ΔRPC3	Docetaxel	211.0
HCC15	ΔΔRPC4	ΔRPC3	2.003
HCC15	ΔRPC3	ΔΔRPC4	1.306
HCC1171	Cispltain	ΔΔRPC4	2.489
HCC1171	Cispltain	ΔRPC3	0.482
HCC1171	ΔΔRPC4	ΔRPC3	2.000
HCC1171	ΔRPC3	ΔΔRPC4	2.000
H1792	Pemetrexed	ΔΔRPC4	66.53
H1819	Etoposide	ΔΔRPC4	1.980
H1648	Etoposide	ΔΔRPC4	1.445
H1648	Cispltain	ΔΔRPC4	1.464
H1648	Pemetrexed	ΔΔRPC4	41.00

Cell Line	Drug A	Drug B	V_{Loewe}
HCC4017	ΔΔRPC4	Docetaxel	10000.42
HCC4017	ΔΔRPC4	Pemetrexed	758.5
HCC4017	Cispltain	ΔΔRPC4	3.522
HCC4017	ΔRPC3	Docetaxel	5600.2
HCC4017	Cispltain	ΔRPC3	27.09
HCC4017	ΔΔRPC4	ΔRPC3	1.760
HCC4017	ΔRPC3	ΔΔRPC4	1.440
H460	ΔΔRPC4	Docetaxel	0.1000
H460	ΔΔRPC4	Pemetrexed	0.9840
H460	Docetaxel	ΔΔRPC4	0.1333
H460	ΔRPC3	Docetaxel	4167.6
H460	Docetaxel	ΔRPC3	1.503
H460	ΔΔRPC4	ΔRPC3	2.000
H460	ΔRPC3	ΔΔRPC4	2.000
H2073	Docetaxel	ΔΔRPC4	1.448
H2073	Docetaxel	ΔRPC3	1.570
H2073	ΔΔTS101	ΔRPC3	1.600
H2073	ΔRPC3	ΔΔRPC4	1.600
H1975	Pemetrexed	ΔΔRPC4	36.08
H596	Etoposide	ΔΔRPC4	2.689
H596	Etoposide	ΔRPC3	2.923
H596	ΔΔRPC4	ΔRPC3	2.000
H596	ΔRPC3	ΔΔRPC4	2.000
H2126	Pemetrexed	ΔΔRPC4	41.00
H2126	Docetaxel	ΔΔRPC4	0.454
H2126	Docetaxel	ΔRPC3	0.363
H2126	ΔΔRPC4	ΔRPC3	1.920
H2126	ΔRPC3	ΔΔTS101	1.280

Appendix 1.2 Cell lines and standard care chemotherapeutic potentiation doublets with corresponding V_{Loewe} synergy index values. Drug A (titrating dose) with drug B (constant IC_{10} dose

References

1. Chabner B, *Cancer Res* (2010), **70**, 428-429.
2. Shen D-W, Pouliot LM, Hall MD, Gottesman MM, *Pharmacological Reviews* (2012), **64**(3):706-721.
3. Owatari S, Akune S, Komatsu M, Ikeda R, Firth SD, Che XF, Yamamoto M, Tsujikawa K, Kitazono M, Ishizawa T, *Cancer Res* (2007), **67**:4860–486
4. Clarke MJ, Zhu F, Frasca DR, *Chem Rev* (1999), **99**: 2511-2534.
5. Yang X, Chen L, Liu Y, Yongguang Y, Chen T, Zheng W, Liu JA, Qing-Yu HE, *Biochimie* (2012), **94**: 345-353
6. Mjos, K. D. & Orvig, C, *Chem. Rev.* (2014), **114**, 4540–4563.
7. Muhammad, N. & Guo, Z, *Curr. Opin. Chem. Biol.* (2014),**19**, 144–153.
8. Galluzzi, L, *Oncogene* (2012), **31**, 1869–1883.
9. D. Griffith, S. Cecco, E. Zangrando, A. Bergamo, G. Sava, and C. J. Marmion, *Journal of Biological Inorganic Chemistry* (2008), **13**, 4, 511–520,.
10. P. Zhang, J. Chen, and Y. Liang, *Acta Biochimica et Biophysica Sinica (*2010) **42,** 7, 440–449,.
11. J. Reedijk, *Platinum Metals Review* (2008), **52**, 1, 2–11.
12. E. Gallori, C. Vettori, E. Alessio, *Archives of Biochemistry and Biophysics* (2000) **376**, 1, 156–162.
13. L. Messori, P. Orioli, D. Vullo, E. Alessio, and E. Iengo, *European Journal of Biochemistry* (2000) **267**, 4, 1206–1213.
14. William M. Motswainyana and Peter A. Ajibade, *Advances in Chemistry* (2015), **21,** 2015 - 2018.
15. Brock S. Howerton, David K. Heidary, and Edith C. Glazer, *J. Am. Chem. Soc.* (2012), ***134,*** (20), 8324–8327.
16. Hufziger KT, Thowfeik FS, Charboneau DJ, *Journal of inorganic biochemistry*. (2014), **130**, 103-111.
17. T. W. Hambley*, Coordination Chemistry Reviews* (1997), **166**, 181–223,.
18. S. H. van Rijt and P. J. Sadler, *Drug Discovery Today* (2009) **14**, 23-24, 1089–1097.
19. Kumar, C. V.; Barton, J. K.; Turro, N. J, *J of American Chemical Society (*1985), **107**, (19), 5518-23.
20. Meggers, Eric, *Chemical Biology* (2007), **11**, 287-292
21. Yadav, Abhishek.; Janarantne, Thanara.; Krishnan, Arthi, *Molecular Cancer Therapeutics* (2013).
22. Abishek, Yadav, *ProQuest* (2008).
23. Dupureur, Cynthia M.; Barton, Jacqueline K, *Inorg. Chem.* (1997), **36**, 33 -43.
24. Liu, Z., Habtemariam, A., Pizarro, A. M., Clarkson, G. J. & Sadler, P. J, *Organometallics* (2011), **30**, 4702–4710.
25. Cynthia Griffith, Adam S. Dayoub, Thamara Jaranatne, Nagham Alatrash, Ali Mohamedi, Kenneth Abayan, Zachary Bierbach, Daniel W. Armstrong, and Frederick M. MacDonnell (in publication que)
26. Borkenstein, Klaus.; Levegruen, Sabine.; Peschke, Peter, *Radiation Research* (2004), **162**, 71-83.
27. Bhat, T. A., Kumar, S., Chaudhary, A. K., Yadav, N. & Chandra, D, *Drug Discovery Today* (2015), **20**, 635–643.
28. Li, F., Collins, J. G. & Keene, F. R, *Chem. Soc. Rev.* (2015), **44**, 2529–2542.
29. Y. Sun, L. E. Joyce, N. M. Dickson and C. Turro, *Chem. Commun (*2010), **46**, 2426-2428.

30. Y.-J. Liu, C.-H. Zeng, Z.-H. Liang, J.-H. Yao, H.-L. Huang, Z.-Z. Li and F.-H. Wu, *Eur. J. Med. Chem.* (2010), **45**, 3087-3095.
31. C. Mari, V. Pierroz, S. Ferrari and G. Gasser, *Chemical Science* (2015), **6**, 2660-2686.
32. A. Wragg, M. R. Gill, D. Turton, H. Adams, T. M. Roseveare, C. Smythe, X. Su and J. A. Thomas, *Chemistry – A European Journal* (2014), **20**, 14004-14011.
33. M. J. Pisani, D. K. Weber, K. Heimann, J. G. Collins and F. R. Keene, *Metallomics* (2010), **2**, 393-396.
34. M. J. Pisani, P. D. Fromm, Y. Mulyana, R. J. Clarke, H. Körner, K. Heimann, J. G. Collins and F. R. Keene, *ChemMedChem* (2011), **6**, 848-858.
35. C. A. Puckett and J. K. Barton, *Biochemistry* (2008), **47**, 11711-11716.
36. M. R. Gill, D. Cecchin, M. G. Walker, R. S. Mulla, G. Battaglia, C. Smythe and J. A. Thomas, *Chemical Science* (2013), **4**, 4512-4519
37. U. Schatzschneider, J. Niesel, I. Ott, R. Gust, H. Alborzinia and S. Wölfl, *ChemMedChem* (2008), **3**, 1104-1109.
38. Niles, A.L, *Anal Biochem. (*2007) **366**, 197–206.
39. Marroquin, L. D., *Toxicol. Sci. (*2007) **97**, 539–47.
40. Puckett, Cindy A.; Barton, Jacqueline K, *Biochemistry* (2008) **47(45)** 11711-11716.
41. Cristina Mari, Vanessa Pierroz, Stefano Ferrari and Gilles Gasser, *Chem. Sci.* (2015), **6**, 2660-2686.
42. Caiping Tan, *Dalton Trans.* (2011), **40**, 8611-8622.
43. W. Guo, W. Zheng, Q. Luo, X. C. Li, Y. Zhao, S. X. Xion and F. Y. Wang, *Inorg. Chem.* (2013), **52,** 5328–5338.
44. Davies, M.S., Berners-Price, S.J., Hambley, T.W, *Inorg. Chem. (*2000), ***39***, 5603-5613.
45. Lim, M.; Song, H.; Olmon, E.; Barton, *J. Inorg. Chem.* (2009), **48**, 5392-5397.
46. Gill, M., Derrat, H., Smythe, C., Battaglia, G., Thomas, J., *Chembiochem* (2011), **12**, 877-880.
47. Wang, J.; Zhang, P.; Qian, C., *J. Biol Inorg. Chem* (2014), **19**, 335 – 348.

48. Amacher DE., *Curr Med Chem*. (2005), **12(16),** 1829-39.

49. O. Zava, S. M. Zakeeruddin, C. Danelon, H. Vogel, M. Gratzel and P. J. Dyson, *ChemBioChem* (2009), **10**, 1796-1800.
50. C. Tan, J. Liu, H. Li, W. Zheng, S. Shi, L. Chen and L. Ji, *J. Inorg. Biochem.* (2008), **102**, 347-358.
51. Aranda A[1], Sequedo L, Tolosa L, Quintas G, Burello E, Castell JV, Gombau L*. Toxicol In Vitro.* (2013), **27(2)**, 954-63.
52. Qian, C., *Metallomics* (2013), **5**, 844–854.
53. Bhat, T. A., Kumar, S., Chaudhary, A. K., Yadav, N. & Chandra, D., *Drug Discovery* (2015), **20**, 635–643.
54. Wen S, Zhu D, Huang P., *Future medicinal chemistry* (2013), **5(1)**, 53-67.
55. Luo Z[1], Yu L, Yang F, Zhao Z, Yu B, Lai H, Wong KH, Ngai SM, Zheng W, Chen T. *Metallomics*. (2014), **6(8)**, 1480-90.

56. E. P. Rogakou, D. R. Pilch, A. H. Orr, V. S. Ivanova and W. M. Bonner, *J. Biol. Chem.*, (1998), **273**, 5858-5868.
57. F. Tommasino, T. Friedrich, B. Jakob, B. Meyer, M. Durante and M. Scholz, *PLoS ONE* (2015), **10**, 129-416.
58. L. J. Mah, A. El-Osta and T. C. Karagiannis, *Leukemia* (2010), **24**, 679-686.
59. S. Burma, B. P. Chen, M. Murphy, A. Kurimasa and D. J. Chen, *J. Biol. Chem.* (2001), **276**, 42462-42467.
60. J. P. Banáth, D. Klokov, S. H. MacPhail, C. A. Banuelos and P. L. Olive, *BMC Cancer* (2010), **10**, 1-12.

61. C. Redon, D. Pilch, E. Rogakou, O. Sedelnikova, K. Newrock and W. Bonner, *Current opinion in genetics & development* (2002), **12**, 162-169.
62. O. J. Bandele and N. Osheroff, *Biochemistry* (2008), **47**, 11900-11908.
63. T. Tanaka, H. D. Halicka, F. Traganos, K. Seiter and Z. Darzynkiewicz, *Cell cycleI (*2007), **6**, 371-376.
64. W. M. Bonner, C. E. Redon, J. S. Dickey, A. J. Nakamura, O. A. Sedelnikova, S. Solier and Y. Pommier, *Nat Rev Cancer* (2008), **8**, 957-967.
65. E. Ledesma-Fernández and P. H. Thorpe, *J. of Bio. Methods* (2015), **(2)**, 233-236.
66. Lin, R. Z. and H. Y. Chang, *Biotechnology journal* (2008), **3**, 1172-1184.
67. Longati, P., X. Jia., *BMC cancer* (2013), **13**, 95.
68. McMillin, D. W., J. M. Negri, *Nature reviews Drug discovery* (2013), **12(3)**, 217-228.
69. Petersen, O. W., L. Ronnov-Jessen, *Proceedings of the National Academy of Sciences of the United States of America* (1992), **89(19)**, 9064-9068.
70. Francia, G. and R. S. Kerbel, *Nature biotechnology* (2010), **28(6)**, 561-562.
71. Chitcholtan, K., P. H. Sykes, *Journal of translational medicine* (2012), **10**, 38-41.
72. Vermeulen, L., F. de Sousa e Melo, The lancet oncology (2012), **13(2)**, 83-89.
73. Aljitawi, O. S., D. Li, *Leukemia & lymphoma* (2013), **54(6)**, 1228–34.
74. Debnath, J., S. K. Muthuswamy, *Methods* (2003), **30(3)**, 256-268.
75. Kim, S. H., J. Turnbull, *The Journal of endocrinology* (2011), 209(2), 139-151.
76. McMillin, D. W., J. M. Negri, *Nature reviews Drug discovery* (2013), 12(3, 217-228.
77. Tibbitt, M. W. and K. S. Anseth, *Science translational medicine* (2012), 4(160), 160124.
78. Zschenker, O., T. Streichert, *PloS one* (2012), **7(4),** e34279.
79. Foucquier J, Guedj M.,*Pharmacology Research & Perspectives* (2015), **(3)**, 34-45
80. Oversteegen L, Shah M, Rovini H. *Nat Rev Drug Discov* (2007), **6**, 951–952.
81. Geary N. *Am J Physiol Metab* (2013), **304**, 237–253.
82. Caudle RM, Williams GM. *Pain* (1993), **55**, 313–317.

83. Cokol M, Chua HN, Tasan M, Mutlu B, Weinstein ZB, Suzuki Y, *Mol Syst Biol*. (2011), **7**, 544.
84. Chou T-C. *Pharmacol Rev.* (2006), **58**, 621–681.
85. Greco WR, Bravo G, Parsons JC. *Pharmacol Rev.* (1995), **47(2)**, 331-85.
86. Nelson HS. Advair, *J Allergy Clin Immunol*. (2001), **107**, 398–416.
87. Lee JJ, Kong M., *Stat Biopharm Res*. (2009), **1**, 4–17.
88. Zimmermann GR, Lehar J, Keith CT, *Drug Discov Today* (2007), **12**, 34–42.
89. Woodcock J, Griffin JP, Behrman RE., *N Engl J Med*. (2011), **364**, 985–987.
90. Whitehead A, Su T-L, Thygesen H, Sperrin M, Harbron C. *Pharm Stat*. (2013), **12**, 300–308.
91. Lehár J, Krueger AS, Avery W, Heilbut AM, Johansen LM, Price ER, *Nat Biotechnol* (2009), **27**, 659–666.
92. Loewe SMH. *Exp Pathol*. (1926), **114**, 313–326.
93. Loewe S. *Klin Wochenshrift*. (1927), **6**, 1077–1084.
94. Loewe S*. Arzneimittelforsch - Drug Res*.(1953), **3**, 285–290.
95. Tallarida RJ. *J Pharmacol Exp Ther*. (2001), **298**, 865–872.
96. Tallarida RJ. *J Pharmacol Exp Ther.* (2006), **319**, 1–7.
97. Tallarida RJ. *J Pharmacol Exp Ther*. (2012), **342**, 2–8.
98. Leslie JC, Shaw D, McCabe C, Reynolds DS, Dawson GR. *Neurosci Biobehav Rev*. (2004), **28(3)**, 229-38.
99. Young GT, Zwart R, Walker AS, Sher E, Millar NS *Proc Natl Acad Sci* (2008), **105(38)**, 14686–14691.
100. Michels J, Vitale I, Senovilla L. *Cell Cycle*. (2013), 12(6), 877-884
101. Costa CJB, Free CR, Corradi J, Bouzat C, Sine SM *J Neurosci* (2011), **31(39**), 13870–13879.
102. Thi L, Shaw D, Bird J. *Consult Pharm*. (2009), **24(3)**, 227-30.
103. Cetinats V, Kucukaslan Ali *Cell Biol. Int.* (2012)**, 36**, 261-265
104. Montecucco A, Zanetta F *EXCLI Journal* (2015), **14**, 95-108
105. Comer A, Goa K *Drugs and Aging (2000), **1**, 53-80*
106. Noble S, Goa K *Drugs* (1997), **54**, 447-472
107. Barton, J.K., Danishefsky, A.T. *J. Am. Chem. Soc.,* (1984), ***106***, 2172-2176
108. Hiort, C., Lincoln, P.; Norden, B. *J. Am. Chem. Soc.,* (1993), ***115***, 3448-3455
109. Tysoe, A., Kopelman, R.; Schelzig, D. *Inorg. Chem.,* (1999), ***38***, 5196-5197
110. Lincoln, P., Norden, B. *Chem. Commun.,* (1996), 2145-2146
111. Barton J.K.. *Biochemistry* 2008**, *47,*** 11711–11716
112. Guanying Li, Lingli Sun, Liangnian Ji and Hui Chao. . *Dalton Trans.*, 2016, **45**, 13261-13276
113. Martin R. **Gill**, Denis Cecchin, Michael G. Walker, Raminder S. Mulla, Giuseppe Battaglia, Carl Smythe and Jim A. Thomas*Chem. Sci*., 2013, **4**, 4512